Golden Jublee Year 1969-2019
ಹೈದ್ರಾಬಾದ ಕರ್ನಾಟಕ ಶಿಕ್ಷಣ ಸಂಸ್ಥೆಯ
ಶ್ರೀ ಪ್ರಭು ಕಲಾ, ವಿಜ್ಞಾನ ಹಾಗೂ ಜಿ. ಎಂ. ಬೋಹ್ರಾ ವಾಣಿಜ್ಯ ಪದವಿ ಮಹಾವಿದ್ಯಾಲಯ
ಶೋರಾಪೂರ - 585 224 ಜಿ. ಯಾದಗಿರ,
ಸ್ಥಾಪನೆ : 1969
ಫ್ಯಾಕ್ಸ : 08443 - 257039
ಕಛೇರಿ: 08443 - 256039
H.K.E. Society's
Shri Prabhu Arts, Science and J. M. Bohra Commerce Degree College
Shorapur - 585 224 Dist. Yadgiri - Karnataka - Email : spjmbcollege@gmail.com- web : spjmbcollege.org
(Accredited 'B+' grade by NAAC (2nd Cycle),

Ref. No. SPJMB/DEGREE/ /20

Date : 23/12/2024

3.2.1 Number of papers published per teacher in the Journals notified on UGC website during the year

Title of paper	Name of the author/s	Department of the teacher	Name of journal	Year of publication	ISSN number
Samaja mukhi Bhava Pragneya Madivalappanavar Tatva Padagalu	Dr. Saibanna	Sociology	AKSHARASURYA	2024	2583-620X
Intrinsic Burst-Blinking Nanographenes for Super-Resolution Bioimaging	Dr. Goudappagouda	Chemistry	Journal of the American Chemical Society (JACS)	2024	0002-7863 (print); 1520-5126 (web)
Solvent-FreeOrganic Liquids :An Efficient Fluid Matrix for Unexplored Functional Hybrid Materials	Dr. Goudappagouda	Chemistry	Accounts of Chemical Research (ACS)	2023	0001-4842 (print); 1520-4898 (web)
A Detailed exploration on termites (Isopteran; Termitidae) Ecology of vegetative gradient in Gulbarga University Campus, Kalaburagi	Dr. Md Varis	Zoology	International Journal of Entomology Research	2023	2455-4758
MHD Carreau hybrid nanoliquid flow over a stagnation region of poignant needle: An enhanced heat transmission model	Dr. Samrat	Mathematics	Scandinavian Journal of Information Systems	2023	0905-0167

Total of five publications has been published in the academic year 2023-24

PRINCIPAL
S.P.& J.M.B. DEGREE COLLEGE
SHORAPUR 585 224 Dist: YADGIR

AKSHARASURYA

E-ISSN: 2583-620X

PEER-REVIEWED, MULTI LINGUAL E-JOURNAL

THIS IS TO CERTIFY THAT THE ARTICLE ENTITLED

ಸಮಾಜಮುಖಿ ಭಾವ ಪ್ರಜ್ಞೆಯ ಮಡಿವಾಳಪ್ಪನವರ ತತ್ವಪದಗಳು

AUTHORED BY

ಸಾಯಿಬಣ್ಣ

ಸಹಾಯಕ ಪ್ರಾಧ್ಯಾಪಕರು, ಸಮಾಜಶಾಸ್ತ್ರ ವಿಭಾಗ, ಶ್ರೀ ಪ್ರಭು ಕಲಾ, ವಿಜ್ಞಾನ ಮತ್ತು ಜೆ. ಎಂ. ಬೋಹರಾ ವಾಣಿಜ್ಯ ಪದವಿ ಮಹಾವಿದ್ಯಾಲಯ, ಸುರಪುರ, ಯಾದಗಿರಿ.

PUBLISHED IN:

AKSHARASURYA

Peer-Reviewed, Multi Lingual E-Journal.

Volume-03, Issue-02, February 2024.

Publisher

Mr. Mahesh M.

AKSHARASURYA

Peer-Reviewed, Multi lingual E-Journal.

E-ISSN: 2583-620X | Volume-03, Issue-02, February 2024.

Peer-Reviewed,
Multi lingual E-Journal.
E-ISSN: 2583-620X

Publisher
Mahesh M.
59/A, Maddenahatti
Village, G. Bhommanahalli
Post, Devalapura Hobli,
Nagamangala Taluk,
Mandya District-571 425.
m143che@gmail.com
9008559583

Editor in Chief
'AKSHARA', No. 697, 4th
Main, Raghavendra Block,
Srinagara, Bengaluru- 50.
editor@aksharasurya.com
9008588133

AKSHARASURYA

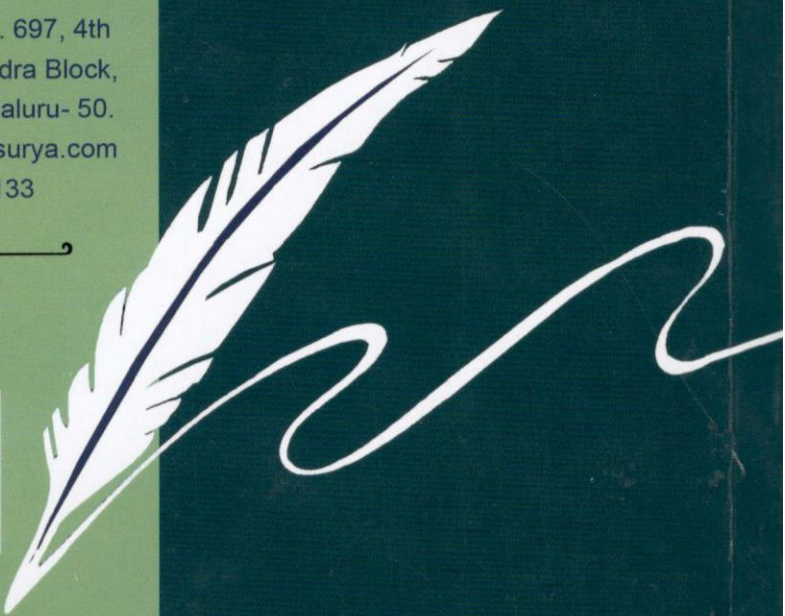

AKSHARASURYA

Peer-Reviewed, Multi Lingual E-Journal

E-ISSN: 2583-620X

VOLUME – 03, ISSUE – 02, FEBRUARY 2024.

PUBLISHER:

Mahesh M.

[illegible], Maddenahatti Village, G. Bhomanahalli Post, DevalapuraHobli,

Nagamangala Taluk, Mandya District, Karnataka State- 571425.

9008559583

m143che@gmail.com

https://aksharasurya.com/

ಸಮಾಜಮುಖಿ ಭಾವ ಪ್ರಜ್ಞೆಯ ಮಡಿವಾಳಪ್ಪನವರ ತತ್ವಪದಗಳು

ಸಾಯಿಬಣ್ಣ
ಸಹಾಯಕ ಪ್ರಾಧ್ಯಾಪಕರು
ಸಮಾಜಶಾಸ್ತ್ರ ವಿಭಾಗ
ಶ್ರೀ ಪ್ರಭು ಕಲಾ, ವಿಜ್ಞಾನ ಮತ್ತು
ಜೆ. ಎಂ. ಬೋಹರಾ ವಾಣಿಜ್ಯ
ಪದವಿ ಮಹಾವಿದ್ಯಾಲಯ
ಸುರಪುರ, ಯಾದಗಿರಿ.

Article Link: https://aksharasurya.com/2024/02/saibanna-m.php

ABSTRACT:

ಪ್ರಸ್ತುತ ಸಮಕಾಲಿನ ಸಾಮಾಜಿಕ ಸಂದರ್ಭದಲ್ಲಿ ತತ್ವಪದಗಳು ಮತ್ತು ತತ್ವಪದಕಾರರ ತಾತ್ವಿಕತೆಯನ್ನು ಅಭಿವ್ಯಕ್ತಿಪಡಿಸುತ್ತದೆ. ಆಧುನಿಕರಣ, ಜಾಗತಿಕರಣ, ನಗರಿಕರಣದಲ್ಲಿ ಮಿಂದೆಳುತ್ತಿರುವ ಇಂದಿನ ಸಮಾಜವು ಮೌಲ್ಯಾಧಾರಿತ ವಾತಾವರಣವನ್ನು ಮೀರಿ ನಾಗರಿಕತೆಯೆನ್ನುವ ವೈಭೋಗದ ಬದುಕಿಗೆ ಅಂಟಿಕೊಂಡು, ಮೌಲ್ಯ, ಆದರ್ಶ, ನೈತಿಕತೆಯನ್ನು ಬರಿದಾಗಿಸಿಕೊಳ್ಳುತ್ತಿದೆ. ಮನುಷ್ಯ ಕಲ್ಯಾಣ, ಸದಾಶಯದ ಭಾವ ಇಂದಿನ ಯುವಸಮುದಾಯಗಳಲ್ಲಿ ಗಣನಿಯವಾಗಿ ಕುಸಿಯುತ್ತಿದೆ. ಪರಿಣಾಮವಾಗಿ ಸಮಾಜದಲ್ಲಿ ಸಮುದಾಯ ಮತ್ತು ವಿವಿಧ ಸಮೂಹಗಳು, ನೈತಿಕ ಮತ್ತು ಅಲಿಂಗನ ಮನೋಭಾವವನ್ನು ಬರಿದಾಗಿಸಿಕೊಳ್ಳುತ್ತಿವೆ. ಇಂತಹ ಕ್ಲಿಷ್ಟಕರವಾದ ಹಾದಿಯೆಡೆಗೆ ಸಾಗುತ್ತಿರುವ ಸಮಾಜವನ್ನು ನೈತಿಕತೆಯೆಡೆಗೆ ಕರೆತರಲು ತತ್ವಪದಗಳು ಅತ್ಯಂತ ಪರಿಣಾಮಕಾರಿ ಮತ್ತು ಕ್ರೀಯಾತ್ಮಕವಾಗಿ ಕೆಲಸ ಮಾಡಿವೆಯೆಂದು ನಿರ್ವಿವಾದವಾಗಿ ಹೇಳಬಹುದು. ಈ ದೆಸೆಯಲ್ಲಿ ಕಡಕೋಳ ಮಡಿವಾಳಪ್ಪನವರ ತತ್ವಪದಗಳು ಸಮಾಜದಲ್ಲಿ ವೈಚಾರಿಕತೆಯ ಕೂಗೆಬ್ಬಿಸಿ, ಸಮಾಜಕ್ಕೆ ಚಲನಾಶೀಲತೆಯೆಂಬ ಮೌಲಿಕತೆಯನ್ನು ತುಂಬಿ ಸಮಾಜದ ಪ್ರಗತಿಗೆ ಕಾರಣವಾಗಿವೆ. ಪ್ರಸ್ತುತ ಲೇಖನವು ತತ್ವಪದ ಸಾಹಿತ್ಯವನ್ನು ಕೇವಲ ಸಾಹಿತ್ಯಕ ಪರಿಧಿಯಿಂದ ಗ್ರಹಿಸದೆ, ಸಾಮಾಜಿಕ ಕಣ್ಣೋಟಗಳಿಂದ ನೋಡಬೇಕಾದ ಅಗತ್ಯತೆಯನ್ನು ಪ್ರತೀಪಾದಿಸುತ್ತದೆ. ಕಡಕೋಳ ಮಡಿವಾಳಪ್ಪನವರನ್ನು ಕೇವಲ ತತ್ವಪದಕಾರನಷ್ಟೆ ಅಲ್ಲ, ಅವರೊಬ್ಬ ಸಮಾಜದ ಬಗ್ಗೆ ಸದಾ ಚಿಂತಿಸುತಿದ್ದ ಸಾಮಾಜಿಕ ಸಹೃದಯಿಯಾಗಿದ್ದರು. ಹಾಗಾಗಿ ಅವರನ್ನು ಸಮಾಜವಿಜ್ಞಾನ ಅಧ್ಯಯನ ಶಿಸ್ತುಗಳು ಸಾಮಾಜಿಕ ಚಿಂತಕರನ್ನಾಗಿ ಪರಿಭಾವಿಸುವ ಅವಶ್ಯಕತೆಯಿದೆ. ಈ ನೆಲೆಯಲ್ಲಿ ಪ್ರಸ್ತುತ ಲೇಖನವು ಅವರ ತತ್ವಪದಗಳ ಸಾಮಾಜಿಕ ಕಾಳಜಿಯನ್ನು ಹೊರಹಾಕುತ್ತದೆ. ಸಮಾಜವನ್ನು ಆವರಿಸಿರುವ ಮೌಢ್ಯ, ಕಂದಾಚಾರ, ಅಗಣಿತ ಸಾಮಾಜಿ-

ಕ ವ್ಯಸನಗಳ ಕುರಿತು ಮಡಿವಾಳಪ್ಪನವರ ಸಾಹಿತ್ಯವು ಧ್ವನಿಯೆತ್ತಿದೆ. ಹೀಗೆ ಪ್ರಸ್ತುತ ಲೇಖನವು ಮಡಿವಾಳಪ್ಪನವರ ಸಾಹಿತ್ಯ ಒಳಗೊಂಡಿರುವ ಸಾಮಾಜಿಕ ನಿಲುವುಗಳನ್ನು ದಾಖಲಿಸುವ ಪ್ರಯತ್ನ ಮಾಡಿದೆ.

KEY WORDS:

ಮಡಿವಾಳಪ್ಪ, ಜನಮುಖಿ ಧೋರಣೆ, ಸಾಮಾಜಿಕ ಅಭಿವೃದ್ಧಿ, ಅಭಿವ್ಯಕ್ತಿ, ಸಾಹಿತ್ಯ, ತತ್ವಪದ.

ಮಡಿವಾಳಪ್ಪನವರನ್ನು ಇಂದು ಬಹುವಾಗಿ ಅರ್ಥಮಾಡಿಕೊಳ್ಳುವ ಸಂಕ್ರಮಣದ ಸನ್ನಿವೇಶ ವಿಶಾಲವಾಗಿ ತೆರೆದುಕೊಳ್ಳುತ್ತಿದೆ. ಮಡಿವಾಳಪ್ಪನವರು ಸಾಹಿತ್ಯಕ್ಕಾಗಿ ತತ್ವಪದಗಳನ್ನು ಸೃಜಸದೆ, ಸಮಾಜದಲ್ಲಿ ವಿಸ್ತೃತವಾಗಿ ಹರಡಿದ್ದ ಅಂಕು ಡೊಂಕುಗಳನ್ನು ತಿದ್ದಲು ತತ್ವಪದಗಳ ಮೊರೆಹೋಗಿ ಸಾಹಿತ್ಯ ಕೃಷಿ ಮಾಡಿರುವದು ಅವರ ಸಮಗ್ರ ಸಾಹಿತ್ಯದಿಂದ ಸಾಬೀತಾಗುತ್ತದೆ. ಸಮಾಜದ ಅವ್ಯವಸ್ಥೆಗಳಿಗೆ ಮಿಡಿದು, ಸಮಾಜದ ವಿಕಾಸಕ್ಕಾಗಿ ಹಂಬಲಿಸಿದ, ಸಾಮಾಜಿಕ ವಿಕಾಸದ ಮುಖವಾಣಿಯಾಗಿ ಶ್ರೀ ಕಡಕೋಳ ಮಡಿವಾಳಪ್ಪನವರು ಕಂಡುಬರುತ್ತಾರೆ. ಸಮಾಜದಲ್ಲಿ ಪರಂಪರೆಯಿಂದ ಬಂದ ಮೇಲು, ಕೀಳು, ಉಚ್ಚ, ನೀಚ, ಕಂದಾಚಾರ, ಮೌಢ್ಯಗಳನ್ನು ನೇರವಾಗಿ ಪ್ರೆಶ್ನಿಸುವ ಎದೆಗಾರಿಕೆಯನ್ನು ಇವರ ತತ್ವಪದಗಳು ಹೊಂದಿವೆ. ಮನುಷ್ಯ ಕಲ್ಯಾಣಕ್ಕಾಗಿ ಇವರ ತತ್ವಪದಗಳು ಶ್ರಮಿಸಿವೆ. ಇಂತಹ ಹಲವು ತತ್ವಪದಗಳಲ್ಲಿ 'ಮುಕನಾಗಬೇಕು ಜಗದೊಳು ಜ್ವಾಕ್ಯಾಗಿರಬೇಕು' ಎನ್ನುವ ಸಮಾಜ ಮುಖಿ ತತ್ವಪದವು ಕೂಡಾ ಒಂದು. ಇಂದಿನ ಆಧುನಿಕ ಸಂಕೀರ್ಣ ಸಮಾಜಕ್ಕೆ ಅನ್ವಯಿಸುವಂತಹ ಬದುಕಿನ ವಾಸ್ತವ ಚಿತ್ರಣವನ್ನು ಹಿಡಿದಿಡುವಂತಹ ಬದುಕಿನ ಅಪ್ಪಟ ಸತ್ಯ ಈ 'ಮುಕನಾಗಬೇಕು ಈ ಜಗದೊಳು ಜ್ವಾಕ್ಯಾಗಿರಬೇಕು' ಎನ್ನುವ ಕಡಕೋಳ ಮಡಿವಾಳಪ್ಪನವರ ತತ್ವಪದ. ಸಮತೋಲನದ ಬದುಕನ್ನು ಕಟ್ಟಿಕೊಳ್ಳುವಲ್ಲಿ ಜೀವನದಲ್ಲಿ ಮೌನವು ಬಹುಮುಖ್ಯವಾದದ್ದು ಎನ್ನುವದನ್ನು ಸಾಕ್ಷೀಕರಿಸುವ ಈ ತತ್ವಪದ ತನ್ನದೆಯಾದ ಮಹತ್ವವನ್ನು ಪಡೆದಿದೆ. ಜಗದ ವ್ಯತ್ಯಾಸಗಳನ್ನು, ಶ್ರೇಣೀಕರಣವನ್ನು, ಬೇಧಭಾವಗಳನ್ನು ಗಟ್ಟಿಯಾದ ಧ್ವನಿಯಲ್ಲಿ ಝೇಂಕರಿಸುವ ಚಲನಾಶೀಲತೆಯ ಮನೋಭಾವದ ಪ್ರಗತಿಪರರನ್ನು ಸಮಾಜದ ಒಂದು ವರ್ಗ ಕಡುವಾಗಿ ವಿರೋಧಿಸುತ್ತ ಬಂದಿರುವದು ಇತಿಹಾಸವನ್ನು ಗಮನಿಸಿದಾಗ ಮನದಟ್ಟಾಗುತ್ತದೆ. ಸಮಾಜದ ಉಗಮದ ಇತಿಹಾಸದಿಂದಲೂ ಇಲ್ಲಿಯವರೆಗೆ ಸಮತೆಯೆನ್ನುವದು ಸಮಾಜದ ಬಹುದೊಡ್ಡ ಸವಾಲಾಗಿದೆ. ಇಂತಹ ಸವಾಲಿಗೆ ಪ್ರತಿರೋಧವಾಗಿ ಹಲವು ಚಳುವಳಿಗಳು ಜನ್ಮತಾಳಿದವು, ಇಂತಹ ಚಳುವಳಿಗಳ

ಜೊತೆಗೆ ಪ್ರತಿರೋಧದ ಕೊಗು ಸಾಹಿತ್ಯದಲ್ಲೂ ಕಂಡುಬಂದವು. ಪ್ರಮುಖವಾಗಿ ಬಂಡಾಯ ಸಾಹಿತ್ಯ ಮತ್ತು ತತ್ವಪದಗಳು ಈ ಬಗೆಯನ್ನು ಪ್ರಭಲವಾಗಿ ವಿರೋಧಿಸಿದವು. ಈ ವಿಧದ ಸಾಹಿತ್ಯದ ಮೂಲಕ ಸಮಾಜದಲ್ಲಿ ಜಾಗೃತಿಯನ್ನು ಹಮ್ಮಿಕೊಂಡ ಸಾಹಿತಿ ಮತ್ತು ತತ್ವಪದಕಾರರಿಗೆ ಅನೇಕ ಸಂಕಟಗಳು ಎದುರಾದವು. ಇಂತಹ ಸಂಕಟಗಳಿಗೆ ಕೊರಳೋಡ್ಡಿ ಮೈಗೆಡವಿಕೊಂಡ ಅದೆಷ್ಟೋ ಸಾಮಾಜಿ–ಕ ಚಿಂತಕರು ಸಮಾಜದ ಸುಗಮಕ್ಕಾಗಿ ತಮ್ಮನ್ನು ಸಮರ್ಪಿಸಿಕೊಂಡಿದ್ದಾರೆ. ಸಮಾಜದಲ್ಲಿ ಗಟ್ಟಿಯಾಗಿ ತಳವುರಿದ್ದ ಅಸಹ್ಯಗಳನ್ನು ಬಯಲಾಗಿಸುವ ಶ್ರಮಿಕರನ್ನು ಪಟ್ಟಭದ್ರರು ಸಾಧ್ಯವಿರುವಷ್ಟು ಅವರಿಗೆ ತೊಂದರೆ ನೀಡಿದ್ದಾರೆ. ಅಂತಹ ಸಂಕ್ರಮಣದ ಸನ್ನಿವೇಶದಲ್ಲಿ ಮಡಿವಾಳಪ್ಪನವರಿಂದ ತಯಾರಾದ ಅರ್ಥ ಪೂರ್ಣ ಭಾವಪೂರ್ಣ ತತ್ವಪದವೆ ಈ ಮೂಕನಾಗಬೇಕು ಈ ಜಗದೊಳು ಜ್ವಾಕ್ಯಾಗಿರಬೇಕು ಎನ್ನುವ ಸಾರ್ವಕಾಲಿಕವಾದ ಸತ್ಯ. ಸತ್ಯವನ್ನು ಸಾರಲು ಹೊರಟವರಿಗೆ ಎದುರಾಗುವ ಭೀತಿಯ ಸ್ವರೂಪವನ್ನು ಅಭಿವ್ಯಕ್ತಿಪಡಿಸಲು ಈ ತರಹದ ಭಾವಗಳು ಪ್ರಕಟಿತ ರೂಪವಾಗುತ್ತವೆ ಎನ್ನುವದನ್ನು ಮಡಿವಾಳಪ್ಪನವರು ನಿರೂಪಿಸಿದ್ದಾರೆ. ಸಮಚಿತ್ತದಿಂದ ಸಮಾಜದ ಆಗುಹೋಗುಗಳನ್ನು ಗಮನಿಸಿದರು, ಪ್ರತಿಕ್ರಿಯಿಸದೆ ಮೌನಕ್ಕೆ ಶರಣಾಗಿ ದುರ್ಜನರ ನಿಂದನೆಗಳಿಂದ ದೂರವಿರಬೇಕು ಎನ್ನುವ ಮೂಲಕ ಸತ್ವಯುತವಾದ ವೈಚಾರಿಕವಾದವನ್ನು ಸ್ವೀಕರಿಸುವಷ್ಟು ಸಮಾಜ ಪ್ರಭುದ್ವವಾಗಿರುವಲ್ಲಿ ಮಿತಿಗಳನ್ನು ಎದುರಿಸುತ್ತಿರುವದನ್ನು ಮಡಿವಾಳಪ್ಪನವರು ಗುರುತಿಸುತ್ತಾರೆ. ನೈಜತೆಯನ್ನು ಅಪ್ಪಿಕೊಳ್ಳುವಲ್ಲಿ ಸಮಾಜದ ಬಹುಸಂಖ್ಯಾತ ಜನಸಮುದಾಯಗಳು ತಿಳುವಳಿಕೆ ಮತ್ತು ದೂರದೃಷ್ಟಿಯನ್ನು ಬೆಳೆಸಿಕೊಂಡಿಲ್ಲ. ಮಿಥ್ಯೆವಾದಿಗಳ ಮಿಥ್ಯೆಗಳಿಗೆ ತಮ್ಮ ಮೆದಳೊಪ್ಪಿಸಿರುವದನ್ನು ತಮ್ಮ ತತ್ವಪದಗಳ ಮುಖೇನ ಮಡಿವಾಳಪ್ಪನವರು ದೃಡೀಕರಿಸುತ್ತಾರೆ. ಮೌನದ ಅವಲೋಕನದ ಬದುಕು ಸಮಸ್ಯೆಗಳಿಂದ ಮುಕ್ತವಾಗಿರುತ್ತದೆ ಎನ್ನುವದು ಒಂದರ್ಥದಲ್ಲಿ ಸತ್ಯವಾದರೂ, ಸತ್ಯವನ್ನು ಮೌನದ ಮೂಲಕ ನಗ್ನವಾಗಿಸುವದು ಆತ್ಮದ್ರೋಹವಾಗುತ್ತದೆ. ಮೌನ ಜೀವನದ ಶ್ರೇಷ್ಠ ಆಭರಣವೆ ಆದರೂ ಪ್ರತಿಕ್ರಿಯಿಸುವ, ಪ್ರತಿಸ್ಪಂದಿಸುವ ಭಾವವನ್ನು ಮೋಟಕುಗೊಳಿಸುತ್ತದೆ. ಹಾಗಾಗಿ ಅತಿ ಮೌನವು ಕೂಡಾ ಅಪಾಯಕಾರಿ. ಮಡಿವಾಳಪ್ಪನವರ ದೃಷ್ಟಿಕೋನದಲ್ಲಿ ಅಂದಾಜಿಸುವದಾದರೆ ಸಮಾಜ ಸಮಕಾಲಿನ ವಾಸ್ತವವನ್ನು ಗಟ್ಟಿಯಾಗಿ ಅಭಿವ್ಯಕ್ತಿಸುವದರಿಂದ ಅಭಿವ್ಯಕ್ತಿಕಾರನ ಮೇಲೆ ಸಮಸ್ಯೆಗಳನ್ನ ಸೃಷ್ಟಿಸುವ ಸಾಧ್ಯತೆಗಳು ಹೆಚ್ಚಾಗಿರುತ್ತವೆ. ಕಾರಣ ಸಮಾಜದ ವಿಧ್ಯಮಾನಗಳನ್ನು ಕ್ಷ–ಕಿರಣದಿಂದ ಗಮನಿಸಿದರು ಮಾತಾಡದೆ ಮೂಕನಾಗಿ ಸುರಕ್ಷಿತವಾಗಿರುವದು ಒಳಿತೇನೋ ಎನ್ನುವ ಭಾವಕ್ಕೆ ಒಂದು ಕ್ಷಣಕ್ಕೆ ಬಂದಾಗ

ಮೂಕನಾಗಬೇಕು ಜಗದೊಳು ಜ್ವಾಕ್ಯಾಗಿರಬೇಕು ಎನ್ನುವ ಭಾವ ಅವರಿಂದ ಪ್ರಕಟವಾಗಿರಬಹುದು ಎನ್ನುವ ಅನುಮಾನವನ್ನು ವ್ಯಕ್ತಪಡಿಸಬಹುದು. ಏಕೆಂದರೆ ಮಡಿವಾಳಪ್ಪನವರು ಯಾವ ಮುಲಾಜಿಗೆ, ಭೀತಿಗೆ ಹೆದರಿದವರಲ್ಲ, ನಿರ್ಭಿತಿ ನಿರ್ಭಿಡೆ ತತ್ವಪದಗಳ ವಾರಸುದಾರರಾದ ಅವರು ಯಾವ ಅಂಜಿಕೆಯನ್ನು ಪರಿಗಣನೆಗೆ ತೆಗೆದುಕೊಂಡವರಲ್ಲ. ನೇರವಂತಿಕೆಯನ್ನೇ ತಮ್ಮ ತತ್ವಪದಗಳ ಶಕ್ತಿಯಾಗಿಸಿಕೊಂಡ ತತ್ವಪದಕಾರರಾದ ಇವರಿಂದ ಅನೇಕ ಬಹುಮುಖಿ ಕೊಡುಗೆಗಳು ಸಮಾಜಕ್ಕೆ ಹೆರಳವಾಗಿ ಲಭ್ಯವಾಗಿವೆ. ಮೂಕನಾಗಬೇಕು ಈ ಜಗದೊಳು ಜ್ವಾಕ್ಯಾಗಿರಬೇಕು ಎನ್ನುವ ಈ ತತ್ವಪದಗಳ ಹಲವು ಗುಡಾರ್ಥಗಳನ್ನು ಒಳಗೊಂಡ ಒಂದು ಅರ್ಥಪೂರ್ಣ ಸಂದೇಶವಾಹಕವಾಗಿದೆ. ಸಮಕಾಲಿನ ಸಂದರ್ಭದ ನೆಲೆಯಲ್ಲಿಯು ಇದನ್ನು ಪರೀಕ್ಷಿಸಿದಾಗ ಮೌನವು ಬಹುದೊಡ್ಡ ಸಮಾಧಾನದ ಅಂಶವಾಗಿ ಕಂಡುಬರುವದರಲ್ಲಿ ಯಾವುದೆ ಅನುಮಾನಗಳಿಲ್ಲ. ಮಡಿವಾಳಪ್ಪನವರಿಂದ ನೂರಾರು ವರ್ಷಗಳಿಂದ ಹಿಂದೆಯೇ ಮೂಡಿಬಂದ ಈ ತತ್ವಪದವು ಪ್ರಸ್ತುತ ಸಮಾಜಕ್ಕೂ ಸಾಕಷ್ಟು ಅನ್ವಯವಾಗುತ್ತದೆ. ಅನಾವಶ್ಯಕ ಮಾತುಗಳು ನಿಯಂತ್ರಿಸಿ ಬದುಕಲ್ಲಿ ಸಂತೋಷವನ್ನು ಬರಮಾಡಿಕೊಳ್ಳಬಹುದು. ಪ್ರಗತಿಪರವಾದ ಆಶಯಗಳನ್ನು ಬದಿಗೊತ್ತುವ ಪೊಳ್ಳುಗಳನ್ನು ಹೆರಳವಾಗಿಸಿಕೊಂಡ ಸಮಾಜದಲ್ಲಿ ನಾವಿಂದು ಜೀವಿಸುತಿದ್ದೇವೆ. ಸತ್ಯವನ್ನು ಗಟ್ಟಿಯಾಗಿ ಹೇಳುಲು ಪೂರಕವಾದ ಪರಿಸರದ ಕೊರತೆಯ ಸಂದರ್ಭದ ಸಮಾಜದಲ್ಲಿ ಇಂದು ಬದುಕನ್ನು ಸವೆಸಬೇಕಾದ ಅನಿವಾರ್ಯತೆಯಿದೆ. ಈ ಹಿನ್ನಲೆಯಲ್ಲಿ ಮೂಕ ಮನಸ್ಥಿತಿಗೆ ಒಗ್ಗಿಕೊಂಡವರು ತಮ್ಮ ಸುರಕ್ಷತೆಯನ್ನು ಕಾಯ್ದುಕೊಂಡು ಜೀವನ ಸಾಗಿಸುತ್ತಾರೆ. ಸತ್ಯವನ್ನು ತಡೆಯಬಹುದು ನಿರ್ಮೂಲನೆಗೊಳಿಸಲು ಅಸಾಧ್ಯ. ಈ ತರಹದಲ್ಲಿ ಕಡಕೋಳ ಮಡಿವಾಳಪ್ಪನವರ ಈ ತತ್ವಪದ ಅನೇಕ ಸಾಧ್ಯತೆಗಳಿಗೆ ತನ್ನನ್ನು ತೆರೆದುಕೊಳ್ಳುತ್ತದೆ.

ಪರಿವರ್ತನಾಶೀಲಾ ಸಮಾಜಕ್ಕೆ ಸಹಾಯಕವಾದ ಮಡಿವಾಳಪ್ಪನವರ ಸಾಹಿತ್ಯ:

ಜಗತ್ತಿನಲ್ಲಿ ಅನೇಕ ರಾಷ್ಟ್ರಗಳು ತಮ್ಮದೇಯಾದ ಹಲವು ಸಮಸ್ಯೆಗಳನ್ನು ಎದುರಿಸುತ್ತಿದ್ದವು. ಅಂತಹ ದೇಶಗಳ ಅಬ್ಯುದಯಕ್ಕೆ ಹಲವು ಸುಧಾರಕರು ಅವತರಿಸಿ ಆಯಾ ಸಮಾಜದ ಪರಿವರ್ತನೆಗೆ ಕಾರಣವಾಗಿದ್ದು ಇತಿಹಾಸ. ನಮ್ಮ ದೇಶವು ಅಂತಹ ಹತ್ತು ಹಲವು ಸಮಸ್ಯೆಗಳ ಆಗರವಾಗಿತ್ತು. ಇಂತಹ ಸಂಧರ್ಭದಲ್ಲಿ ಅನೇಕ ಸಮಾಜಸುಧಾರಕರು, ಚಿಂತಕರು, ಶಿವಶರಣರು, ದಾರ್ಶನಿಕರು, ಇಲ್ಲಿ ಜನ್ಮವೆತ್ತಿ ಸಮಾಜದ ಅನೇಕ ಸಮಸ್ಯೆಗಳಿಗೆ ಪರಿಹಾರವನ್ನು ಕೊಟ್ಟಿರುವಂತದ್ದು ಎಲ್ಲರಿಗೂ ತಿಳಿದಿರುವ ವಿಚಾರ. ಅಂತಹ ಅನೇಕ ಶಿವಶರಣರು, ದಾರ್ಶನಿಕರಲ್ಲಿ

ಕಡಕೋಳ ಮಡಿವಾಳಪ್ಪನವರು ಕೂಡ ಒಬ್ಬರು. ಮಡಿವಾಳಪ್ಪನವರು ಕೇವಲ ಸಾಹಿತ್ಯದ ದೃಷ್ಟಿಯಿಂದ ತತ್ವಪದಗಳನ್ನು ರಚಿಸದೆ, ಸಮಾಜದ ಪರಿವರ್ತನೆಯ ನೆಲೆಯಲ್ಲಿ ತತ್ವಪದಗಳನ್ನು ಸಮಾಜಕ್ಕೆ ನೀಡಿರುವದು ಸ್ಪಷ್ಟವಾಗುತ್ತದೆ. ಇವರ ತತ್ವಪದಗಳಲ್ಲಿ ಅನೇಕ ರೀತಿಯ ಮಾನವೀಯ ಮೌಲ್ಯಗಳು, ಆದರ್ಶಗಳು, ಸಂಸ್ಕಾರ, ಜೀವಪರನಿಲುವು ಮುಂತಾದವುಗಳು ಸಮೃದ್ಧವಾಗಿವೆ. ಇಂತಹ ಅನೇಕ ಮೌಲ್ಯಗಳು ಸಮಾಜದ ಪರಿವರ್ತನೆಗೆ ಕಾರಣವಾಗುತ್ತವೆ. ಸಾಮಾಜಿಕ ಬದ್ಧತೆ, ಕಾಳಜಿಗಳನ್ನು ಆರಂಭದಿಂದಲೆ ರೂಡಿಸಿಕೊಂಡ ಮಡಿವಾಳಪ್ಪನವರು ಯಾವಾಗಲೂ ಸಮಾಜದ ಕುರಿತು ಚಿಂತಿಸುತ್ತಿದ್ದರು, ಸಮಾಜದ ಒಳಿತು ಅವರ ಕನಸಾಗಿತ್ತು, ಈ ದೆಸೆಯಲ್ಲಿ ಸದಾ ಅವರು ಅನೇಕ ಕಾರ್ಯಗಳು ಕೈಗೊಳ್ಳುತ್ತಿದ್ದರು. ಮಡಿವಾಳಪ್ಪನವರ ಈ ರೀತಿಯ ಬದುಕು ಅವರ ಸಮಾಜಮುಖಿಯ ಚಿಂತನೆಯನ್ನು ಪ್ರತಿಬಿಂಬಿಸುತ್ತದೆ. ಹಾಗಾಗಿ ಮಡಿವಾಳಪ್ಪನವರನ್ನು ಸಮಾಜ ಸುಧಾರಕರ ನೆಲೆಯಲ್ಲಿ ಅರ್ಥಮಾಡಿಕೊಳ್ಳಬೇಕಿದೆ. ಆದ್ಯಾತ್ಮಿಕ ಮತ್ತು ತತ್ವಪದಿಯ ಕ್ಷೆತ್ರಗಳ ಆಚೆಯ ಅವರ ವ್ಯಕ್ತಿತ್ವದ ಪರಿಚಯ ಮಾಡಿಸಬೇಕಿದೆ. ಮಾನವ ಸಮೂಹದ ಅನೇಕ ಸಂವೇದನೆಗಳಿಗೆ ಅವರು ಧ್ವನಿಯಾಗಿದ್ದಾರೆ ಸಮಾಜಲ್ಲಿದ್ದಂತಹ ಅನೇಕ ಬೂಟಾಟಿಕೆಗಳಿಗೆ ತಿಕ್ಷಣವಾಗಿ ಪ್ರತಿಕ್ರಿಯಿಸಿದ್ದಾರೆ. ಅಂಧಾನುಚಾರಣೆಗಳನ್ನು ಬಲವಾಗಿ ವಿರೋಧಿಸಿದ್ದಾರೆ. ದೇವರು ದೈವದ ಬಗ್ಗೆ ಸ್ಪಷ್ಟವಾದ ನಿಲುವನ್ನು ಹೊಂದಿದ್ದರು. ದೇವರನ್ನು ಒಲಿಸಿಕೊಳ್ಳಲು ಪರಿಶುದ್ಧವಾದ ಭಕ್ತಿಯೆ ಮುಖ್ಯ ಹೊರತು ಮತ್ತಾವ ವಿಧಿವಿಧಾನಗಳಲ್ಲ ಎನ್ನುವ ಅಂತಿಮ ಸತ್ಯವನ್ನು ಸಮಾಜಕ್ಕೆ ಸಾರಿದ್ದಾರೆ. ಮನುಷ್ಯನಲ್ಲಿರುವ ಅಜ್ಞಾನ, ಅಂಧಕಾರಗಳನ್ನು ಹೋಗಲಾಡಿಸುವಲ್ಲಿ ಇವರ ತತ್ವಪದಗಳು ಗಂಭೀರವಾಗಿ ಕೆಲಸ ಮಾಡಿವೆ. ಮಡಿವಾಳಪ್ಪನವರ ಸಾಹಿತ್ಯ ಕೆಲವೆ ವಿಷಯಗಳಿಗೆ ಸೀಮಿತವಾಗದೆ, ಹಲವು ಉಪಯುಕ್ತ ವಿಷಯಗಳ ಆಗರವಾಗಿದೆ. ಸಮಾಜದ ಅನೇಕ ಜ್ವಲಂತ ಸಮಸ್ಯೆಗನ್ನು ಹೋಗಲಾಡಿಸಿ, ವೈಚಾರಿಕ ಸಮಾಜವನ್ನು ಸ್ಥಾಪಿಸುವ ಮೂಲ ಆಶಯಗಳನ್ನು ಇವರ ಸಾಹಿತ್ಯ ಹೊಂದಿದ್ದು, ಇವರು ಸಮಾಜದ ಕುರಿತಾಗಿ ಹೊಂದಿರುವ ಕಾಳಜಿಯನ್ನು ತೋರಿಸುತ್ತದೆ. ಹಾಗಾಗಿ ಮಡಿವಾಳಪ್ಪನವರನ್ನು ಕೇವಲ ಕೆಲವೆ ನೆಲೆಗಳಲ್ಲಿ ಗ್ರಹಿಸಿಕೊಳ್ಳದೆ ಬಹುಮುಖಿ ನೆಲೆಗಳಲ್ಲಿ ಮಡಿವಾಳಪ್ಪನವರನ್ನು ಗ್ರಹಿಸಿಕೊಳ್ಳಬೇಕಾಗಿದೆ. ಆ ಮೂಲಕ ಇವರನ್ನು ಸಮಾಜ ಸುಧಾರಕರನ್ನಾಗಿ ಗ್ರಹಿಸಿಕೊಳ್ಳಬೇಕು. ಇವರ ಚಿಂತನೆಗಳು ಖಂಡಿತವಾಗಿ ಸಮಾಜದ ಪರಿವರ್ತನೆಗೆ ಕಾರಣವಾಗಿವೆ. ಇವರ ಎಲ್ಲಾ ಚಿಂತನೆಗಳನ್ನು ಜಾಗತಿಕವಾಗಿ ಮುಟ್ಟಿಸಬೇಕಾದ ಅಗತ್ಯತೆ ಇದೆ. ಆ ಮೂಲಕ ಮಡಿವಾಳಪ್ಪನವರನ್ನು ಜಾಗತಿಕ ಚಿಂತಕರನ್ನಾಗಿ ಗ್ರಹಿಸುವ ಅವಶ್ಯಕತೆಯಿದೆ. ಈ

ಮೂಲಕ ಮಡಿವಾಳಪ್ಪನವರ ಕೊಡುಗೆಗಳನ್ನು ಅಮರವಾಗಿಸೋಣ. ಮಹಾಜ್ಞಾನಿ, ತತ್ವಪದಕಾರರು ವೈಚಾರಿಕ ಚಿಂತಕರಾದ, ಕಡಕೋಳ ಮಡಿವಾಳಪ್ಪ ಅವರ ಕು-ರಿತು ಬಹುಮುಖಿ ನೆಲೆಯಲ್ಲಿ ಚರ್ಚೆಯಾಗಬೇಕಿದೆ. ಕನ್ನಡ ಸಾಹಿತ್ಯ ಮತ್ತು ಚ-ರಿತ್ರೆಯಲ್ಲಿ ಅವರ ಅಚ್ಚಳಿಯದ ಹೆಜ್ಜೆಗುರುತುಗಳನ್ನು ಹೆಚ್ಚು ಪ್ರಚುರ ಪಡಿಸಬೇಕಿದೆ. ಕಡಕೋಳ ಮಡಿವಾಳಪ್ಪನವರ ತತ್ವಪದಗಳನ್ನು ಪ್ರೇರಣೆಯಾಗಿಸಿಕೊಂಡು ಕೆಲ ಸಾಹಿತಿಗಳು ಬಂಡಾಯದ ರೀತಿಯ ಕಾವ್ಯ, ಕಥನ ಸೃಷ್ಟಿಸಿ ಮುನ್ನೆಲೆಗೆ ಬಂದಿದ್ದಾರೆ. ಮಡಿವಾಳಪ್ಪನವರ ತತ್ವಪದಗಳು ಸಮಾಜದಲ್ಲಿ ಹೊಸ ಪರಿವರ್ತನೆಗೆ ಕಾರಣವಾಗಿವೆ. ಇವು ಕೇವಲ ತತ್ವಪದಗಳಲ್ಲದೆ ಸಮಾಜದಲ್ಲಿ ಬೇರುರಿದ್ದ ಹಲವು ಜಾಡ್ಯಗಳನ್ನು ಹೋಗಲಾಡಿಸುವಲ್ಲಿ ಕೆಲಸ ಮಾಡಿವೆ. ಇದ್ದದ್ದನ್ನು ಇದ್ದ ಹಾಗೆ ಖಂಡಿಸಿದ ಇಂತಹ ಮೇಧಾವಿಯನ್ನು ಜಗತ್ತಿನಲ್ಲಿ ಎಲ್ಲಿಯೂ ಸಿಗುವದಿಲ್ಲ. ನವ ಸಮಾಜದ ಪರಿಕಲ್ಪನೆಗಳನ್ನು ಇವರ ಚಿಂತನೆಗಳಲ್ಲಿ ಕಾಣಬಹುದಾಗಿದೆ. ಸಮಾಜದ ಕುರಿತಾಗಿ ಇವರು ಹೊಂದಿದ್ದ ಮುನ್ನೋಟಗಳು ಇಂದಿಗೂ ಪ್ರಸ್ತುತವಾಗಿವೆ. ಬಹುಮುಖಿ ನೆಲೆಯಿಂದ ಸಮಾಜವನ್ನು ಗ್ರಹಿಸಿದ ಅಪರೂಪದ ಸಾಮಾಜಿ-ಕ ಚಿಂತಕರನ್ನಾಗಿ ಇಂದು ಸಮಾಜ ಇವರನ್ನು ಅರ್ಥಮಾಡಿಕೊಳ್ಳಬೇಕಿದೆ. ಅಂದಶ್ರದ್ಧೆ, ಕಂದಾಚಾರ, ಮೈಲಿಗೆ, ಮೂಡಿಚಟ್ಟು ಮುಂತಾದ ಮನಸಿನ ವ್ಯಸನಗಳನ್ನು ಮುಲಾಜಿಲ್ಲದೆ ಅವುಗಳನ್ನು ಕಡುವಾಗಿ ವಿರೋಧಿಸಿದ್ದಾರೆ. ಹಲವು ಸಾಮಾಜಿಕ ಅಂಶಗಳನ್ನು ಆಧ್ಯಾತ್ಮಿಕ ನೆಲೆಯಲ್ಲಿ ಪರಿಶೋದಿಸಿದ್ದಾರೆ. ಆದ್ಯಾ-ತ್ಮಿಕ ಕ್ಷೇತವು ಸಾಮಾಜಿಕ ಬದಲಾವಣೆಗಳಿಗೆ ತೆರೆದುಕೊಳ್ಳಬೇಕೆಂದು ಬಲವಾಗಿ ಹಂಬಲಿಸಿದ್ದವರು. ವೈಯಕ್ತಿಕ ಬದಲಾವಣೆ, ಸಮುದಾಯದ ಬದಲಾವಣೆಗೆ ಆ ಮೂಲಕ ಸಾಮಾಜಿಕ ಬದಲಾವಣೆಗೆ ಕಾರಣವಾಗುತ್ತದೆ ಎಂದು ಗ್ರಹಿಸಿದ್ದ ಒಬ್ಬ ಸಾಮಾಜಿಕ ತಜ್ಞರಾಗಿದ್ದರು. ಇವರ ಎಲ್ಲಾ ತತ್ವಪದಗಳನ್ನು ಸೂಕ್ಷ್ಮವಾಗಿ ಗಮನಿಸಿದಾಗ ಇವರು ಅತಿಯಾಗಿ ಕಾಳಜಿವಹಿಸುತ್ತಿದ್ದುದ್ದು ಏಣಿಶ್ರೇಣಿ ಮುಕ್ತ ಸಮಾಜ, ಕಂದಾಚಾರ ರಹಿತ ಸಮಾಜವನ್ನು. ಹಾಗಾಗಿ ಇವರ ಚಿಂತನೆಗಳು ಸಮುದಾಯಿಕ ಅಂಶಗಳನ್ನು ಪುಷ್ಟಿಕರಿಸುತ್ತವೆ. ಜಗತ್ತನ್ನು ಕವಿದಿರುವ ಅಂ-ಧಕಾರವನ್ನು ಹೋಗಲಾಡಿಸುವಲ್ಲಿ ವೈಚಾರಿಕ ಮನಸ್ಥಿತಿ ಬಹಳ ಮುಖ್ಯವೆಂದು ನಂಬಿದ್ದರು. ವೈಚಾರಿಕತೆಯ ಪ್ರಸರಣವೆ ಪ್ರಧಾನ ಅಂಶವಾಗಿ ಇವರ ತತ್ವಪದಗಳನ್ನು ನಾವು ಗ್ರಹಿಸಬಹುದಾಗಿದೆ. ಮಡಿವಾಳಪ್ಪನವರು ಕೇವಲ ತತ್ವಪದಕಾರರಾಗಿ, ಸಾಹಿತ್ಯವನ್ನು ಪ್ರಚುರಪಡಿಸುವ ವ್ಯಕ್ತಿಯಾಗಿ ಕಾಣಿಸದೆ, ಅವರೊಬ್ಬ ಸಮಾಜ ಸುಧಾರಕರಾಗಿ ಕಂಡುಬರುತ್ತಾರೆ. ಹೀಗೆ ಇಂದಿನ ನಾಡಿನ ವಿದ್ವತ್ ವಲಯ ಮಡಿವಾಳಪ್ಪನವರನ್ನು ಗ್ರಹಿಸಬೇಕಿದೆ. ಉತ್ತಮ ಸಮಜ ನಿರ್ಮಾಣದ ಹಲವು

ಅಂಶಗಳನ್ನು ತಮ್ಮ ಚಿಂತನೆಗಳಲ್ಲಿ ದಾಖಲಿಸಿದ್ದಾರೆ. ಇಂತಹ ಅನೇಕ ಅಂಶಗಳನ್ನು ಸಾಮಾಜಿಕ ಅಭಿವೃದ್ಧಿಯಲ್ಲಿ ಇಂದಿನ ಸಮಾಜ ಬಳಸಿಕೊಳ್ಳಬೇಕಾಗಿದೆ.

ಪರಾಮರ್ಶನ ಗ್ರಂಥಗಳು:

1. ರೆಹಮತ್ ತರೀಕೆರೆ. (2017). ತತ್ವಪದಗಳ ಪ್ರವೇಶಿಸುವಿಕೆ. ರಾಷ್ಟ್ರೀಯ ಸಂತ ಕನಕದಾಸ ಅಧ್ಯಯನ ಮತ್ತು ಸಂಶೋಧನಾ ಕೇಂದ್ರ, ಬೆಂಗಳೂರು.
2. ಲಟ್ಟೆ ಎಂ. ಎಸ್. (1994). ಕಡಕೋಳ ಮಡಿವಾಳಪ್ಪ. ಕನ್ನಡ ಸಾಹಿತ್ಯ ಅಕಾಡೆಮಿ. ಬೆಂಗಳೂರು.
3. ನಾಗಭೂಷಣ ಬುಗನಡ್ಡು. (2015). ಕಡಕೋಳ ಮಡಿವಾಳಪ್ಪ. ಬಸವ ಅಧ್ಯಯನ ಪೀಠ, ಮೈಸೂರು ವಿಶ್ವವಿದ್ಯಾಲಯ. ಮೈಸೂರು.
4. ರೆಹಮತ್ ತರೀಕೆರೆ. (2018). ಕನ್ನಡ ಸಂಶೋಧನೆ ತಾತ್ವಿಕ ವಿಚಾರ. ಪ್ರಸಾರಾಂಗ, ಕನ್ನಡ ವಿಶ್ವವಿಧ್ಯಾಲಯ. ಹಂಪಿ.
5. ಆಲ್ದಾಳ ಎಲ್. ಬಿ. ಕೆ. (2019). ಕಡಕೋಳ ಮಡಿವಾಳಪ್ಪನವರು. ಕನ್ನಡ ಸಾಹಿತ್ಯ ಪರಿಷತ್. ಬೆಂಗಳೂರು.
6. ಮೀನಾಕ್ಷಿ ಬಾಳಿ (ಸಂ). (2017). ಕಡಕೋಳ ಮಡಿವಾಳಪ್ಪ ಮತ್ತು ಶಿಷ್ಯರ ತತ್ವಪದಗಳು. ರಾಷ್ಟ್ರೀಯ ಸಂತಕವಿ ಕನಕದಾಸ ಅಧ್ಯಯನ ಮತ್ತು ಸಂಶೋಧನಾ ಕೇಂದ್ರ, ಬೆಂಗಳೂರು.
7. ವಿಶ್ವರಾದ್ಯ ಸತ್ಯಂಪೇಟಿ. (2017). ಅನುಭಾವಿ ಕವಿ ಮಡಿವಾಳಪ್ಪ (ಲೇ). ಬಸವಮಾರ್ಗ ಪ್ರತಿಷ್ಠಾನ ಪ್ರಕಾಶನ. ಶಹಾಪುರ.
8. ಮೀನಾಕ್ಷಿ ಬಾಳಿ. (2015). ಬಂಡಾಯದ ಕಿಡಿ ಮಡಿವಾಳಪ್ಪ. ನ್ಯಾಷನಲ್ ಬುಕ್ ಟ್ರಸ್ಟ್, ಇಂಡಿಯಾ.
9. ಮಲ್ಲಿಕಾರ್ಜುನ ಕಡಕೋಳ (ಸಂ) (2022). ಕಡಕೋಳ ನೆಲದ ನೆನಪುಗಳು. ಶ್ರೀ ವೀರೇಶ್ವರ ಪ್ರಕಾಶನ, ಕಡಕೋಳ ಮಹಾಮಠ. ಕಡಕೋಳ.
10. ಮೋಹನದಾಸ್ ಮುಖರ್ಜಿ. (2012). ಸಾಹಿತ್ಯ ಮತ್ತು ಸಮಾಜ. ಪ್ರಕಾಶ ಪಬ್ಲಿಕೇಷನ್ಸ್, ಸಹನಾಪುರ.

JACS
JOURNAL OF THE AMERICAN CHEMICAL SOCIETY
pubs.acs.org/JACS

Article

Intrinsic Burst-Blinking Nanographenes for Super-Resolution Bioimaging

Xingfu Zhu,[#] Qiang Chen,[#] Hao Zhao,[#] Qiqi Yang, Goudappagouda, Márton Gelléri, Sandra Ritz, David Ng, Kaloian Koynov, Sapun H. Parekh, Venkatesh Kumar Chetty, Basant Kumar Thakur, Christoph Cremer, Katharina Landfester, Klaus Müllen, Marco Terenzio, Mischa Bonn,* Akimitsu Narita,* and Xiaomin Liu*

Cite This: https://doi.org/10.1021/jacs.3c11152

Read Online

ACCESS | Metrics & More | Article Recommendations | Supporting Information

ABSTRACT: Single-molecule localization microscopy (SMLM) is a powerful technique to achieve super-resolution imaging beyond the diffraction limit. Although various types of blinking fluorophores are currently considered for SMLM, intrinsic blinking fluorophores remain rare at the single-molecule level. Here, we report the synthesis of nanographene-based intrinsic burst-blinking fluorophores for highly versatile SMLM. We image amyloid fibrils in air and in various pH solutions without any additive and lysosome dynamics in live mammalian cells under physiological conditions. In addition, the single-molecule labeling of nascent proteins in primary sensory neurons was achieved with azide-functionalized nanographenes via click chemistry. SMLM imaging reveals higher local translation at axonal branching with unprecedented detail, while the size of translation foci remained similar throughout the entire network. These various results demonstrate the potential of nanographene-based fluorophores to drastically expand the applicability of super-resolution imaging.

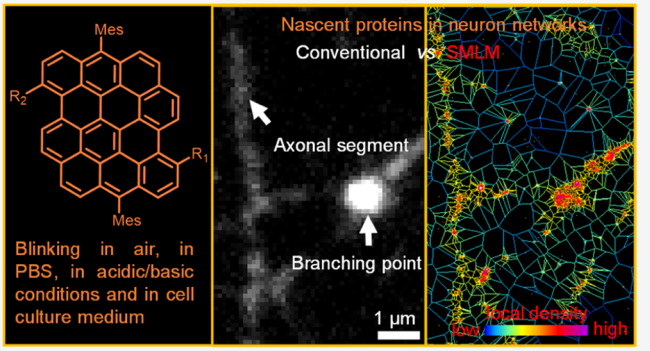

INTRODUCTION

Optical super-resolution microscopy (SRM) has emerged as a powerful tool to visualize nanostructures below the optical diffraction limit in life science[1,2] and material science[3−5]. An increasing number of single-molecule localization microscopy (SMLM) techniques are currently being developed to construct super-resolved images, including photoactivated localization microscopy (PALM),[6] stochastic optical reconstruction microscopy (STORM),[7] and second-generation optical super-resolution imaging techniques, i.e., MINFLUX,[8] SIMFLUX,[9] and MINSTED.[10] All of the SRM techniques mentioned above share the same basic principle of separating and localizing adjacent fluorophores in a diffraction-limited area by their different time-dependent behavior, known as blinking. Thus, the development of blinking fluorophores that are able to automatically switch between fluorescent and nonfluorescent states under measurement conditions is key to the improvement of SRM methods.

In addition to organic fluorophores and fluorescent proteins, different types of fluorescent nanoparticles, such as semiconductor quantum dots (QDots), carbon-based nanodots (CDots), polymer dots (PDots), and fluorescent nanodiamonds (FNDs), have been extensively investigated as blinking fluorophores with higher brightness and stability.[11,12] Among them, CDots have emerged as one of the most promising candidates with unique optical properties that are advantageous for SMLM imaging.[13−17] CDots can be very small (∼2 and 5 nm) and demonstrate the so-called burst-blinking with a long and complete off state, which are crucial to achieving SRM imaging of high-density labeling samples. Moreover, CDots display buffer-independent fluorescence properties, enabling SRM imaging under a wide range of conditions, such as imaging of materials in air, live-cell imaging under physiological conditions,[13−17] and potentially correlative light-electron microscopy (CLEM) in vacuum and hydrophobic environments.[18] Precise control of the chemical structures of CDots, which are typically heterogeneous and mostly undefined at the molecular level, however, remains challenging and constitutes a hurdle for the unambiguous elucidation of their structure−property relationship and fluorescence mechanism,[11,12,17] thus prohibiting an accurate control of their optical properties. Furthermore, conjugation of

Received: October 9, 2023
Revised: January 11, 2024
Accepted: January 11, 2024

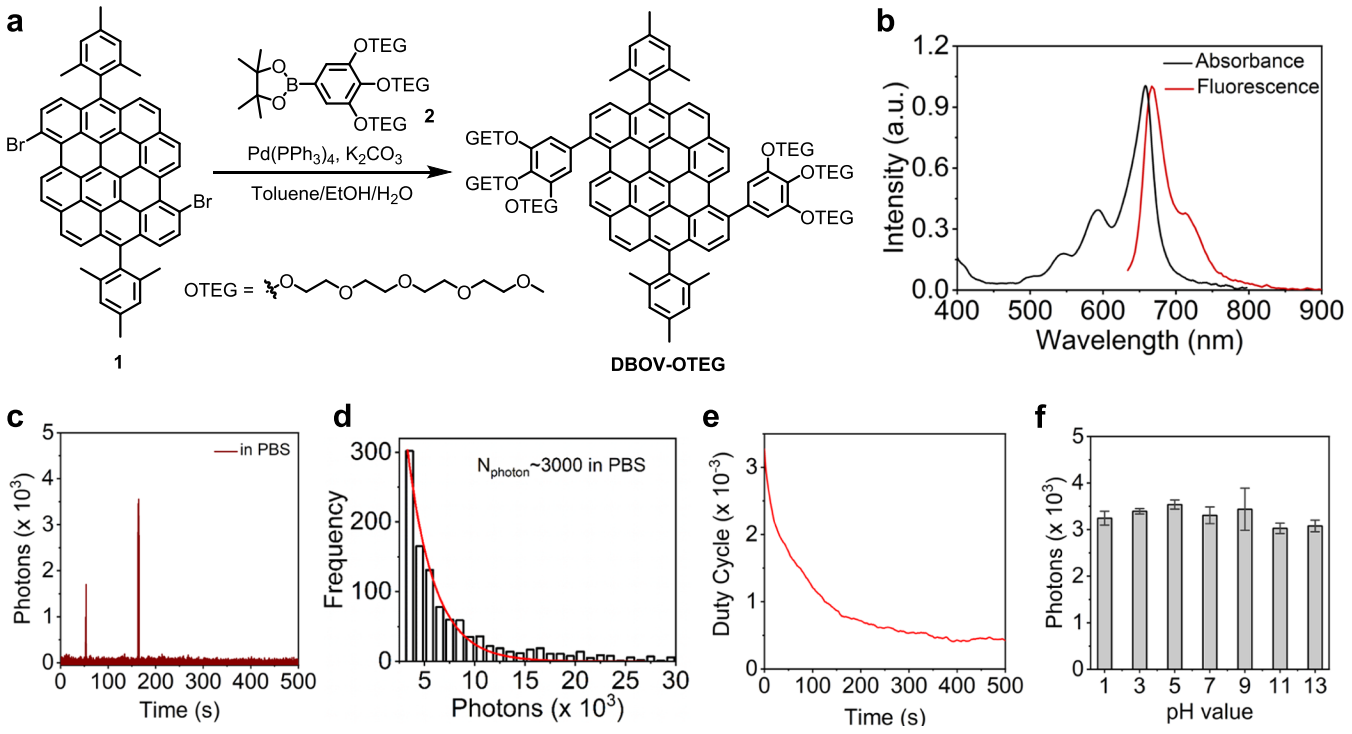

Figure 1. Synthesis and optical characterization of DBOV-OTEG. (a) Chemical structure and synthesis of DBOV-OTEG. (b) UV−vis absorption and emission spectra of DBOV-OTEG in aqueous solution. (c) Single-molecule fluorescence time trace of DBOV-OTEG in PBS solution. (d) Histogram of detected photons per switching event and single-exponential fit of DBOV-OTEG in PBS solution. (e) On−off duty cycle of DBOV-OTEG in PBS solution. (f) Detected photons per switching event of DBOV-OTEG in solutions of various pH.

CDots to biomolecules remains challenging at the single-molecule level,[11,12,17] restricting their applicability in bioimaging and biosensing of specific targets.

In this work, we report the synthesis of nanographene-based biocompatible fluorophores for super-resolution bioimaging under a wide range of imaging conditions, which have real-life applications for studying biological systems. Nanographenes, namely, large polycyclic aromatic hydrocarbons with nanoscale graphene structures, can be bottom-up synthesized with atomic precision by synthetic organic chemistry. Some nanographenes have recently been shown to have outstanding burst-blinking properties,[19,20] similar to CDots, although their application in SRM bioimaging has remained elusive.[21] Through the decoration of nanographene with hydrophilic side groups, we achieved the SMLM imaging of amyloid fibrils both in air and in various pH solutions. We also imaged lysosome dynamics in live cells under physiological conditions without any additive or irradiation with ultraviolet (UV) light. Finally, we achieved super-resolution imaging of nascent polypeptides in primary sensory neurons using *O*-propargyl-puromycin (OPP) and azide-functionalized nanographenes. Using these data, we were able to document at the single-molecule level how local translation is unevenly distributed along the axonal network, with axonal branching displaying higher levels of translational activity. These results highlight the exciting potential of functionalized nanographenes as intrinsic burst-blinking fluorophores for expanding SRM applications.

RESULTS AND DISCUSSION

Synthesis and Photophysical Properties of DBOV-OTEG. We chose dibenzo[*hi*,*st*]ovalene (DBOV) as the blinking nanographene for this study, considering its highly stability, well-resolved absorption and emission bands like those of best-performing organic dyes, and red emission with photoluminescence quantum yield of ∼80%.[19,22] To synthesize hydrophilic and biocompatible nanographenes for the bioimaging, six hydrophilic tetraethylene glycol (TEG) chains were introduced onto the DBOV core (DBOV-OTEG). DBOV-OTEG was synthesized through the Suzuki coupling of dibromo-DBOV **1**[23] and boronic ester **2** in 88% yield (Figure 1a), unambiguously characterized by nuclear magnetic resonance (NMR) spectroscopy and high-resolution mass spectrometry (HRMS) (see the Supporting Information (SI), Figures S1−S9). DBOV-OTEG could be molecularly dissolved in dimethyl sulfoxide (DMSO) as confirmed by fluorescence correlation spectroscopy (FCS) measurements[24] while the presence of small aggregations with a size of ∼10 nm was indicated in PBS (Figure S18). Since the aggregates are sufficiently small, the impact on the performed SRM imaging is negligible.

UV−visible (UV−vis) absorption and emission spectra of DBOV-OTEG were measured in aqueous solution, exhibiting maxima at 658 and 667 nm with a Stokes shift of 205 cm^{-1} and full width at half-maximum (fwhm) bandwidths of 40 and 38 nm, respectively (Figure 1b). For SMLM imaging, two key blinking properties, photon numbers (detected average photon numbers per blinking event) and on−off duty cycle (fraction of time a molecule resides in its fluorescent state), are crucial for securing high-quality images. While high photon numbers provide better localization precision, a low on−off duty cycle enables better localization accuracy with high labeling density.[25] Unlike other organic fluorophores that can only blink under optimal blinking buffer conditions or irradiation with UV light, DBOV-OTEG blinks in air and aqueous environments, such as PBS, which are often used in biological applications (Figures 1c and S19). Using single-molecule

https://doi.org/10.1021/jacs.3c11152
J. Am. Chem. Soc. XXXX, XXX, XXX−XXX

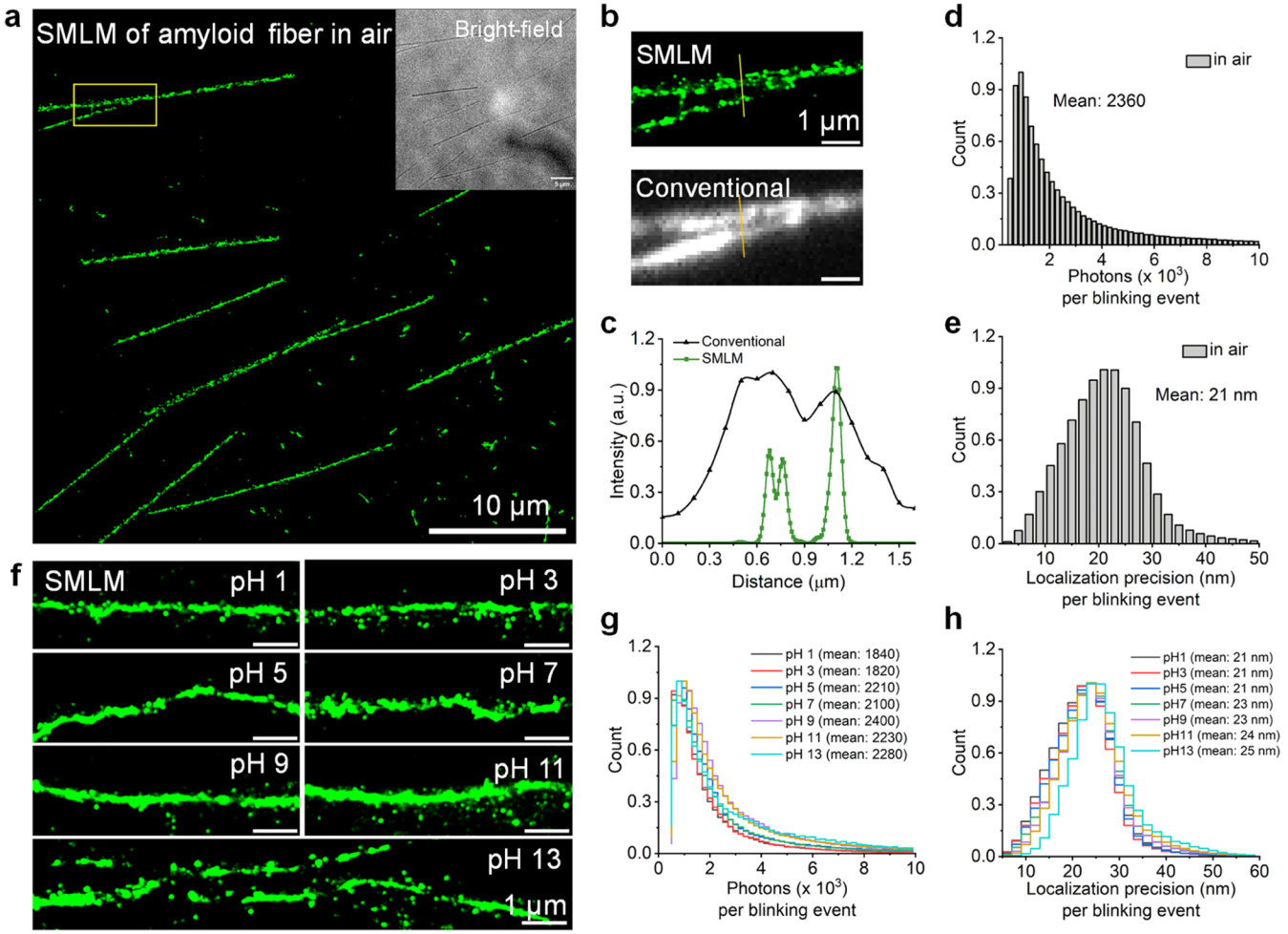

Figure 2. SMLM images of amyloid fibrils labeled with DBOV-OTEG in air and various pH solutions. (a) Reconstructed SMLM image of amyloid fibrils labeled with DBOV-OTEG from 15,000 frames in air. Inset: bright-field image of amyloid fibrils. (b) Magnification of yellow box (top) and the corresponding conventional wide-field fluorescence image (bottom). (c) Cross-line profiles of localization, corresponding regions lined in yellow in (b). (d) Distribution of photon counts per single switching event at 50 ms exposure time in air, with its average value. (e) Distribution of localization precision per single switching event at 50 ms exposure time in air, with its average value. (f) Reconstructed SMLM image of amyloid fibrils from 15,000 frames in various pH solutions. (g) Distribution of photon counts per single switching event at 50 ms exposure time in various pH solutions, with their average values. (h) Distribution of localization precision per single switching event at 50 ms exposure time in various pH solutions, with their average values.

fluorescence analysis, high photon numbers of ~3000 per blinking event (Figure 1d) and low on−off duty cycle of 10^{-3} (Figure 1e) with a blinking time of approximately 71 ms were revealed with a 642 nm laser at a laser density of 5 kW/cm^2, which are comparable to the gold standard Alexa647 under optimized special blinking buffer conditions.[19]

In addition, the blinking properties of DBOV-OTEG were measured over a wide range of pH (from pH 1 to 13) and no obvious change was observed (Figure 1f), indicating that DBOV-OTEG is pH-insensitive and can be used in various pH environments. Unlike most photoswitchable/blinking fluorophores,[26,27] DBOV-OTEG can, therefore, be used in a wide range of environments, including acidic microenvironment inside lysosomes (pH 4.5−5),[28] and can withstand sample preparation conditions for hydrogel used in expansion microscopy (pH 7) and surface functionalization of nanocarriers, e.g., for drug delivery (pH 2.7−11).[29,30]

Nanographenes for SMLM Imaging of Biomaterials in Different Environments. Amyloid fibrils, the aggregates of peptides and proteins, are essential elements in biosystems with various physiological functions.[31] To demonstrate the robustness of DBOV-OTEG under different environments, we performed SMLM imaging of amyloid fibrils (Aβ1−42) in air as well as in aqueous solutions with various pH values (Figure 2). DBOV-OTEG was conjugated to the amyloid fibrils via physisorption (see the SI for details of sample preparation). The formation of DBOV-OTEG-labeled amyloid fibrils was confirmed by bright-field image (Figure 2a, inset) and verified by co-staining of Thioflavin T (ThT). This commonly used fluorescent dye binds specifically to amyloid fibrils (Figure S20) and showed a good colocalization with DBOV-OTEG (Pearson correlation coefficient = 0.71). SMLM imaging of amyloid fibrils was then performed in air without imaging buffer or illumination with UV light and reconstructed (Figure 2a and Supporting Video 1). SMLM could resolve amyloid fibrils labeled with DBOV-OTEG with high resolution and high signal-to-noise ratio, which are difficult to distinguish in the conventional wide-field image (Figure 2b,c). Note that the SMLM image displays a clear gap (Figure 2b), whereas conventional wide-field image shows a continuous fluorescence

https://doi.org/10.1021/jacs.3c11152
J. Am. Chem. Soc. XXXX, XXX, XXX−XXX

signal, which might be due to the on/off time and high density of emitters where the SMLM analysis algorithm sorts out overlapping emitters. The image quality of SMLM is typically limited by the fluorophore's brightness (number of photons) and on−off duty cycle, together with its labeling density.[25] The high average photon number of 2360 and a remarkable average localization precision of around 20 nm per frame were achieved at 50 ms exposure time for the SMLM image reconstruction of amyloid fibrils (Figure 2d,e). Furthermore, DBOV-OTEG-labeled amyloid fibrils could be imaged in aqueous solutions of various pH values ranging from pH 1 to 13 (Figure 2f and Supporting Videos 2, 3, 4, 5, 6, 7, and 8) with photon numbers and imaging localization precision comparable to those measured in air (Figure 2g,h). These results demonstrate the versatility of DBOV-OTEG and its advantages over environment-dependent fluorophores, such as Cy5, which requires a special blinking buffer[32] and spiropyran, which is only applicable in air with UV illumination.[33]

Nanographenes for SMLM Imaging of Lysosomes in Live Cells. Live-cell super-resolution imaging is critical to studying the dynamic biological processes, avoiding the introduction of structural artifacts due to cell fixation. SMLM is capable of imaging subcellular structures/organelles in living cells with nanoscale resolution as long as their speed of movement is slow compared to the imaging speed. For live-cell SMLM imaging, the fluorophores should have low toxicity and good cell permeability in addition to optimal blinking properties.[21] We confirmed the low cytotoxicity of DBOV-OTEG using an MTT assay (Figure S21), indicating the possibility of long-term live-cell imaging. DBOV-OTEG was also able to cross the plasma membrane in U2OS cells and selectively accumulated into lysosomes after endocytosis,[21] which was confirmed by co-labeling with commercial dye LysoTracker Green (Figures 3a and S22). Lysosomes are multifunctional organelles inside cells that play crucial roles in mediating cellular metabolism and signaling,[34] but their acidic microenvironments (pH 4.5−5) prevent SMLM imaging with the typical pH-sensitive fluorophores. Notably, the pH-independent blinking properties of DBOV-OTEG enabled SMLM imaging of lysosomes in live U2OS cells in a standard cell culture medium without any additives or irradiation with UV light under physiological conditions suitable for live-cell studies (Figure 3b). The dynamic movement as well as the change in morphology of lysosomes were monitored in 30 s time intervals (Figure 3c). The time sequence super-resolution images of three subareas within one cell clearly revealed the diversity of lysosomes' movements at a nanoscale. These results highlight the advantages of DBOV-OTEG over state-of-the-art lysosome markers for SMLM,[28] achieving 1.5 times improvement in localization precision and 7 times brighter fluorescence, and a substantially enhanced accuracy in the imaging localization and lysosome dynamics analysis enabled by a lower duty cycle. The pH-independent blinking properties also potentially allow for the simultaneous targeting and imaging of multiple organelles in addition to lysosomes by the proper functionalization of other nanographenes.

Nanographenes for SMLM Imaging of Global Nascent Proteins in Neurons. Single-molecule imaging of specific targets (e.g., DNA, RNA, proteins) in complex cellular environments is very desirable and allows for unprecedented insights into biological systems. To achieve site-specific labeling of DBOV, we designed DBOV-azide with three triethylene glycol chains to ensure water solubility and an azide

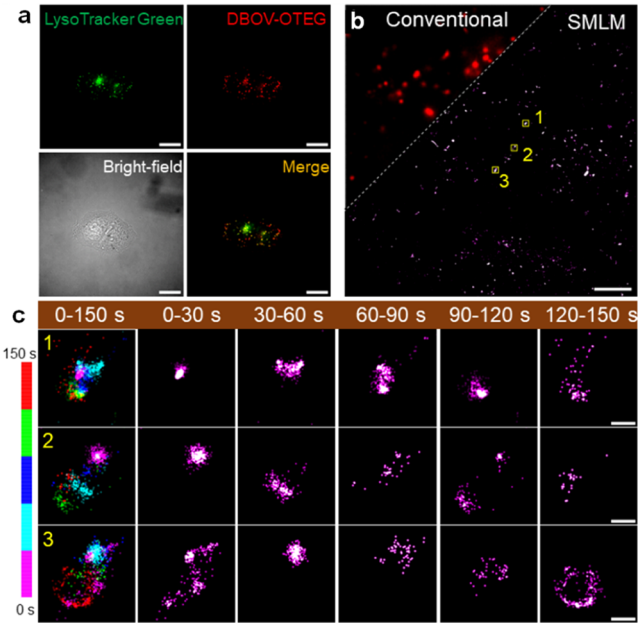

Figure 3. SMLM imaging of lysosomes with DBOV-OTEG in live U2OS cells. (a) Colocalization of DBOV-OTEG and LysoTracker Green. (b) Conventional wide-field fluorescence image of lysosomes and corresponding SMLM image of lysosomes. SMLM imaging was performed in DMEM (supplement 10% FBS) at room temperature, with 642 nm laser of 1 kW/cm^2 and 23 ms per frame. A total of 6,500 frames were acquired to reconstruct the SMLM image. (c) Time sequence super-resolution images of lysosomes at 30, 60, 90, 120, and 150 s. Three lysosomes were selected in (b), and corresponding SMLM images were reconstructed every 30 s. Scale bars: 20 μm for (a), 5 μm for (b), and 200 nm for (c).

residue suitable for the click reaction. For the synthesis of DBOV-azide, dibromo-DBOV **1** was subjected to a Suzuki coupling with two different boronic esters **3** and **4**, which statistically gave DBOV bromide **5** in 25% yield (Figure 4a). DBOV bromide **5** was then reacted with sodium azide to afford DBOV-azide in 85% yield (see the SI for details). The blinking properties of DBOV-azide were found to be similar to those of DBOV-OTEG (Figure S23).

Local protein synthesis is critical in cells with extreme morphology, particularly neurons that transport, localize, and translate mRNAs in axons during axonal development.[35,36] Local mRNAs are crucial to axonal homeostasis, allowing for fast and localized on-demand translation,[37] which enables spatial and temporal regulation of the axonal protein content,[38] and rapid response to external and/or internal stimuli. Thus, axonal protein translation plays a crucial role in axonal development and homeostasis,[39] as well as in response to stimuli[40] and nerve injury.[41] Axonal local translation has also recently risen to prominence in the context of neurodegenerative diseases.[42] To study axonal translation, biochemical labeling and imaging of nascent synthesized proteins has been performed in neurons and even in vivo in mice,[43,44] but current fluorescence imaging of nascent proteins based on confocal microscopy is restricted by the diffraction limit.[41]

To gain a deeper insight into the synthesis of nascent proteins by SMLM imaging, we labeled newly synthesized nascent polypeptides in dorsal root ganglia (DRG) sensory neurons via the incorporation of *O*-propargyl-puromycin (OPP)[45] and subsequent click reaction with DBOV-azide, based on the copper-catalyzed azide−alkyne cycloaddition

https://doi.org/10.1021/jacs.3c11152
J. Am. Chem. Soc. XXXX, XXX, XXX−XXX

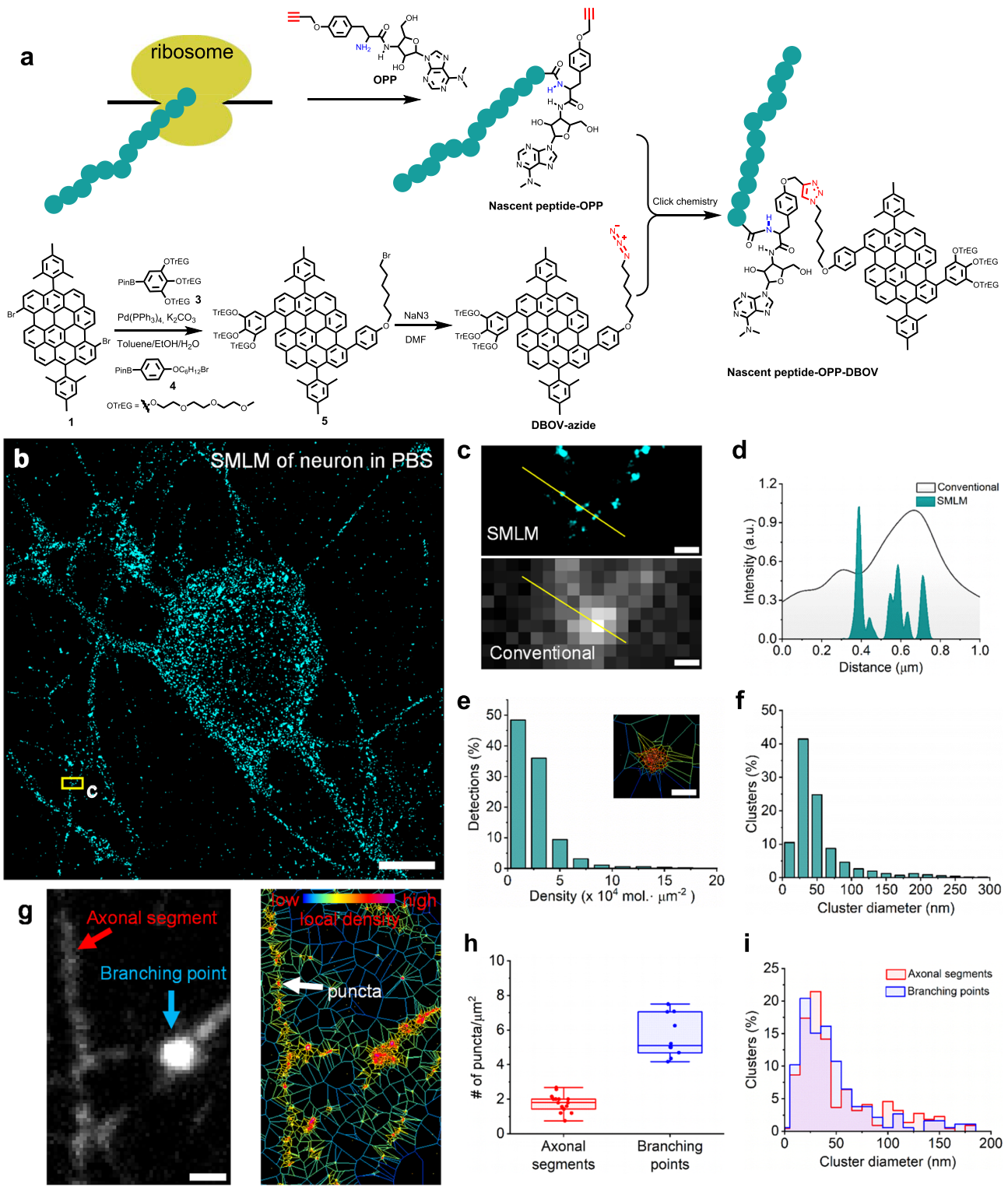

Figure 4. SMLM imaging of global nascent proteins labeled with DBOV-azide in DRG neurons. (a) Reaction schematic illustrating the synthesis of DBOV-azide and the labeling of global nascent proteins in neurons via click chemistry. (b) Reconstructed SMLM image of global nascent proteins in neurons. Imaging was performed in PBS solution. (c) Magnification of SMLM image and conventional wide-field fluorescence image for the yellow box region in (b), respectively. (d) Cross-line profiles of SMLM image and conventional wide-field fluorescence image lined in yellow in (c). (e) Distribution of the first-rank density (single-molecule localizations/μm^2) of global nascent proteins in (b). The inset shows one representative protein cluster by the Voronoi diagram segment (the red line is the estimated outline of this protein cluster). (f) Cluster size distribution for global nascent proteins in (b) (~2900 clusters). (g) Conventional wide-field fluorescence image of networks in neurons (left) and corresponding Voronoi diagram image (right) of the same position. The red arrow in (g) (left) indicates the linear axon, and the light blue arrow in (g) (left) shows the branching point (intersection between multiple axons). The white arrow in (g) (right) indicates one puncta in linear axon in reconstructed SMLM image. (h) Number of puncta (cluster)/μm^2 of axonal segments and branching points in neuron networks. (i) Cluster size distribution of axonal segments and branching points in neuron networks. Scale bar: 5 μm for (b), 1 μm for (g), 200 nm for (c), 50 nm for (e).

https://doi.org/10.1021/jacs.3c11152
J. Am. Chem. Soc. XXXX, XXX, XXX−XXX

(CuAAC) (Figure 4a).[46] Conventional wide-field imaging showed that a fluorescence signal was homogeneously distributed within the neuronal cell body and axons (Figure S24). DBOV-azide on its own did not react with other biomolecules in neurons, confirming the high selectivity of DBOV-azide to the cytosolic protein and OPP. Little labeling could also be observed when neurons were treated with anisomycin, another antibiotic that stops ribosome translation and competes with OPP prior to the treatment with OPP and the subsequent click reaction with DBOV-azide, confirming the high labeling selectivity of OPP to nascent proteins.

One of the unique advantages of SMLM over other fluorescence imaging techniques is its inherent capability to detect individual blinking events of single molecules. These events can be used to investigate, e.g., protein clustering. However, the quantification of exact protein numbers in clusters is difficult due to over- and undercounting of molecules.[47−49] SMLM imaging of nascent proteins in neurons could be achieved in PBS solution without any additives, providing super-resolved images after the reconstruction (Figure 4b and Supporting Video 9). Notably, SMLM imaging enabled us to clearly distinguish three protein clusters in a branch of an axon, which could not be resolved in its corresponding wide-field image (Figure 4c,d). To obtain a detailed map of nascent proteins in neuronal axons, we further performed the cluster analysis of all localization data based on Voronoi diagrams,[50] which could effectively segment protein clusters and calculate the local density and diameter of global nascent proteins (Figure 4e,f). The Voronoi cluster analysis revealed a mean cluster size of 50 nm in diameter with an average density of 2.5×10^4 localizations/μm^2. Although the conventional wide-field fluorescence imaging revealed that the extent of local translation at branch points is greater than the one in axonal fragments between branches (Figure 4g (left) and Figure S25), it could not provide an accurate analysis of the number of translation foci and their cluster size distribution due to the diffraction limit. In contrast, with cluster analysis of SMLM images, the average number of puncta/μm^2 at the branch points (intersection between multiple axons) could be calculated (5.1 punctas/μm^2) to be around 2.8 times that of the axonal fragments in between (1.8 punctas/μm^2, Figure 4h). On the other hand, the cluster size and density of translation foci in branching points are comparable with those puncta in axon fragments (Figures 4i and S25b). These results suggest that local translation at axonal branching is higher in terms of the number of synthesized proteins, while the sizes of translation foci remain similar throughout the network. This technology offers the opportunity to obtain a detailed map of translationally active foci in neuronal axons at a resolution that was not possible before and could help shed new light on the phenomena of axonal translation, which has broad implications on both neuronal injury and neurodegenerative diseases. Taken together, our data demonstrate the potential of DBOV-azide for studying axonal translation and other cellular metabolism.

CONCLUSIONS AND OUTLOOK

In summary, hydrophilic, biocompatible, and functionalized nanographenes were synthesized as intrinsic burst-blinking fluorophores for SRM applications, successfully deployed for amyloid fibrils imaging both in air and various pH conditions as well as live-cell imaging under physiological conditions, as a proof of concept. DBOV-OTEG displayed an excellent intrinsic blinking behavior, uncoupled from imaging buffer conditions, irradiation of UV light, and pH, making it suitable for super-resolution imaging in various applications, ranging from materials to live/fixed cell imaging, and with the potential to further explore the relationship of functions and structures of materials as well as the interaction of materials and biosystems. Furthermore, we performed SMLM imaging of global nascent proteins of neurons labeled with DBOV-azide via click chemistry in a PBS solution. The unique cluster analysis of SMLM enabled a detailed map of translationally active foci in neuronal axons at the single-molecule level. This kind of resolution has not been achieved before for the visualization of global local translation in sensory neuron axons, and it allows for much greater mechanistic insights into this biological phenomenon, which is critical to axonal physiology and pathology. Thus, this technology could help us better understand local translation in response to internal and external stimuli.

While DBOV-OTEG and DBOV-azide serve as excellent prototypes of DBOV-based blinking fluorophores, the synthetic protocol that we have established also allows for the introduction of other functional groups for various bioorthogonal reactions from the literature[51] or conjugation with nanobody or antibody used in immunofluorescence, as well as ligands for specific tags, such as SNAP-tag, Halo-tag, and Clip-tag, for directly targeting specific proteins and subcellular structures in the live-cell SMLM. We also envision that multicolor SMLM imaging using nanographenes is enabled by the readily tunable absorption and emission wavelengths by tuning the spatial extent of the aromatic structures.[19,52]

Besides the conventional SMLM imaging presented here, the intrinsic blinking properties of nanographenes may also be compatible with second-generation optical super-resolution imaging techniques, e.g., MINFLUX, SIMFLUX, and MINSTED, to achieve ultrahigh-precision localization (1−3 nm) of individual molecules. Furthermore, the robust chemical structures and intrinsic blinking properties of nanographenes may contribute to their potential applications in CLEM,[18] which combines the advantages of optical fluorescence microscopy and electron microscopy in the long term. Overall, the intrinsic burst-blinking fluorophores based on nanographenes have clear advantages and substantially expand new possibilities for super-resolution imaging in materials and life science.

ASSOCIATED CONTENT

Supporting Information

The Supporting Information is available free of charge at https://pubs.acs.org/doi/10.1021/jacs.3c11152.

SMLM imaging of DBOV-OTEG in air (Movie 1) (AVI)

SMLM imaging of DBOV-OTEG in solution of pH 1 (Movie 2) (AVI)

SMLM imaging of DBOV-OTEG in solution of pH 3 (Movie 3) (AVI)

SMLM imaging of DBOV-OTEG in solution of pH 5 (Movie 4) (AVI)

SMLM imaging of DBOV-OTEG in solution of pH 7 (Movie 5) (AVI)

SMLM imaging of DBOV-OTEG in solution of pH 9 (Movie 6) (AVI)

https://doi.org/10.1021/jacs.3c11152
J. Am. Chem. Soc. XXXX, XXX, XXX−XXX

SMLM imaging of DBOV-OTEG in solution of pH 11 (Movie 7) (AVI)
SMLM imaging of DBOV-OTEG in solution of pH 13 (Movie 8) (AVI)
SMLM imaging of DBOV-azide labeled neurons in PBS (Movie 9) (AVI)
Experimental details and data analysis; synthesis and characterizations of new compounds; and NMR spectra (PDF)

AUTHOR INFORMATION

Corresponding Authors

Mischa Bonn − *Max Planck Institute for Polymer Research, 55128 Mainz, Germany;* orcid.org/0000-0001-6851-8453; Email: bonn@mpip-mainz.mpg.de

Akimitsu Narita − *Max Planck Institute for Polymer Research, 55128 Mainz, Germany; Organic and Carbon Nanomaterials Unit, Okinawa Institute of Science and Technology Graduate University, Kunigami-gun, Okinawa 904-0495, Japan;* orcid.org/0000-0002-3625-522X; Email: akimitsu.narita@oist.jp

Xiaomin Liu − *Max Planck Institute for Polymer Research, 55128 Mainz, Germany*; Email: liuxiaomin@mpip-mainz.mpg.de

Authors

Xingfu Zhu − *Max Planck Institute for Polymer Research, 55128 Mainz, Germany*

Qiang Chen − *Max Planck Institute for Polymer Research, 55128 Mainz, Germany;* orcid.org/0000-0001-5612-1504

Hao Zhao − *Organic and Carbon Nanomaterials Unit, Okinawa Institute of Science and Technology Graduate University, Kunigami-gun, Okinawa 904-0495, Japan;* orcid.org/0000-0002-9125-617X

Qiqi Yang − *Max Planck Institute for Polymer Research, 55128 Mainz, Germany*

Goudappagouda − *Organic and Carbon Nanomaterials Unit, Okinawa Institute of Science and Technology Graduate University, Kunigami-gun, Okinawa 904-0495, Japan*

Márton Gelléri − *Institute of Molecular Biology (IMB), 55128 Mainz, Germany;* orcid.org/0000-0003-2145-838X

Sandra Ritz − *Institute of Molecular Biology (IMB), 55128 Mainz, Germany*

David Ng − *Max Planck Institute for Polymer Research, 55128 Mainz, Germany;* orcid.org/0000-0002-0302-0678

Kaloian Koynov − *Max Planck Institute for Polymer Research, 55128 Mainz, Germany;* orcid.org/0000-0002-4062-8834

Sapun H. Parekh − *Max Planck Institute for Polymer Research, 55128 Mainz, Germany*

Venkatesh Kumar Chetty − *Department of Pediatrics III, University Hospital Essen, 45147 Essen, Germany*

Basant Kumar Thakur − *Department of Pediatrics III, University Hospital Essen, 45147 Essen, Germany*

Christoph Cremer − *Max Planck Institute for Polymer Research, 55128 Mainz, Germany; Institute of Molecular Biology (IMB), 55128 Mainz, Germany*

Katharina Landfester − *Max Planck Institute for Polymer Research, 55128 Mainz, Germany;* orcid.org/0000-0001-9591-4638

Klaus Müllen − *Max Planck Institute for Polymer Research, 55128 Mainz, Germany;* orcid.org/0000-0001-6630-8786

Marco Terenzio − *Molecular Neuroscience Unit, Okinawa Institute of Science and Technology Graduate University, Kunigami-gun, Okinawa 904-0495, Japan*

Complete contact information is available at: https://pubs.acs.org/10.1021/jacs.3c11152

Author Contributions

#X.Z., Q.C., and H.Z. contributed equally to this work.

Funding

Open access funded by Max Planck Society.

Notes

The authors declare the following competing financial interest(s): X. Liu, A. Narita, Q. Chen, S. Parekh, C. Cremer, K. Land-fester, K. Mllen, and M. Bonn are listed as inventors on a patent (PCT/EP2019/076496, WO2020070085) and Q. Chen, A. Narita, K. Mllen, S. Parken, M. Bonn and X. Liu are listed as inventors on a patent (PCT/EP2019/076497, WO 2020070086) related to the work presented in this manuscript. All other authors have nothing to disclose.

ACKNOWLEDGMENTS

This work was financially supported by the Max Planck Society, the Okinawa Institute of Science and Technology Graduate University, the ANR-DFG NLE Grant GRANAO by DFG 431450789, JSPS KAKENHI Grant No. JP21KK0091 and JP23KF0075, and the Microscopy Core Facility at IMB for use of microscopes. X.Z. and Q.Y. acknowledge support from the Chinese Scholarship Council (CSC). H.Z. and G. appreciate the JSPS Postdoctral Fellowships for Research in Japan. The authors thank Shih-Ya Chen, Yanfei Li, Jingjing Yu, Hilmar Strickfaden, Kaifa Xin, Yu-Liang Tsai, Seah-Ling Kuan, Bellinda Lantzberg, and Martin Möckel for some test experiments and insightful discussions.

REFERENCES

(1) Sahl, S. J.; Hell, S. W.; Jakobs, S. Fluorescence Nanoscopy in Cell Biology. *Nat. Rev. Mol. Cell Biol.* **2017**, *18* (11), 685−701.

(2) Schermelleh, L.; Ferrand, A.; Huser, T.; Eggeling, C.; Sauer, M.; Biehlmaier, O.; Drummen, G. P. C. Super-Resolution Microscopy Demystified. *Nat. Cell Biol.* **2019**, *21* (1), 72−84.

(3) Pujals, S.; Feiner-Gracia, N.; Delcanale, P.; Voets, I.; Albertazzi, L. Super-Resolution Microscopy as a Powerful Tool to Study Complex Synthetic Materials. *Nat. Rev. Chem.* **2019**, *3* (2), 68−84.

(4) Wöll, D.; Flors, C. Super-Resolution Fluorescence Imaging for Materials Science. *Small Methods* **2017**, *1* (10), No. 1700191.

(5) Chen, T.; Dong, B.; Chen, K.; Zhao, F.; Cheng, X.; Ma, C.; Lee, S.; Zhang, P.; Kang, S. H.; Ha, J. W.; Xu, W.; Fang, N. Optical Super-Resolution Imaging of Surface Reactions. *Chem. Rev.* **2017**, *117* (11), 7510−7537.

(6) Betzig, E.; Patterson, G. H.; Sougrat, R.; Lindwasser, O. W.; Olenych, S.; Bonifacino, J. S.; Davidson, M. W.; Lippincott-Schwartz, J.; Hess, H. F. Imaging Intracellular Fluorescent Proteins at Nanometer Resolution. *Science* **2006**, *313* (5793), 1642−1645.

(7) Rust, M. J.; Bates, M.; Zhuang, X. Sub-Diffraction-Limit Imaging by Stochastic Optical Reconstruction Microscopy (STORM). *Nat. Methods* **2006**, *3* (10), 793−795.

(8) Balzarotti, F.; Eilers, Y.; Gwosch, K. C.; Gynnå, A. H.; Westphal, V.; Stefani, F. D.; Elf, J.; Hell, S. W. Nanometer Resolution Imaging and Tracking of Fluorescent Molecules with Minimal Photon Fluxes. *Science* **2017**, *355* (6325), 606−612.

(9) Cnossen, J.; Hinsdale, T.; Thorsen, R. Ø.; Siemons, M.; Schueder, F.; Jungmann, R.; Smith, C. S.; Rieger, B.; Stallinga, S. Localization Microscopy at Doubled Precision with Patterned Illumination. *Nat. Methods* **2020**, *17* (1), 59−63.
(10) Weber, M.; Leutenegger, M.; Stoldt, S.; Jakobs, S.; Mihaila, T. S.; Butkevich, A. N.; Hell, S. W. MINSTED Fluorescence Localization and Nanoscopy. *Nat. Photonics* **2021**, *15* (5), 361−366.
(11) Li, W.; Schierle, G. S. K.; Lei, B.; Liu, Y.; Kaminski, C. F. Fluorescent Nanoparticles for Super-Resolution Imaging. *Chem. Rev.* **2022**, *122* (15), 12495−12543.
(12) Jin, D.; Xi, P.; Wang, B.; Zhang, L.; Enderlein, J.; Van Oijen, A. M. Nanoparticles for Super-Resolution Microscopy and Single-Molecule Tracking. *Nat. Methods* **2018**, *15* (6), 415−423.
(13) He, H.; Liu, X.; Li, S.; Wang, X.; Wang, Q.; Li, J.; Wang, J.; Ren, H.; Ge, B.; Wang, S.; Zhang, X.-D.; Huang, F. High-Density Super-Resolution Localization Imaging with Blinking Carbon Dots. *Anal. Chem.* **2017**, *89* (21), 11831−11838.
(14) He, H.; Chen, X.; Feng, Z.; Liu, L.; Wang, Q.; Bi, S. Nanoscopic Imaging of Nucleolar Stress Enabled by Protein-Mimicking Carbon Dots. *Nano Lett.* **2021**, *21* (13), 5689−5696.
(15) Mao, J.; Xue, M.; Guan, X.; Wang, Q.; Wang, Z.; Qin, G.; He, H. Near-Infrared Blinking Carbon Dots Designed for Quantitative Nanoscopy. *Nano Lett.* **2023**, *23* (1), 124−131.
(16) Ye, Z.; Wei, L.; Geng, X.; Wang, X.; Li, Z.; Xiao, L. Mitochondrion-Specific Blinking Fluorescent Bioprobe for Nanoscopic Monitoring of Mitophagy. *ACS Nano* **2019**, *13* (10), 11593−11602.
(17) Sun, X.; Mosleh, N. Fluorescent Carbon Dots for Super-Resolution Microscopy. *Materials* **2023**, *16* (3), No. 890.
(18) Sochacki, K. A.; Shtengel, G.; Van Engelenburg, S. B.; Hess, H. F.; Taraska, J. W. Correlative Super-Resolution Fluorescence and Metal-Replica Transmission Electron Microscopy. *Nat. Methods* **2014**, *11* (3), 305−308.
(19) Liu, X.; Chen, S. Y.; Chen, Q.; Yao, X.; Gelléri, M.; Ritz, S.; Kumar, S.; Cremer, C.; Landfester, K.; Müllen, K.; Parekh, S. H.; Narita, A.; Bonn, M. Nanographenes: Ultrastable, Switchable, and Bright Probes for Super-Resolution Microscopy. *Angew. Chem., Int. Ed.* **2020**, *59* (1), 496−502.
(20) Jin, E.; Yang, Q.; Ju, C. W.; Chen, Q.; Landfester, K.; Bonn, M.; Müllen, K.; Liu, X.; Narita, A. A Highly Luminescent Nitrogen-Doped Nanographene as an Acid- And Metal-Sensitive Fluorophore for Optical Imaging. *J. Am. Chem. Soc.* **2021**, *143* (27), 10403−10412.
(21) Lin, H. A.; Sato, Y.; Segawa, Y.; Nishihara, T.; Sugimoto, N.; Scott, L. T.; Higashiyama, T.; Itami, K. A Water-Soluble Warped Nanographene: Synthesis and Applications for Photoinduced Cell Death. *Angew. Chem., Int. Ed.* **2018**, *57* (11), 2874−2878.
(22) Chen, Q.; Thoms, S.; Stöttinger, S.; Schollmeyer, D.; Müllen, K.; Narita, A.; Basché, T. Dibenzo[Hi, St]Ovalene as Highly Luminescent Nanographene: Efficient Synthesis via Photochemical Cyclodehydroiodination, Optoelectronic Properties, and Single-Molecule Spectroscopy. *J. Am. Chem. Soc.* **2019**, *141* (41), 16439−16449.
(23) Chen, Q.; Wang, D.; Baumgarten, M.; Schollmeyer, D.; Müllen, K.; Narita, A. Regioselective Bromination and Functionalization of Dibenzo[Hi,St]Ovalene as Highly Luminescent Nanographene with Zigzag Edges. *Chem. - Asian J.* **2019**, *14* (10), 1703−1707.
(24) Schmitt, S.; Nuhn, L.; Barz, M.; Butt, H. J.; Koynov, K. Shining Light on Polymeric Drug Nanocarriers with Fluorescence Correlation Spectroscopy. *Macromol. Rapid Commun.* **2022**, *43* (12), No. 2100892.
(25) Dempsey, G. T.; Vaughan, J. C.; Chen, K. H.; Bates, M.; Zhuang, X. Evaluation of Fluorophores for Optimal Performance in Localization-Based Super-Resolution Imaging. *Nat. Methods* **2011**, *8* (12), 1027−1040.
(26) Szczurek, A.; Klewes, L.; Xing, J.; Gourram, A.; Birk, U.; Knecht, H.; Dobrucki, J. W.; Mai, S.; Cremer, C. Imaging Chromatin Nanostructure with Binding-Activated Localization Microscopy Based on DNA Structure Fluctuations. *Nucleic Acids Res.* **2017**, *45* (8), No. e56.
(27) Uno, S. N.; Kamiya, M.; Yoshihara, T.; Sugawara, K.; Okabe, K.; Tarhan, M. C.; Fujita, H.; Funatsu, T.; Okada, Y.; Tobita, S.; Urano, Y. A Spontaneously Blinking Fluorophore Based on Intramolecular Spirocyclization for Live-Cell Super-Resolution Imaging. *Nat. Chem.* **2014**, *6* (8), 681−689.
(28) Qiao, Q.; Liu, W.; Chen, J.; Wu, X.; Deng, F.; Fang, X.; Xu, N.; Zhou, W.; Wu, S.; Yin, W.; Liu, X.; Xu, Z. An Acid-Regulated Self-Blinking Fluorescent Probe for Resolving Whole-Cell Lysosomes with Long-Term Nanoscopy. *Angew. Chem., Int. Ed.* **2022**, *61* (21), No. e202202961.
(29) Zwettler, F. U.; Reinhard, S.; Gambarotto, D.; Bell, T. D. M.; Hamel, V.; Guichard, P.; Sauer, M. Molecular Resolution Imaging by Post-Labeling Expansion Single-Molecule Localization Microscopy (Ex-SMLM). *Nat. Commun.* **2020**, *11* (1), No. 3388, DOI: 10.1038/s41467-020-17086-8.
(30) Tonigold, M.; Simon, J.; Estupiñán, D.; Kokkinopoulou, M.; Reinholz, J.; Kintzel, U.; Kaltbeitzel, A.; Renz, P.; Domogalla, M. P.; Steinbrink, K.; Lieberwirth, I.; Crespy, D.; Landfester, K.; Mailänder, V. Pre-Adsorption of Antibodies Enables Targeting of Nanocarriers despite a Biomolecular Corona. *Nat. Nanotechnol.* **2018**, *13* (9), 862−869.
(31) Knowles, T. P. J.; Vendruscolo, M.; Dobson, C. M. The Amyloid State and Its Association with Protein Misfolding Diseases. *Nat. Rev. Mol. Cell Biol.* **2014**, *15* (6), 384−396.
(32) Albertazzi, L.; Van Der Zwaag, D.; Leenders, C. M. A.; Fitzner, R.; Van Der Hofstad, R. W.; Meijer, E. W. Probing Exchange Pathways in One-Dimensional Aggregates with Super-Resolution Microscopy. *Science* **2014**, *344* (6183), 491−495.
(33) Yan, J.; Zhao, L.; Li, C.; Hu, Z.; Zhang, G.; Chen, Z.-Q.; Chen, T.; Huang, Z.; Zhu, J.; Zhu, M. Optical Nanoimaging for Block Copolymer Self-Assembly. *J. Am. Chem. Soc.* **2015**, *137* (7), 2436−2439.
(34) Lawrence, R. E.; Zoncu, R. The Lysosome as a Cellular Centre for Signalling, Metabolism and Quality Control. *Nat. Cell Biol.* **2019**, *21* (2), 133−142.
(35) Glock, C.; Heumüller, M.; Schuman, E. M. MRNA Transport & Local Translation in Neurons. *Curr. Opin. Neurobiol.* **2017**, *45*, 169−177.
(36) Rangaraju, V.; tom Dieck, S.; Schuman, E. M. Local Translation in Neuronal Compartments: How Local Is Local? *EMBO Rep.* **2017**, *18* (5), 693−711.
(37) Vargas, J. N. S.; Sleigh, J. N.; Schiavo, G. Coupling Axonal MRNA Transport and Local Translation to Organelle Maintenance and Function. *Curr. Opin. Cell Biol.* **2022**, *74*, 97−103.
(38) Jung, H.; Gkogkas, C. G.; Sonenberg, N.; Holt, C. E. Remote Control of Gene Function by Local Translation. *Cell* **2014**, *157* (1), 26−40.
(39) Batista, A. F. R.; Martínez, J. C.; Hengst, U. Intra-Axonal Synthesis of SNAP25 Is Required for the Formation of Presynaptic Terminals. *Cell Rep.* **2017**, *20* (13), 3085−3098.
(40) Graber, T. E.; Hébert-Seropian, S.; Khoutorsky, A.; David, A.; Yewdell, J. W.; Lacaille, J. C.; Sossin, W. S. Reactivation of Stalled Polyribosomes in Synaptic Plasticity. *Proc. Natl. Acad. Sci. U.S.A.* **2013**, *110* (40), 16205−16210.
(41) Terenzio, M.; Koley, S.; Samra, N.; Rishal, I.; Zhao, Q.; Sahoo, P. K.; Urisman, A.; Marvaldi, L.; Oses-prieto, J. A.; Forester, C.; Gomes, C.; Kalinski, A. L.; Pizio, A.; Di; Doron-mandel, E.; Perry, R. B.; Koppel, I.; Twiss, J. L.; Burlingame, A. L.; Fainzilber, M. Locally Translated MTOR Controls Axonal Local Translation in Nerve Injury. *Science* **2018**, *359* (6382), 1416−1421.
(42) Nagano, S.; Araki, T. Axonal Transport and Local Translation of MRNA in Neurodegenerative Diseases. *Front. Mol. Neurosci.* **2021**, *14*, No. 697973.
(43) Holt, C. E.; Martin, K. C.; Schuman, E. M. Local Translation in Neurons: Visualization and Function. *Nat. Struct. Mol. Biol.* **2019**, *26* (7), 557−566.
(44) Koppel, I.; Fainzilber, M. Omics Approaches for Subcellular Translation Studies. *Mol. Omics* **2018**, *14* (6), 380−388.

https://doi.org/10.1021/jacs.3c11152
J. Am. Chem. Soc. XXXX, XXX, XXX−XXX

(45) Liu, J.; Xu, Y.; Stoleru, D.; Salic, A. Imaging Protein Synthesis in Cells and Tissues with an Alkyne Analog of Puromycin. *Proc. Natl. Acad. Sci. U.S.A.* **2012**, *109* (2), 413−418.
(46) Hein, J. E.; Fokin, V. V. Copper-Catalyzed Azide-Alkyne Cycloaddition (CuAAC) and beyond: New Reactivity of Copper(i) Acetylides. *Chem. Soc. Rev.* **2010**, *39* (4), 1302−1315.
(47) Baumgart, F.; Arnold, A. M.; Leskovar, K.; Staszek, K.; Fölser, M.; Weghuber, J.; Stockinger, H.; Schütz, G. J. Varying Label Density Allows Artifact-Free Analysis of Membrane-Protein Nanoclusters. *Nat. Methods* **2016**, *13* (8), 661−664.
(48) Annibale, P.; Scarselli, M.; Kodiyan, A.; Radenovic, A. Photoactivatable Fluorescent Protein MEos2 Displays Repeated Photoactivation after a Long-Lived Dark State in the Red Photo-converted Form. *J. Phys. Chem. Lett.* **2010**, *1* (9), 1506−1510.
(49) Sengupta, P.; Jovanovic-Talisman, T.; Skoko, D.; Renz, M.; Veatch, S. L.; Lippincott-Schwartz, J. Probing Protein Heterogeneity in the Plasma Membrane Using PALM and Pair Correlation Analysis. *Nat. Methods* **2011**, *8* (11), 969−975.
(50) Levet, F.; Hosy, E.; Kechkar, A.; Butler, C.; Beghin, A.; Choquet, D.; Sibarita, J. SR-Tesseler: A Method to Segment and Quantify Localization-Based Super-Resolution Microscopy Data. *Nat. Methods* **2015**, *12* (11), 1065−1071.
(51) Jewett, J. C.; Bertozzi, C. R. Cu-Free Click Cycloaddition Reactions in Chemical Biology. *Chem. Soc. Rev.* **2010**, *39* (4), 1272−1279.
(52) Gu, Y.; Wu, X.; Gopalakrishna, T. Y.; Phan, H.; Wu, J. Graphene-like Molecules with Four Zigzag Edges. *Angew. Chem., Int. Ed.* **2018**, *57* (22), 6541−6545.

https://doi.org/10.1021/jacs.3c11152
J. Am. Chem. Soc. XXXX, XXX, XXX−XXX

ACCOUNTS of chemical research

pubs.acs.org/accounts Article

Solvent-Free Organic Liquids: An Efficient Fluid Matrix for Unexplored Functional Hybrid Materials

Vivek Chandrakant Wakchaure, Goudappagouda Channareddy, and Sukumaran Santhosh Babu*

Cite This: *Acc. Chem. Res.* 2024, 57, 670−684 Read Online

ACCESS | Metrics & More | Article Recommendations

CONSPECTUS: The invention of solvent-free organic liquids (SOLs) was serendipitous. However, the curiosity-driven research in the later stage delivered new soft materials with exciting optical, and optoelectronic properties along with appealing physical characteristics suitable for the futuristic applications. A slight change in the molecular design resulted in a drastic change in the physical state of molecules demonstrating monomer-like features in the bulk. The basic idea of core isolation has been successful in delivering new SOLs with attractive functional properties. The unique fluid matrix associated with SOLs offers a tremendous opportunity for making hybrid materials by simple mixing. The chance to study the fundamentally important electron transfer, energy transfer, charge transfer interactions, triplet-state emissions, and even detailed NMR experiments in the solvent-free neat state is the major attraction of SOLs. Usually, solvents and their polarity control such molecular properties, and in the case of SOLs, it avoids the use of solvents to study such fundamentally important properties. Besides, SOLs protect the triplet emitters and excited state processes involving triplet states from quenchers and make the analysis possible under ambient conditions.

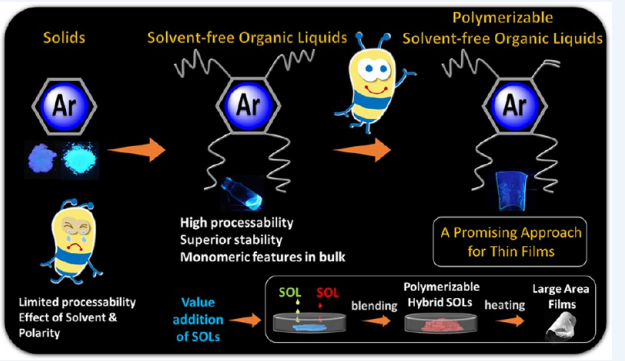

Our effort in this direction was focused on tuning the ground and excited state properties by transforming conventional organic molecules to SOLs and further value addition by preparing the hybrid SOLs. We developed a series of hybrid SOLs, exploring room-temperature phosphorescence, thermally activated delayed fluorescence, charge or energy transfer between donor and acceptor SOLs, selective explosive sensing, etc. A slight variation in the chemical structure or optoelectronic properties of the individual components imparted exciting optical features for the hybrid SOLs. It includes nonemissive charge transfer, tunable emission exciplex, room temperature phosphorescence, and thermally activated delayed fluorescence SOLs. The liquid matrix of donor SOLs accommodated varying amounts of acceptor SOLs to tune the ground and excited state features. In all examples of donor−acceptor-based hybrid SOLs, even a low amount of acceptor, such as a donor−acceptor ratio of 1000:1, can cause pronounced optical properties. Hence, the evaluation of the optical properties of SOLs, especially, in the absence of solvents is so special that it avoids the interference of solvent molecules. Still, the major drawback of SOLs remains unsolved until we report polymerizable SOLs. Although a large variety of SOLs have been reported in the literature, the long-lasting problem of surface stickiness of SOLs was resolved by polymerizable SOLs. It enabled the development of flexible, foldable, and stretchable large-area luminescent films suitable for lighting and display devices. In this Account, we summarize our work on SOLs, hybrid SOLs, polymerizable SOLs, and the application of SOLs in selective sensing of explosives. Finally, an outlook on the feasibility of luminescent polymerizable SOLs in futuristic applications is provided.

KEY REFERENCES

- Goudappagouda; Manthanath, A.; Wakchaure, V. C.; Ranjeesh, K. C.; Das, T.; Vanka, K.; Nakanishi, T.; Babu, S. S. Paintable Room Temperature Phosphorescent Liquid Formulations of Alkylated Bromonaphthalimide. *Angew. Chem., Int. Ed.* **2019**, *58*, 2284−2288.[1] This is the first report based on room-temperature phosphorescence of a solvent-free organic liquid phosphor in air.
- Wakchaure, V. C.; Goudappagouda; Das, T.; Ravindranathan, S.; Babu, S. S. An Excimer to Exciplex Transition through Realization of Donor−Acceptor Interaction in Luminescent Solvent-free Liquid. *Nanoscale* **2021**, *13*, 10780−10784.[2] Donor−acceptor based

Received: October 25, 2023
Revised: January 9, 2024
Accepted: January 19, 2024
Published: February 13, 2024

https://doi.org/10.1021/acs.accounts.3c00670
Acc. Chem. Res. 2024, 57, 670−684

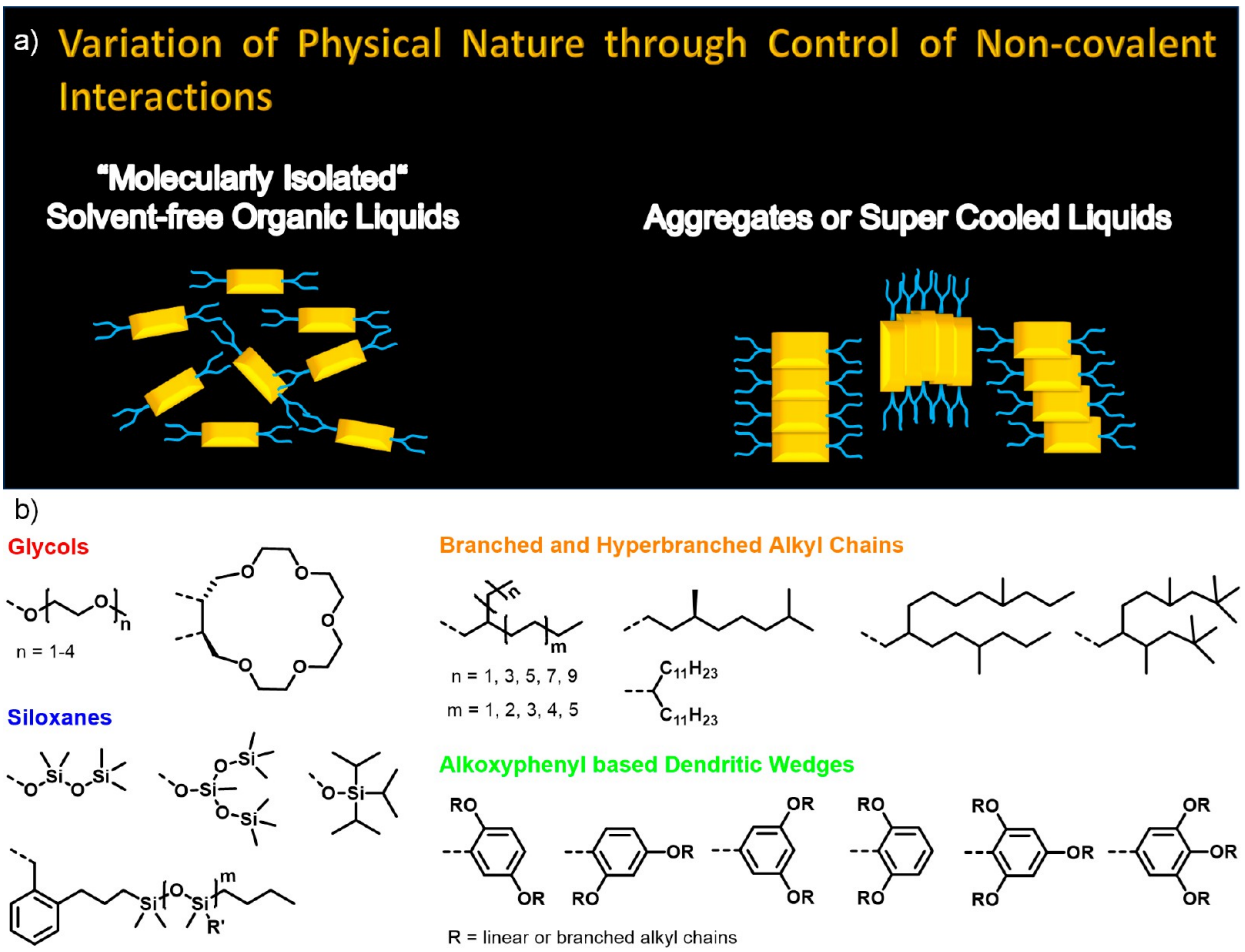

Figure 1. (a) Schematic of the molecularly isolated solvent-free organic liquids and aggregated Supercooled Liquids. (b) Chemical structure of the representative examples of types of glycol, siloxane, or alkyl chains used to achieve stable SOLs.

luminescent "exciplex liquid" efficient in selective sensing application.

- Nidhankar, A. D.; Goudappagouda; Kothavade, P. A.; Dongre, S. D.; Veer, S. D.; Dash, S. R.; Rajeev, K.; Unni, K. N. N.; Shanmuganathan, K.; Babu, S. S. Thermally Activated Delayed Fluorescent Solvent-free Organic Liquid Hybrids for Tunable Emission Applications. *Chem.—Asian J.* **2023**, *18*, e202300276.[3] SOLs exhibiting cyan to red thermally activated delayed fluorescence with luminescence quantum yields up to 80% and lifetimes between 10 to 45 μs.
- Wakcahure, V. C.; Veer, S. D.; Nidhankar, A. D.; Kumar, V.; Narayanan, A.; Babu, S. S. Polymerizable Solvent-free Organic Liquids: A New Approach for Large Area Flexible and Foldable Luminescent Films. *Angew. Chem., Int. Ed.* **2023**, *62*, e202307381.[4] Here we demonstrated polymerizable SOLs. Thermal polymerization of SOLs delivered stable, nonsticky, flexible, foldable, and free-standing large-area films with reasonably high quantum yield.

1. INTRODUCTION

In recent years, room-temperature (RT) solvent-free organic liquids (SOLs) gathered wide attention as a new soft matter.[5−9] The most efficient way to generate SOLs is to regulate intermolecular interactions of functional chromophores by attaching low-viscosity, flexible linear/branched side chains as an integral part of the molecule.[10] An efficient wrapping by the bulky side chains around the π-core controls the physical state of the molecules.[11] The fine-tuning of functional properties by a delicate balance of intermolecular interactions such as interchromophoric $\pi-\pi$ interactions and the interchain van der Waals (vdW) forces have realized a new soft material called SOLs (Figure 1a). Otherwise, it will result in supercooled liquids that transform into solid aggregates upon storage due to the strong $\pi-\pi$ stacking between the aromatic units and vdW interaction between the chains (Figure 1a).[12] In the development course, SOLs composed of various side chains such as branched/hyper-branched alkyl/glycol/siloxane chains have been reported (Figure 1b).[13−16] A general selection rule for components of SOLs is not applicable due to a limited structural correlation between the π and alkyl parts of SOLs, and the choice of the alkyl chains mostly varies from case to case. At the moment, only the trial-and-error method is valid for selecting the alkyl part. The chain length and branching, use of dendritic wedges to incorporate more chains, etc. are taken into consideration after selecting the π-core. Literature reports show that among a series of different π-cores, SOLs with both short and long-branched chains solidify over time. Hence retaining a stable liquid feature at RT depends on various facts such as the type of π-core and alkyl chains and the ratio between them, planarity of the π-core, symmetry of the molecule, etc. In short, a slight enhancement in $\pi-\pi$ or vdW interactions in SOLs results in the aggregation of molecules and subsequent loss of the liquid feature. However, an overview of the selection of the

https://doi.org/10.1021/acs.accounts.3c00670
Acc. Chem. Res. 2024, 57, 670−684

chains is as follows. SOLs of small planar π-conjugated molecules can make use of glycol, siloxanes, and small branched alkyl chains. As the size of the π-unit increases long branched alkyl chains and alkoxy phenyl-based dendritic wedges can be used. For instance, molecules with a high tendency for aggregation such as fullerenes or dyes (diketopyrrolopyrrole, porphyrin) dendritic alkyl wedges are preferred. Figure 1b displays the representative examples of various types of chains used to achieve stable SOLs. It is expected that in the future, more comprehensive investigations coupled with theoretical modeling will enable the molecular design of SOLs.

The physical characteristics of SOLs can be measured by various characterization methods such as rheology, differential scanning calorimetry (DSC), X-ray diffraction (XRD), etc. For SOLs, the rheology experiments demonstrate that the loss modulus G'' surpasses the storage modulus G' across the range of angular frequencies, ω = 0.1−100 rad s^{-1}.[17] DSC helps to determine the glass transition temperature (T_g) of a molecule, which signifies the temperature at which the material transform from a rigid, glass-like state to a more fluid, viscous state. T_g of SOLs always remains below RT, and the lower the T_g, the better the fluidity of SOLs.[18] The amorphous state of SOLs evident from XRD analysis is due to the presence of bulky side chains surrounding the chromophore, preventing $\pi-\pi$ stacking.[17]

SOLs offer a host of advantages beyond their straightforward preparation, positioning them as a compelling choice in the realm of organic materials. One of their notable merits lies in enhanced stability, attributed to the bulky side chains enveloping the chromophore. This protective shield mitigates photoinduced side reactions, air oxidation, and other quenching processes.[19] Additionally, their fluidic nature enhances processability, enabling SOLs to adapt to diverse shapes under bending, twisting, and stretching conditions. The liquid behavior of SOLs also makes them accommodating hosts for various useful dopants. Moreover, the fluid matrix opens new avenues for investigating molecular-level interactions in bulk without the need for solvents. SOLs facilitate the characterization of functional properties in bulk, ushering in a transition from solution-based analyses to solvent-free conditions, thus avoids the influence of solvents and their polarity. Furthermore, the fluid matrix fosters efficient donor−acceptor interactions, facilitating charge and energy transfers (CT and ET). Finally, their free-flowing nature makes SOLs a versatile, paintable material for coating on various substrates such as glass, wood, paper, and more, enabling the creation of continuous, large-area thin films.

Liquefaction of conventional photoluminescent organic molecules has proven to be an efficient method to minimize concentration caused quenching originating from $\pi-\pi$ stacking and thereby offers an intense monomer-like emission in the bulk liquid.[20] Hence most of the reported SOLs were exploited as luminescent organic liquids with reasonably high luminescence quantum yield (QY) in the solvent-free state. These emissive liquids have found substantial use in low-cost, low-energy, flexible light-emitting devices.[21] In most solution-processable devices, color stability and purity are unattainable to a large extent as solvent evaporation after film casting often leads to molecular assemblies and random aggregates.[22] In this context, luminescent SOLs with stable emission and processability offer new opportunities.[23,24] Many attractive SOLs of tetrazine, naphthalene, anthracene, pyrene, carbazole, and tetraphenylethene (TPE), exhibited reasonably high QY and stability. The mono and disubstituted tetrazine derivatives remain liquid at least down to −60 °C and display very low viscosities (28 mPa·s for mono, 58 mPa·s for di)[25] and are used for a unique application in determining local friction measurements.[26] Carbazole is one of the strongest candidates in this category and many carbazole-based SOLs have been investigated for their hole mobility and light-emitting features in the liquid state.[27−30] In 2018, Mizuno and co-workers reported a wide-energy-gap naphthalene-based semiconductor as a host for liquid deep-blue OLEDs.[31] Circularly polarized luminescence of chiral chain appended naphthalene[32] and siloxybinaphthyl SOLs[33] are also reported. Besides, a full-color luminescence tuning was achieved by dye doping to 9,10-diphenyl anthracene SOLs.[17] Adachi and co-workers fabricated a degradation-free liquid OLED by taking advantage of the capillary action of the pyrene liquid emitter.[34] In the case of tetraphenylethenes (TPEs), the viscous nature favored the restriction of the molecular motion, and the isolated TPE molecule was found significantly responsible for the enhanced photoluminescence compared to the solid TPE derivatives.[35]

One of the widely exploited features of SOLs is the availability of the fluid matrix and its use for blending with other suitable candidates to develop new hybrid functional materials, which are otherwise not possible to prepare using the corresponding solid counterparts. The blending experiments in the solid state mostly failed due to the noncompatibility of the dopants with the host material. Hence a rational choice on the compatibility of fluid matrix and dopant is highly required. In SOLs, the fluid matrix enables doping with a variety of external dopants. However, the crystalline dopants limited the shelf life and performance of the hybrid liquids due to phase separation. SOLs provide a low viscous fluid matrix suitable for doping with other functional components through simple physical mixing to develop new hybrid materials. Without altering the liquid nature of SOLs, a tiny amount of dopants adds extra functionality to this hybrid liquid. Even multicomponent hybrid liquids can be developed with these SOLs and provide an added advantage to creating various functional materials. A careful selection of dopants and reasonably controlling the doping ratio will deliver hybrid liquids for different applications.[36] Compared to conventional functional organic materials, SOLs are known for their many unique molecular properties and the recent developments in SOLs are quite promising; however, the shortcomings have to be corrected.

This account discusses the salient features of SOLs as an efficient fluid matrix to develop hybrid materials with attractive features. Moreover, it will provide an overview of the most recent advancements in this field, with a particular focus on the significant contributions made by our team. To be more precise, this review comprises five sections: charge transfer SOLs (CT-SOLs); exciplex SOLs (E-SOLs); room temperature phosphorescence SOLs (RTP-SOLs); thermally activated delayed fluorescence SOLs (TADF-SOLs); polymerizable SOLs (P-SOLs). Furthermore, potential avenues for future research on SOLs are addressed in the concluding section.

1.1. Charge Transfer Solvent-free Organic Liquids (CT-SOLs)

Delving into the realm of optoelectronically active materials reveals that donor−acceptor (D−A) assemblies offer distinct advantages.[37] Within this context, the utilization of charge transfer (CT) interactions emerges as a sophisticated approach for constructing these assemblies.[38] Among various D−A combinations explored, the pair of dialkoxynaphthalene

https://doi.org/10.1021/acs.accounts.3c00670
Acc. Chem. Res. 2024, 57, 670−684

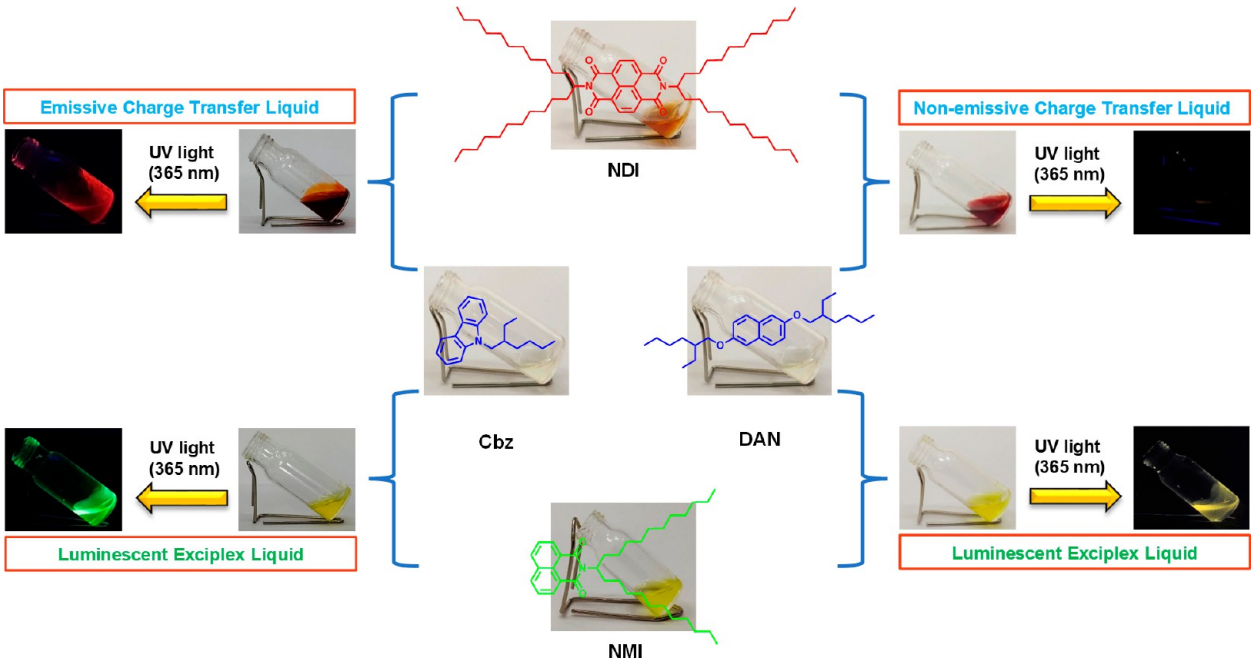

Figure 2. Chemical structures of **NDI**, **DAN**, **NMI**, and **Cbz** and corresponding photographs of SOLs and their (1:1) complex under visible and UV (365 nm) lights.

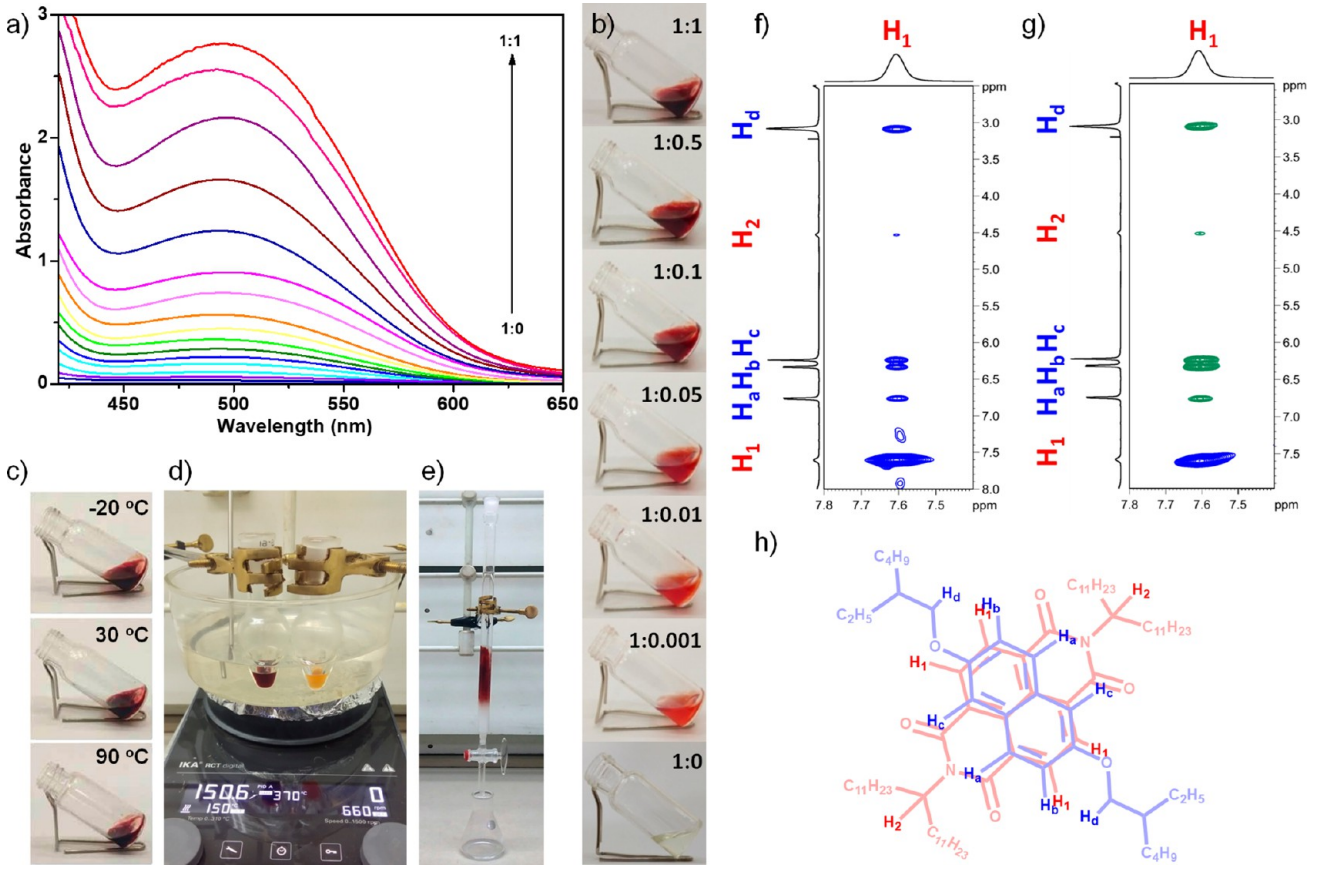

Figure 3. (a) Absorption spectral variation of **DAN** with increasing equivalents of **NDI** (5 mg on 1 × 1 cm^2 area of quartz) and (b) the corresponding daylight photographs of CT-SOL. (c) Photographs of CT-SOL (1:1), stored at −20, 30, and 90 °C, (d) showing stability even at 150 °C (D:A ratio of 1:1 (left) and 1:0.001 (right)) and (e) eluting as a single band in column chromatography separation. 2D-NMR spectra (f) NOESY and (g) ROESY at 250 ms mixing time, showing intermolecular cross-peaks in the CT liquid with D:A ratio 1:0.15. (h) Possible stacking interactions in the CT-SOL (1:1). Reproduced with permission from ref 40. Copyright 2019 Royal Society of Chemistry.

https://doi.org/10.1021/acs.accounts.3c00670
Acc. Chem. Res. 2024, 57, 670−684

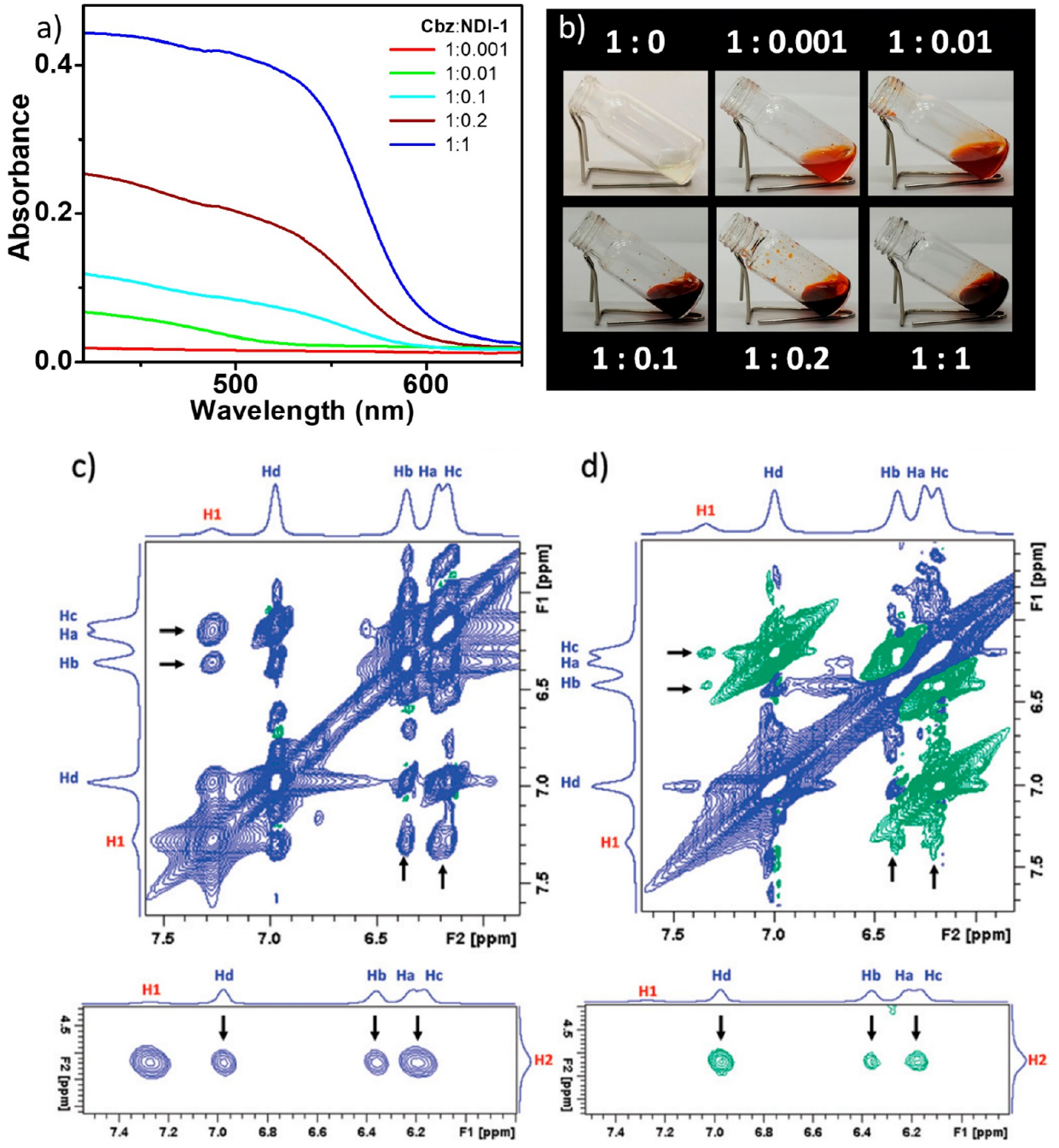

Figure 4. (a) Absorption spectral variation of **Cbz** with increasing equivalents of **NDI** (5 mg on a 1 × 1 cm^2 area of quartz) and (b) corresponding photographs of CT liquids. 2D-NMR spectra (c) NOESY and (d) ROESY spectra of **Cbz**:**NDI** (1:0.2) at 250 and 100 ms, respectively, recorded at 318 K. Intermolecular cross-peaks are indicated by arrows. Reproduced with permission from ref 41. Copyright 2022 Royal Society of Chemistry.

(**DAN**) as a donor and naphthalenediimide (**NDI**) as an acceptor has proven successful.[39] However, CT in solution is normally controlled by concentration, solvents and their polarity, temperature, etc. In contrast, here the CT within a SOL has been studied, specifically their D−A interaction.[40]

As a first example of CT-SOLs, the CT interactions between the donor **DAN** and acceptor **NDI** (Figure 2) were studied.[41] To exclude any impact of solvents and their polarity on CT interactions, a solvent-free method was demonstrated by utilizing **DAN** and **NDI** derivatives and **DAN** was mixed with varying amounts of **NDI**. A pronounced red-brown hue indicative of CT complex formation emerged when **DAN** and **NDI** were manually mixed with a spatula, with evidence of CT formation even at the lowest acceptor concentration, i.e., 0.001 equiv (Figure 3a,b). The low melting point of **NDI** and the liquid nature of **DAN** facilitated the dissolution of the acceptor within the donor matrix. Remarkably, even at a 1:1 D−A ratio, the resulting mixture maintained its fluidic state at RT.

The significant advantages of this solvent-free approach were evident, notably in the enhancement of D−A interactions, even at minimal acceptor concentrations, where only one acceptor molecule was present for every 1000 donor molecules. The CT complex remains stable across a range of temperatures, and the intensity of its characteristic CT band color was sustained even after many years (Figure 3c). Impressively, the CT liquid exhibits exceptional stability even at the elevated temperature of

https://doi.org/10.1021/acs.accounts.3c00670
Acc. Chem. Res. 2024, 57, 670−684

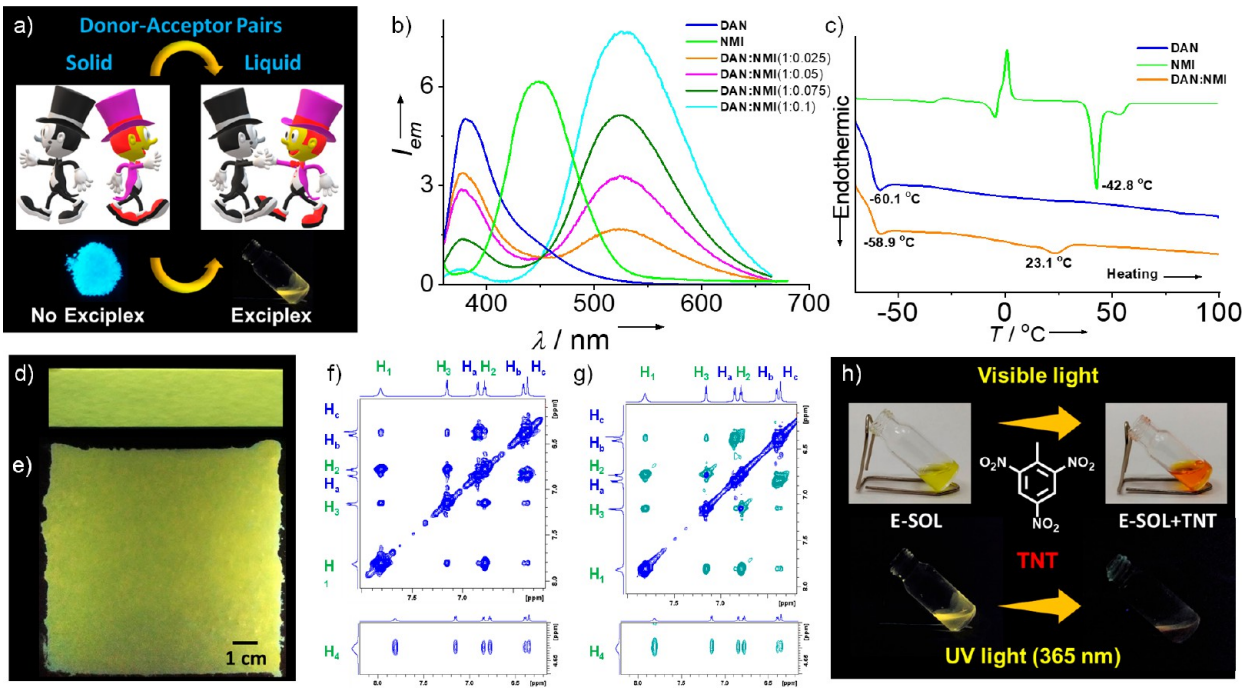

Figure 5. (a) Schematic of the physical interaction between the donor and acceptor molecules. (b) Variation of steady-state emission of **DAN** with an increasing equivalence of **NMI**. (c) Comparison of DSC of **DAN**, **NMI**, and **DAN**:**NMI** (1:1). Photographs of **DAN**:**NMI** (1:1) coated on (d) Whatman filter paper strips from solution and (e) on glass (10×10 cm^2) under UV light (365 nm). 2D-NMR (f) NOESY and (g) ROESY spectra at 100 and 250 ms mixing time, respectively, in the E-SOL. (h) Photographs of E-SOL showing a visible color change (top) and fluorescence quenching with TNT in the dark (bottom). Reproduced with permission from ref 2. Copyright 2021 Royal Society of Chemistry.

150 °C (Figure 3d). Additionally, it elutes as a single band in column chromatography, as shown in Figure 3e.

To gain an insight into the D−A interaction within the CT liquid at the molecular level, detailed NMR experiments were carried out. By introducing varying quantities of **NDI** into the **DAN** liquid, chemical shifts of **DAN** protons were observed. These shifts allowed us to calculate the "interaction constant" (K = 1.32 ML^{-1}) between **DAN** and **NDI**. Besides, 2D NMR experiments helped to explore the intricate interactions between **DAN** and **NDI**. Both nuclear Overhauser effect spectroscopy (NOESY) (Figure 3f) and rotating frame Overhauser effect spectroscopy (ROESY) (Figure 3g) revealed intra- and intermolecular cross-peaks. The intermolecular cross-peak intensities in the ROESY spectrum supported a staggered face-to-face stacking orientation between **DAN** and **NDI** in the CT-SOL, as illustrated in Figure 3h. This stacking arrangement closely matched the theoretical model derived from atomistic molecular dynamics simulations.

In another example of CT-SOLs, exploring a slight difference in the electron affinity of the donor, the same acceptor delivered RTP.[41] In this work, the focus was on the D−A interaction of carbazole (**Cbz**) with **NDI** derivatives in the SOL state (Figures 2, 4). The absorption spectra of both **Cbz** and **NDI** do not exhibit any peaks at wavelengths greater than 400 nm, as depicted in Figure 4a. Similar to the first example, the formation of the CT complex is evident even at the minimal acceptor loading, specifically at 0.001 equiv (Figure 4b). A strong reddish-brown coloration was observed in the CT liquid when the donor **Cbz** was mixed with varying ratios of **NDI** under neat conditions (Figure 4b). Even in a 1:1 D−A ratio, the low melting solid acceptor **NDI** featuring a long-branched alkyl chain maintained its liquid feature supportive of the CT liquid at RT.

NMR spectroscopy has been used to gain a deeper understanding of the molecular-level interaction between the donor and acceptor in the CT liquid. The 2D NMR spectra of **Cbz**:**NDI** exhibit broader signals (Figure 4c,d) and it suggests that **Cbz**:**NDI** experiences slower exchange dynamics and a longer lifetime for the D−A pair. When comparing the spectra of the complex to that of **Cbz**, it becomes evident that the signals of **Cbz** in the complex undergo a downfield shift, providing evidence for a stronger stacking interaction. Furthermore, the intensity pattern of the cross peaks supports a more face-to-face orientation of the aromatic ring planes in **Cbz**:**NDI**. It came to our attention that the **Cbz**:**NDI** hybrid in a 1:1 ratio is only slightly emissive when in solution. However, under solvent-free conditions, the same CT complex exhibits emission, and that will be discussed in the later section. In contrast to the solution state, where the effective CT is hindered at high temperatures and lower concentrations due to the rapid motion of solvated molecules, the CT liquid remains stable and exhibits high efficiency. This can be attributed to the low-polarity, viscous environment provided by the liquid donor scaffold to **NDI**.

1.2. Exciplex Solvent-Free Organic Liquids (E-SOLs)

An exciplex is formed when two different molecules interact in an electronically excited state.[42] This interaction creates a temporary, unique species with distinct electronic properties and energy levels compared to the individual molecules. Exciplexes play a vital role in applications such as photochemical reactions, OLEDs, lasers, and molecular spectroscopy.[43] The examples of E-SOLs highlighted the advantages of transitioning from materials in solid or solution to SOLs, showcasing their ability to achieve extraordinary optical properties that are otherwise unattainable using the former forms (Figure 5a). As mentioned previously, the interaction between **DAN** and **NDI** leads to CT, however, decreasing the acceptor strength by using

https://doi.org/10.1021/acs.accounts.3c00670
Acc. Chem. Res. 2024, 57, 670−684

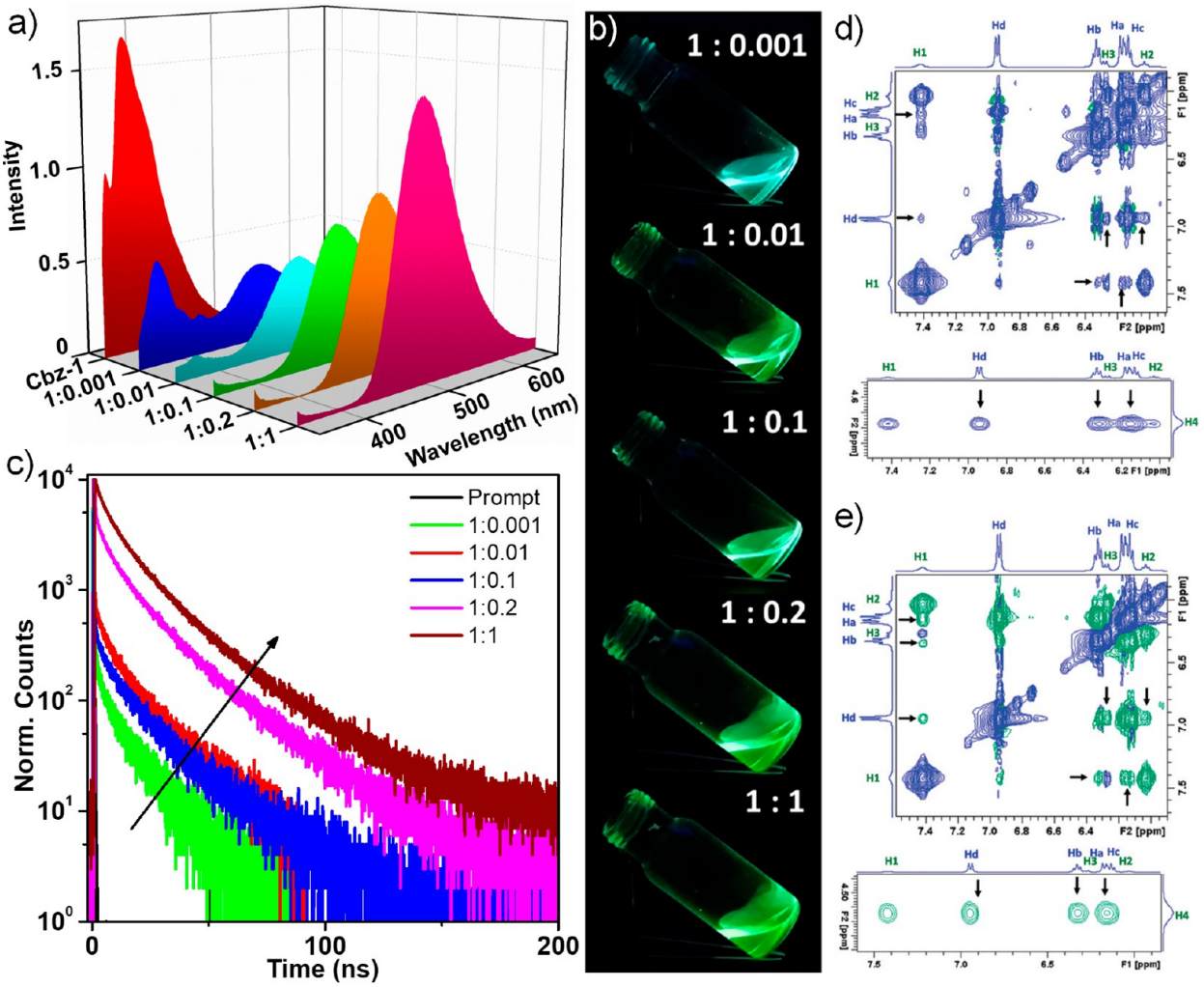

Figure 6. Variation of (a) steady-state emission, (b) corresponding photographs under UV light (λ_{ex} = 365 nm), and (c) fluorescence lifetime of **Cbz**:**NMI** with an increasing equivalence of **NMI** (λ_{ex} = 374 nm, λ_{mon} = 495 nm). (d) NOESY and (e) ROESY spectra of **Cbz**:**NMI** (1:0.2) at 250 ms, recorded at 318 K. Reproduced with permission from ref 41. Copyright 2022 Royal Society of Chemistry.

NMI, resulted in an emissive exciplex in the liquid state (Figure 5b).[2] Notably, there was no observable CT band when monitoring the absorbance of **DAN** and **NMI** in the solvent-free state. Furthermore, DSC analysis confirmed the uniform distribution of D−A molecules in this hybrid liquid as the heating trace of the **DAN**-**NMI** composite liquid showed T_g at −58.9 °C and melting point (T_m) at 23.1 °C (Figure 5c). E-SOL has proven to be practically useful as it can be applied as a coating on filter paper strips and glass surfaces (10 × 10 cm^2) without altering its optical properties (Figure 5d,e). More importantly, the solid counterparts of both the donor and acceptor molecules failed to exhibit exciplex formation.

NMR investigations showed the chemical shift variations in the alkyl ($-OCH_2$) groups and it helps us to estimate an "interaction constant", denoted as K (0.61 ML^{-1}). This value is notably lower than that observed in CT liquids of **DAN** and **NDI**, indicating a comparatively weaker D−A interaction in the E-SOL. Furthermore, 2D NMR results provide support for the stacking arrangement of **DAN**-**NMI** pairs in a staggered configuration within the neat liquid. The 2D spectra revealed the presence of both intra- and intermolecular cross-peaks and the intensities in the ROESY spectrum suggest an average aromatic ring separation of 4.0−4.5 Å between **DAN** and **NMI** (Figure 5f,g). Additionally, this emissive exciplex liquid has been effectively employed for exclusive dual-mode sensing, both colorimetric and fluorometric, of explosives in direct contact mode (Figure 5h). Detecting and distinguishing trinitrotoluene (TNT) from other nitroaromatic compounds is challenging due to similar fluorescence signal responses. However, the E-SOL demonstrates dual-mode sensing of TNT, and further analysis indicated its high selectivity toward TNT compared to other nitroaromatic and nitro group containing nonaromatic explosives.

A similar exciplex formation was observed when the donor was changed to **Cbz** and this exciplex emission in the solvent-free state is noticed even in the low amount of **NMI** (Figure 6a,b). A noticeable increase in the emission lifetime (26 ns) of the E-SOL (1:1) is observed when compared with the individual components, as depicted in Figure 6c. An extended lifetime and the red-shifted broad emission strongly suggest the formation of E-SOL. NMR techniques were employed to investigate the molecular-level interactions between **Cbz** and **NMI** within the E-SOL. In the presence of donor **Cbz**, the **NMI** acceptor signals exhibit a shift toward the upfield, indicating the presence of $\pi-\pi$ stacking interactions between **Cbz** and **NMI**. To gain a more comprehensive understanding of this interaction, 2D NOESY and ROESY experiments were conducted at a temperature of 318 K (Figure 6d,e). These experiments revealed strong

https://doi.org/10.1021/acs.accounts.3c00670
Acc. Chem. Res. 2024, 57, 670−684

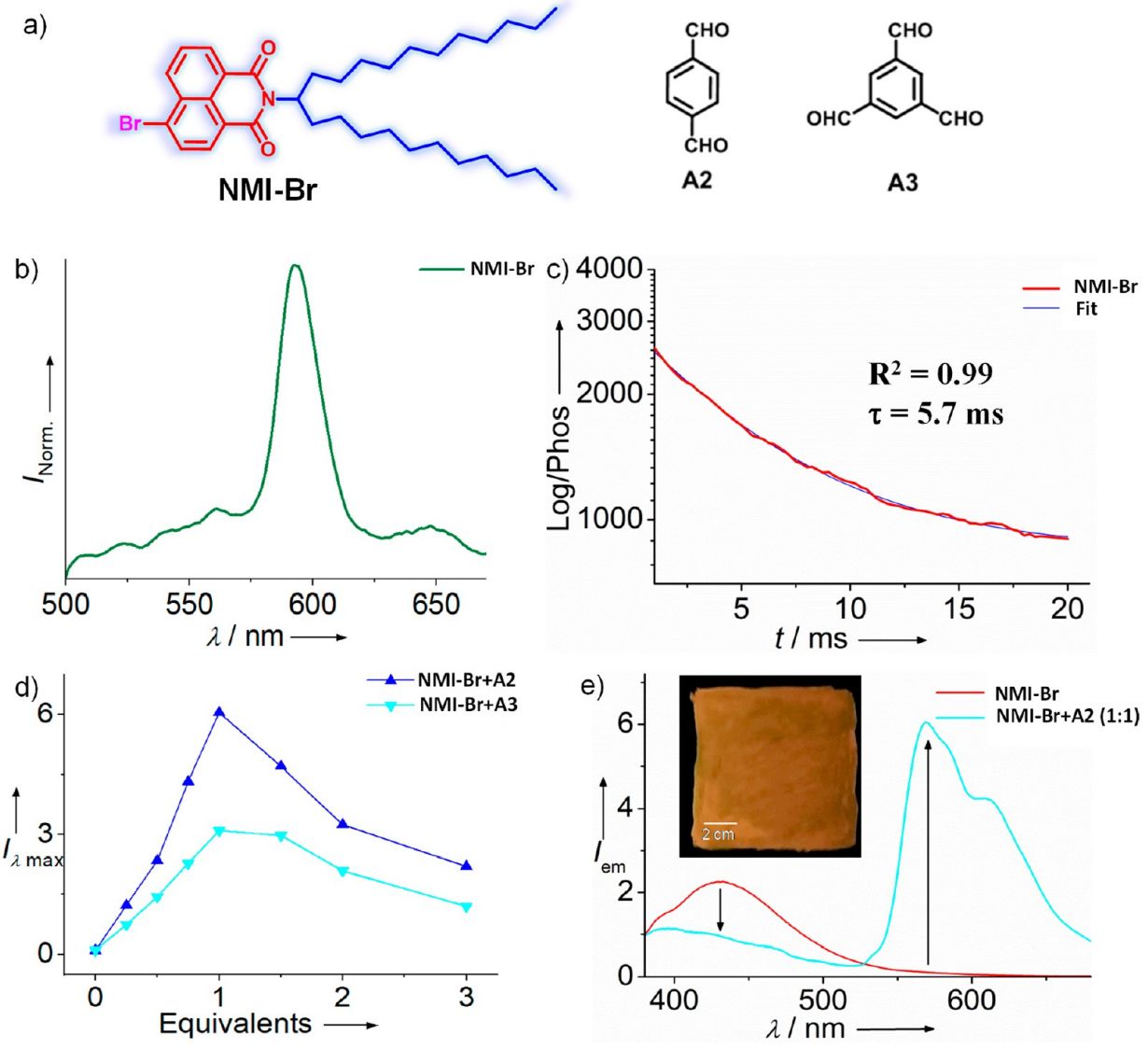

Figure 7. (a) Chemical Structure of **NMI-Br**, **A2** and **A3**. (b) Phosphorescence spectra, and (c) phosphorescence lifetime decay of **NMI-Br** at 298 K (λ_{ex} = 345 nm and λ_{mon} = 594 nm). (d) Variation of phosphorescence intensity at λ_{max} of RTP hybrid liquids of **NMI-Br+A2** and **NMI-Br+A3** (λ_{ex} = 345 nm). (e) Enhanced luminescence of RTP hybrid liquid **NMI-Br+A2** (1:1) at ambient condition and inset shows the photograph of a large-area (10 × 10 cm^2) coating of **NMI-Br+A2** (1:1). Reproduced with permission from ref 1. Copyright 2019 Wiley-VCH Verlag GmbH & Co. KGaA.

intermolecular cross-peaks in the NOESY spectrum, suggesting proximity between the protons of **Cbz** and **NMI** in E-SOL. The findings from the 2D NMR analyses indicate that the aromatic rings of **Cbz** and **NMI** are not parallel to each other but are tilted relative to one another. Recently, Isoda and co-workers also reported a pyromellitic diimide-based SOL, which delivers exciplex after dissolving with electron-donating solid naphthalene.[44]

1.3. Room Temperature Phosphorescence Solvent-Free Organic Liquids (RTP-SOLs)

Advanced synthetic methodologies in organic chemistry have been extensively used to develop many new emissive organic compounds with high quantum yield.[45−48] Organic phosphors are one such class of compounds that have undergone drastic developments in the past decade.[49,50] The recent advancements in this area have delivered numerous RT phosphorescent (RTP) molecules with longer lifetimes and afterglow properties, enabling them in a wide range of applications.[50] However, RTP has been primarily displayed in the crystalline form until SOLs with RTP properties came into existence.[1] The substituted naphthalene monoimide derivatives exhibited RTP[51] and minor alterations in the molecular design resulted in distinct material properties.[52] Toward developing a SOLs with RTP in air, our group introduced a branched alkyl chain on bromonaphthalimide (**NMI-Br**, Figure 7a), the long bulky alkyl chains of **NMI-Br** led to a low T_g (<−38.7 °C) and behaved as a liquid at RT. The phosphorescence spectrum of **NMI-Br** revealed a shifted peak at λ_{max} of 594 nm (Figure 7b) at RT, which closely matches that of the 2-methyltetrahydrofuran (MTHF) solution at −196 °C. This finding supports that **NMI-Br** is exhibiting RTP despite lacking a crystalline molecular arrangement in its design. The phosphorescence lifetimes of **NMI-Br** were 5.7 ms at RT with QY of 0.1% (Figure 7c). This work marks as the first report demonstrating RTP in a SOL. Normally, the absence of molecular ordering in noncrystalline materials support nonradiative decay and reduce triplet emission. However, in the case of **NMI-Br**, its viscous nature

https://doi.org/10.1021/acs.accounts.3c00670
Acc. Chem. Res. 2024, 57, 670−684

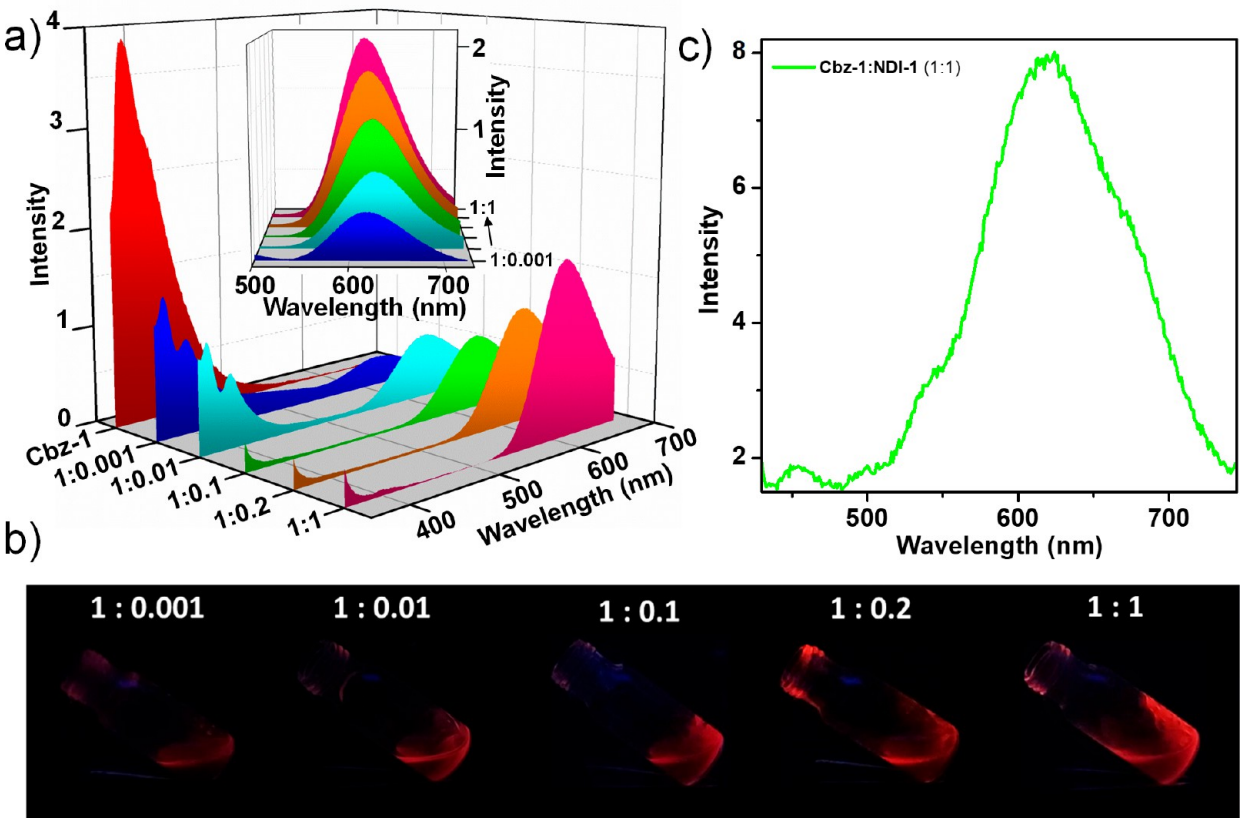

Figure 8. (a) Variation of the steady-state emission of **Cbz** with an increasing equivalence of **NDI** (λ_{ex} = 342 nm) (5 mg on a 1 × 1 cm^2 area of quartz); inset shows the corresponding spectral change by exciting at 370 nm and (b) corresponding photographs under UV (365 nm) light. (c) Phosphorescence spectra of **Cbz**:**NDI** (1:1) at RT in air (λ_{ex} = 350 nm). Reproduced with permission from ref 41. Copyright 2022 Royal Society of Chemistry.

plays a crucial role in regulating nonradiative decay processes and enhancing triplet emission. Furthermore, the significance of weak Br···O halogen bonding becomes evident in facilitating RTP even in the presence of air. Time-dependent density functional theory (TD-DFT) confirmed isoenergic singlet−triplet energy levels that help with intersystem crossing.[1] Utilizing supramolecular two-component assemblies has proven to be a highly effective strategy for enhancing RTP.[53] In line with this, we introduced guest molecules, benzene-1,4-dialdehyde (**A2**) and benzene-1,3,5-tricarboxaldehyde (**A3**), into **NMI-Br** SOL (Figure 7a). The resulting **NMI-Br**:**A2** hybrid in a 1:1 ratio exhibited notable improvements in both phosphorescence lifetime (7.1 ms) and QY (2%) (Figure 7d,e). These enhancements were attributed to the formation of a halogen bond between **NMI-Br** and **A2**. Further a liquid phosphor hybrid was developed by mixing **NMI-Br** with **A2** (1:1), and this combination was used to generate a large-area (10 × 10 cm^2) paintable material with improved RTP (Figure 7e, inset).

Recently, some more efforts have been made to achieve RTP-SOLs materials. Tani and co-workers reported the photo-induced crystal-melt transition followed by phosphorescence emission of an unsymmetrical heteroaromatic 1,2-diketone-based RTP supercooling liquid.[54] Another example of RTP-SOLs is CT-assisted triplet emission from the CT-SOL of **Cbz**:**NDI** hybrid.[41] The hybrid liquid displayed a red emission that extends into the near-infrared region (Figure 8a,b). Notably, after monitoring CT emission at both RT and 77 K, we observed an increase in emission intensity specifically at 640 nm. This enhanced emission arises from the ability to control nonradiative decay due to restricted vibrational and rotational movements within the complex at 77 K. Furthermore, the closely matching emission spectra of CT-SOL at RT and 77 K suggest that both emissions likely stem from the decay of the triplet excited state. The excitation spectrum of **Cbz**:**NDI** (1:1) monitored at 620 nm highlights a significant contribution from the CT peak. In the case of CT-SOLs, its phosphorescence spectrum at RT exhibits a single broad peak spanning from 490 to 720 nm, with the peak maximum at 640 nm (Figure 8c). The concordance between the phosphorescence spectrum of CT-SOL and the corresponding emission spectra at both RT and 77 K confirms RTP. Moreover, increasing the acceptor loading from 0.01 to 1 equiv leads to enhanced RTP, characterized by longer lifetimes ranging from 326 to 485 ms. This extended RTP lifetime, coupled with the improved processability of the RTP-SOL, supports CT-assisted RTP-SOL for large-area red-emitting lighting and display applications.

1.4. Thermally Activated Delayed Fluorescence Solvent-Free Organic Liquids (TADF-SOLs)

Interest in organic luminescent materials exhibiting TADF materials has increased tremendously in the past few years due to their longer lifetime than conventional fluorescent materials.[55−57] Besides, small singlet−triplet energy gap (ΔE_{ST}) of these materials facilitates reverse intersystem crossing from triplet to singlet state and thereby leads to 100% internal quantum yield in the electroluminescence process.[56,57] TADF materials often suffer from severe aggregation-induced quenching (AIQ) due to strong $\pi-\pi$ stacking.[58] Given the difficult nature of molecular packing in the crystal state, blocking

https://doi.org/10.1021/acs.accounts.3c00670
Acc. Chem. Res. 2024, 57, 670−684

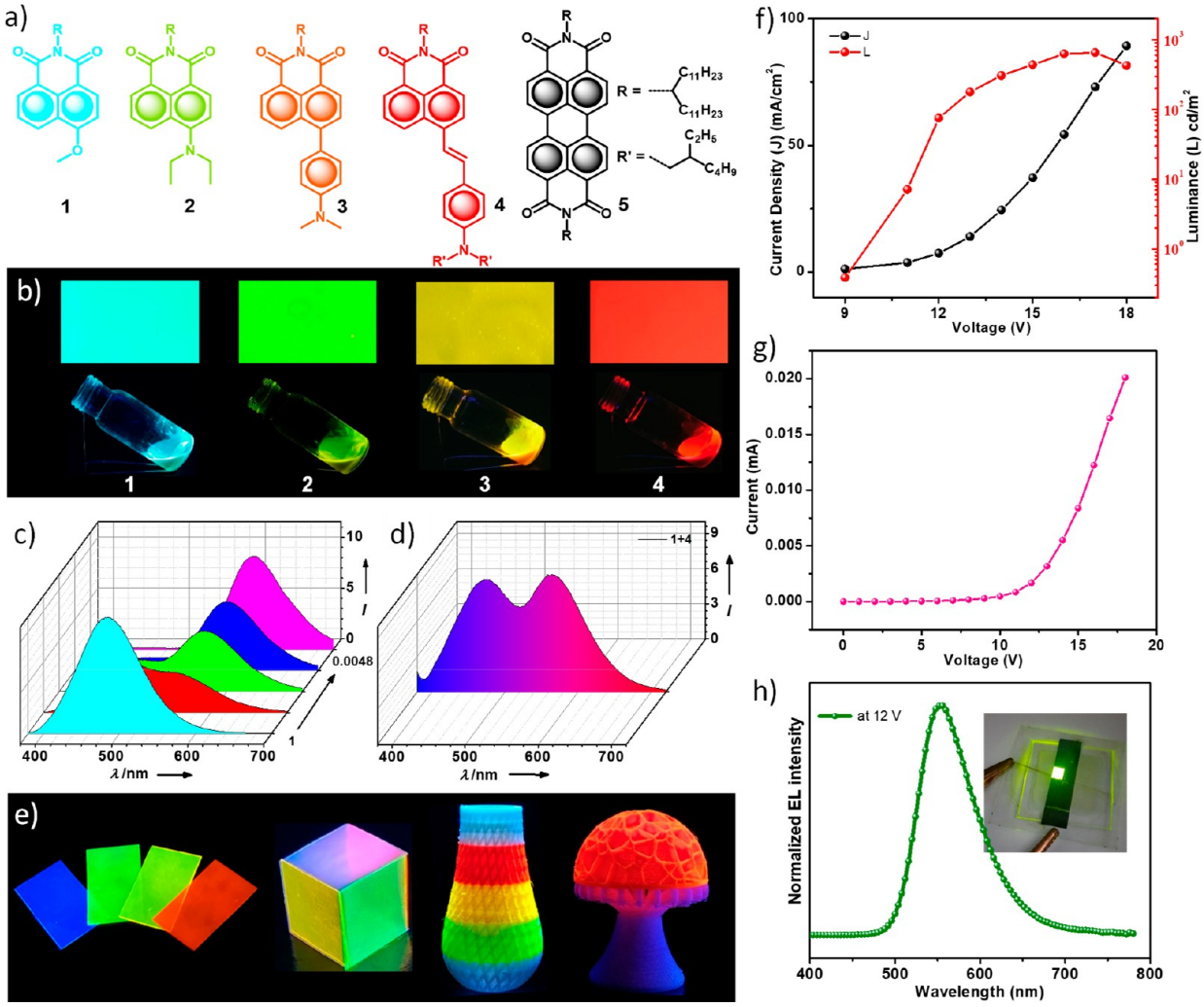

Figure 9. (a) Chemical structures of TADF-SOLs **1**-**4** and fluorescent SOL **5**. (b) Photographs of thin films and neat SOLs of **1**−**4** (λ_{ex} = 365 nm). (c) ET studies of **1** with increasing equivalents of **4** and (d) white light emission achieved by **1**+**4**. (e) Photographs of thin-film of **1**−**4** with PLA and the 3D printed objects using PLA-TADF SOL (1 wt %) hybrids under UV light (λ_{ex} = 365 nm). (f) Current density (J)-voltage (V)-luminance (L) characteristics, (g) current(I)-voltage (V) characteristics, and (h) electroluminescence spectra of the device, inset shows the corresponding photograph. Reproduced with permission from ref 3. Copyright 2023 Wiley-VCH Verlag GmbH & Co. KgaA.

multiple AIQ channels is key. And limitations of existing crystalline luminescent materials such as solubility, self-healing properties, etc., are making challenges for existing organic materials.[59] In this context, current interest has turned to SOL-based emitters.

Electron D−A dyads of naphthalimide with different donors connected through flexible and rigid linkages have been explored for TADF features.[60,61] Based on that our group in the year 2023 reported a series of TADF liquid naphthalimide derivatives **1**−**4** (Figure 9a).[3] A comprehensive investigation was carried out for molecule **1** to understand the role of the liquid medium in facilitating TADF. A similar spectral feature was noticed for **1** in the steady-state emissions at 298 and 77 K. This similarity, along with the substantial overlap between the fluorescence and phosphorescence spectra, serves as confirmation of a minimal ΔE_{ST}. Even in the presence of oxygen, the emission spectra and lifetime of molecule **1** exhibited minimal changes, indicating that the liquid medium functions as a protective barrier. Furthermore, the temperature-dependent decay profile of **1** revealed the typical TADF behavior, with an increase in lifetime (τ_{TADF}) as the temperature was raised from 77 to 298 K. Additionally, we observed a linear correlation between the intensity of delayed fluorescence and excitation power for molecule **1**, providing clear evidence that the emission is attributed to TADF rather than triplet−triplet annihilation.

Similarly, other molecules **2**−**4** show TDAF, and these derivatives were prepared to diversify the emission features by structural modification with emission spanning from green to red (Figure 9b), with luminescence QY up to 80% and lifetimes between 10 and 45 μs. The involvement of the CT state in TADF liquids was confirmed by the presence of solvatochromism. More importantly, all molecules exhibited reasonably high optical stability upon direct irradiation with UV light for 5 h. TADF emitter **1** exhibited ET with various TADF, RTP, and fluorescent dopants (Figure 9a) to achieve tunable and white light emissions (Figure 9c,d).[36] The use of a liquid matrix made it easy to blend with polylactic acid (PLA), a biodegradable polymer, producing solid filament materials suitable for 3D printing applications. The optimized condition required only minimum SOL content (1 wt %) to achieve satisfactory luminescent characteristics with high QYs in thin films (Figure 9e). The excellent compatibility of SOLs in PLA enabled the

https://doi.org/10.1021/acs.accounts.3c00670
Acc. Chem. Res. 2024, 57, 670−684

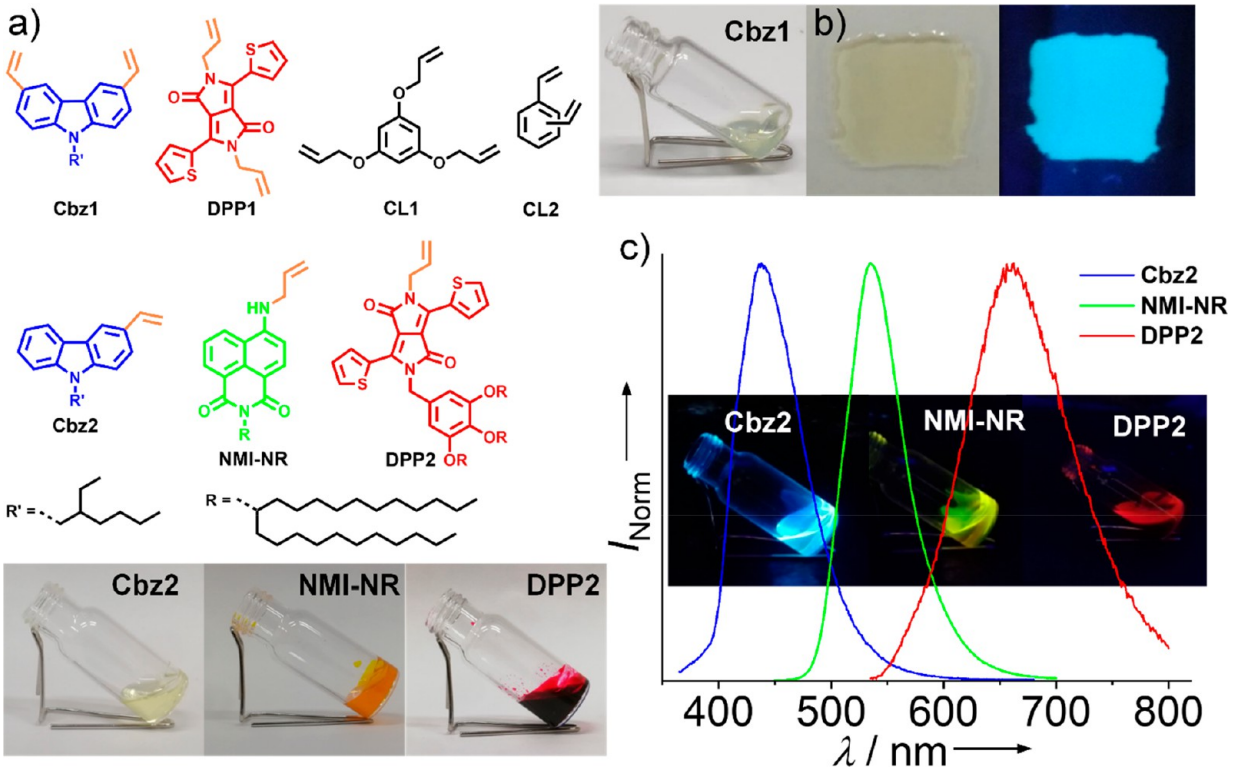

Figure 10. (a) Chemical structure and corresponding daylight photographs of **Cbz1**, **DPP1**, **CL1**, **CL2**, **Cbz2**, **NMI-NR**, and **DPP2**. (b) Photographs of **Cbz1**-**CL1** polymer film under visible (left) and UV (365 nm) (right) lights. (c) Normalized steady-state emission spectra of **Cbz2**, **NMI-NR**, and **DPP2** in neat thin film (inset photographs of **Cbz2**, **NMI**, and **DPP2** under UV (365 nm) lights).

creation of new TADF-based 3D printable materials. Interestingly, SOL-PLA hybrids displayed outstanding thermal stability and processability. Additionally, these TADF-SOLs have been employed in OLED devices, demonstrating reasonably good performance. The device prepared from **3** achieved a maximum luminance of 653 cd/m^2 at 17 V with a current density of 73 mA/cm^2, showcasing the suitability of SOLs as an emitter in OLEDs.

1.5. Polymerizable Solvent-Free Organic Liquids (P-SOLs)

While the recent advancements in SOLs are fascinating,[62,63] it is essential to appropriately address their current limitations, including surface stickiness and the potential irreversibility of film curing. To overcome these challenges while preserving the physical and photophysical attributes of SOLs, one promising approach is the creation of luminescent polymer films through the design of polymerizable SOLs (P-SOL). The concept of P-SOLs holds the potential to surmount numerous hurdles associated with luminescent organic materials. In this context, our group developed polymerizable luminescent SOLs and investigated the suitability of a fluid matrix for other dopants to fine-tune the luminescent properties.[4] Ultimately, the polymerization of this hybrid liquid is uniform and gives large-area thin films that deliver both stable mechanical and optical properties (Figure 10).

In this study, we have opted for mono/di vinyl and mono/di allyl functionalized chromophores as P-SOL luminophores. As the blue-emitting donor P-SOL, liquid divinyl carbazole (**Cbz1**) and monovinyl carbazole (**Cbz2**) have been chosen. While as acceptor polymerizable dopants, diallyl diketopyrrolopyrrole (**DPP1**), mono allyl diketopyrrolopyrrole (**DPP2**), and allyl naphthalene monoimide (**NMI-NR**) have been selected (Figure 10). To enhance the versatility of our films and broaden their applicability, the cross-linkers (**CLs**), namely, 1,3,5-tris-(allyloxy)benzene (**CL1**) and the commercially available divinylbenzene (**CL2**) were selected. These cross-linkers, **CL1** and **CL2**, facilitate the formation of cross-linked polymer structures with the SOLs.

UV light-assisted free-radical polymerization delivered a stable film of **Cbz1**, however, the **Cbz1**-based SOL films were brittle and challenging to peel off from glass surfaces due to their highly cross-linked network formed by the bifunctional monomer (Figure 10b). Similar observations were noticed for the hybrid films of **Cbz1**, **DPP1**, and **CL1**/**CL2**. To overcome this, we selected new liquid monomers, **Cbz2**, **NMI-NR**, and **DPP2**, exhibiting intense blueish-green, green, and red emissions, respectively (Figure 10c). This modification improved film quality and produced free-standing, flexible, foldable, and transparent luminescent films with high QYs. Since all attempts to photochemically polymerize **Cbz1** resulted in the production of brittle films with low QYs, a thermochemical polymerization in an inert atmosphere for **Cbz2** was carried out. After a series of optimizations, it was determined that heating at 100 °C for 1 h was sufficient to produce a self-supporting luminescent film of **Cbz2**, as illustrated in Figures 11a,b. The time-dependent FT-IR spectral changes of **Cbz2** were monitored during the thermochemical polymerization to confirm the complete conversion of monomers (Figure 11c). Subsequently, the ratio of **NMI-NR** and **DPP2** was further optimized to achieve white light emission from the polymer film (Figure 11d). By combining **Cbz2**-**CL2**-**NMI-NR**-**DPP2** in a hybrid liquid, we successfully created a flexible, transparent, and large-area white light-emitting film (Figure 11e,f). This film exhibited a reasonably high QY of 34% and possessed CIE coordinates of $x = 0.32$ and $y = 0.30$. In short, we demonstrated a

https://doi.org/10.1021/acs.accounts.3c00670
Acc. Chem. Res. 2024, 57, 670−684

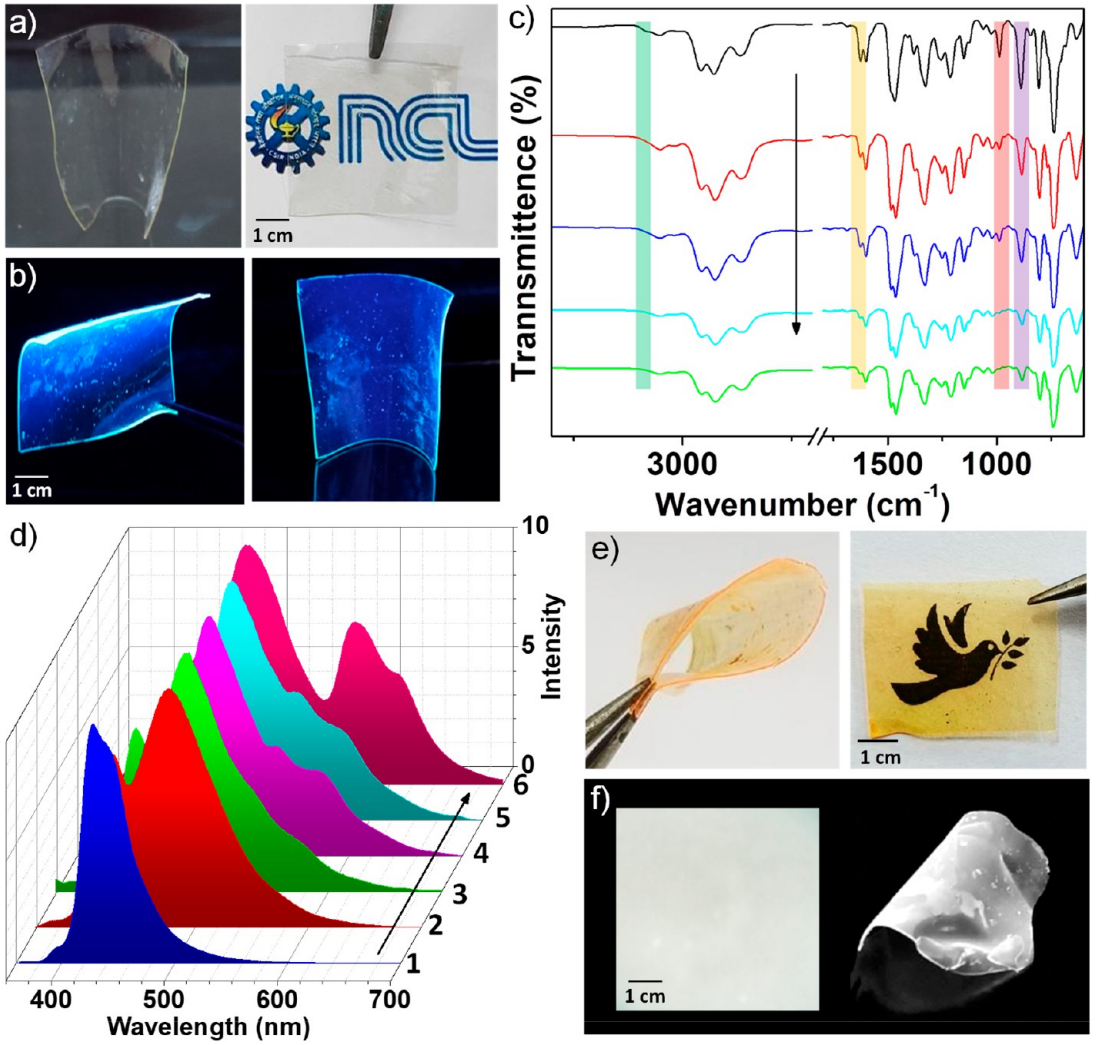

	1	2	3	4	5	6
Cbz2	1	1	1	1	1	1
CL2	0	0.5	0.5	0.5	0.5	0.5
NMI-NR	0	1×10^{-4}	1×10^{-4}	1.4×10^{-4}	1.8×10^{-4}	2.2×10^{-4}
DPP2	0	0	0.6×10^{-5}	1.8×10^{-5}	1.8×10^{-5}	2.2×10^{-5}

Figure 11. Photographs of free-standing large-area flexible and transparent polymer film of **Cbz2** under (a) visible and (b) UV (365 nm) lights. (c) Time-dependent FT-IR spectra of **Cbz2** from 0 to 1.5 h during polymerization. (d) Emission spectral variation of **Cbz2-CL2-NMI-NR-DPP2** polymer leading to white light emission and corresponding mixing ratio in mol %. Photographs of free-standing large-area flexible and transparent films of the white light-emitting polymer **Cbz2-CL2-NMI-NR-DPP2** under (e) visible and (f) UV (365 nm) lights. Reproduced with permission from ref 4. Copyright 2023 Wiley-VCH Verlag GmbH & Co. KGaA.

groundbreaking approach to developing emissive polymers suitable for large-area device applications by introducing the novel concept of P-SOLs.

In a related concept of liquid polymer, Shinohara et al. reported viscoelastic conjugated polymers of a π-conjugated backbone by incorporating bulky and flexible alkyl side chains as internal plasticizers and further utilized as mechanoelectric generator and electret.[64]

2. CONCLUSIONS AND OUTLOOK

In this account, we highlighted the emergence of a new soft material called "organic solvent-free liquid", which can also serve as a fluid matrix for introducing new hybrid materials through doping. Since the design concept of SOLs is based on π-core isolation, the initial developments were limited to luminescent liquids. Later, the advancement in this area displayed the potential of the SOLs to achieve success in responsive materials, light-harvesting, selective sensing applications, etc. Besides, it explored the molecular properties such as charge transfer, energy

https://doi.org/10.1021/acs.accounts.3c00670
Acc. Chem. Res. 2024, 57, 670−684

transfer, room temperature phosphorescence, thermally activated delayed fluorescence, etc. in the liquid matrix. The inevitable support of the liquid matrix is the key to achieving efficient hybrid materials. The most attractive feature of these hybrid liquids is the synergism to deliver exceptional properties that are otherwise unattainable by the individual components. The new concept of polymerizable SOLs is expected to address the significant challenges posed by the inherent limitations of SOLs. This innovative approach paves the way for the development of alternate emissive materials that are well-suited for use in large-area flexible, foldable, and stretchable devices, offering promising prospects for advancements in the field. Besides, the concept of polymerizable SOLs can be extended to other functional properties and develop new hybrid materials. As a new functional material, SOLs exhibited remarkable improvement and the coming years will witness more advancement in the field.

AUTHOR INFORMATION

Corresponding Author

Sukumaran Santhosh Babu − *Organic Chemistry Division, National Chemical Laboratory (CSIR-NCL), Pune 411008, India; Academy of Scientific and Innovative Research (AcSIR), Ghaziabad 201002, India;* orcid.org/0000-0003-1959-6142; Email: sb.sukumaran@ncl.res.in

Authors

Vivek Chandrakant Wakchaure − *Organic Chemistry Division, National Chemical Laboratory (CSIR-NCL), Pune 411008, India; Academy of Scientific and Innovative Research (AcSIR), Ghaziabad 201002, India;* orcid.org/0000-0003-1147-1564

Goudappagouda Channareddy − *Organic Chemistry Division, National Chemical Laboratory (CSIR-NCL), Pune 411008, India; Academy of Scientific and Innovative Research (AcSIR), Ghaziabad 201002, India*

Complete contact information is available at: https://pubs.acs.org/10.1021/acs.accounts.3c00670

Author Contributions

The manuscript was written through contributions of all authors. All authors have given approval to the final version of the manuscript. CRediT: **Vivek Chandrakant Wakchaure** writing-original draft; **Goudappagouda Channareddy** writing-original draft; **Sukumaran Santhosh Babu** conceptualization, funding acquisition, writing-review & editing.

Funding

This work is supported by SERB, Govt. of India, CRG/2019/002539.

Notes

The authors declare no competing financial interest.

Biographies

Dr. Vivek C. Wakchaure completed his Masters in Organic Chemistry in 2013 from Savitribai Phule Pune University, Pune, India. Later, he received his Ph.D. in Chemical Science under the guidance of Dr Sukumaran Santhosh Babu from CSIR-National Chemical Laboratory (CSIR-NCL), Pune, India, in 2021. His thesis mainly focuses on strategies to develop processable 2D-polymers using SOLs.

Dr. Goudappagouda obtained his Masters in Chemistry from Sahyadri Science College, Kuvempu University, Karnataka, India in 2012. Later, he received his Ph.D. in Chemical Science under the guidance of Dr Sukumaran Santhosh Babu from CSIR-National Chemical Laboratory (CSIR-NCL), Pune, India, in 2020. His research work mainly focused on the design and synthesis of donor−acceptor small organic molecules for lighting and light-harvesting applications.

Dr. Sukumaran Santhosh Babu has been a scientist at the Organic Chemistry Division of National Chemical Laboratory (CSIR-NCL) since 2014 and leads his research group focusing on optical and redox properties of organic functional materials. His research interests focus on solvent-free organic liquids, luminescent organic materials, and nanographenes and porous 2D-polymers for catalytic and energy applications.

ACKNOWLEDGMENTS

We acknowledge Dr. Sairam D. Veer and Dr. Aakash D. Nidhankar for their contributions in the area of SOLs from our group.

REFERENCES

(1) Goudappagouda; Manthanath, A.; Wakchaure, V. C.; Ranjeesh, K. C.; Das, T.; Vanka, K.; Nakanishi, T.; Babu, S. S. Paintable Room-Temperature Phosphorescent Liquid Formulations of Alkylated Bromonaphthalimide. *Angew. Chem., Int. Ed.* **2019**, *58*, 2284−2288.

(2) Wakchaure, V. C.; Goudappagouda; Das, T.; Ravindranathan, S.; Santhosh Babu, S. An Excimer to Exciplex Transition through Realization of Donor−Acceptor Interactions in Luminescent Solvent-Free Liquids. *Nanoscale* **2021**, *13*, 10780−10784.

(3) Nidhankar, A. D.; Goudappagouda; Kothavade, P.; Dongre, S. D.; Dnyaneshwar Veer, S.; Ranjan Dash, S.; Rajeev, K.; Unni, K. N. N.; Shanmuganathan, K.; Santhosh Babu, S. Thermally Activated Delayed Fluorescent Solvent-Free Organic Liquid Hybrids for Tunable Emission Applications. *Chem.—Asian J.* **2023**, *18*, No. e202300276.

(4) Wakchaure, V. C.; Veer, S. D.; Nidhankar, A. D.; Kumar, V.; Narayanan, A.; Babu, S. S. Polymerizable Solvent-Free Organic Liquids: A New Approach for Large Area Flexible and Foldable Luminescent Films. *Angew. Chem., Int. Ed.* **2023**, *62*, No. e202307381.

(5) Santhosh Babu, S.; Nakanishi, T. Nonvolatile Functional Molecular Liquids. *Chem. Commun.* **2013**, *49*, 9373−9382.

(6) Li, H.; Choi, J.; Nakanishi, T. Optoelectronic Functional Materials Based on Alkylated-π Molecules: Self-Assembled Architectures and Nonassembled Liquids. *Langmuir* **2013**, *29*, 5394−5406.

(7) Lu, F.; Neal, E. A.; Nakanishi, T. Self-Assembled and Nonassembled Alkylated-Fullerene Materials. *Acc. Chem. Res.* **2019**, *52*, 1834−1843.

(8) Narayan, B.; Nakanishi, T. Room-Temperature Liquid Dyes. In *Functional Organic Liquids*; John Wiley & Sons, Ltd: Hoboken, NJ, 2019; pp 1−20.

(9) Babu, S. S. Paradigms Shift When Solvent-Less Fluids Come into Play. *Phys. Chem. Chem. Phys.* **2015**, *17*, 3950−3953.

(10) Ghosh, A.; Nakanishi, T. Frontiers of Solvent-Free Functional Molecular Liquids. *Chem. Commun.* **2017**, *53*, 10344−10357.

(11) Hollamby, M. J.; Nakanishi, T. The Power of Branched Chains: Optimising Functional Molecular Materials. *J. Mater. Chem. C* **2013**, *1*, 6178−6183.

(12) Lu, F.; Jang, K.; Osica, I.; Hagiwara, K.; Yoshizawa, M.; Ishii, M.; Chino, Y.; Ohta, K.; Ludwichowska, K.; Kurzydłowski, K. J.; Ishihara, S.; Nakanishi, T. Supercooling of Functional Alkyl-π Molecular Liquids. *Chem. Sci.* **2018**, *9*, 6774−6778.

(13) Takeda, T.; Yamamoto, S.; Mitsuishi, M.; Akutagawa, T. Thermoresponsive Amphipathic Fluorescent Organic Liquid. *J. Phys. Chem. C* **2018**, *122*, 9593−9598.

(14) Kamino, B. A.; Bender, T. P. The Use of Siloxanes, Silsesquioxanes, and Silicones in Organic Semiconducting Materials. *Chem. Soc. Rev.* **2013**, *42*, 5119−5130.

(15) Kamino, B. A.; Grande, J. B.; Brook, M. A.; Bender, T. P. Siloxane−Triarylamine Hybrids: Discrete Room Temperature Liquid

Triarylamines via the Piers−Rubinsztajn Reaction. *Org. Lett.* **2011**, *13*, 154−157.
(16) Bender, T. P.; Graham, J. F.; Duff, J. M. Effect of Substitution on the Electrochemical and Xerographic Properties of Triarylamines: Correlation to the Hammett Parameter of the Substituent and Calculated HOMO Energy Level. *Chem. Mater.* **2001**, *13*, 4105−4111.
(17) Babu, S. S.; Hollamby, M. J.; Aimi, J.; Ozawa, H.; Saeki, A.; Seki, S.; Kobayashi, K.; Hagiwara, K.; Yoshizawa, M.; Möhwald, H.; Nakanishi, T. Nonvolatile Liquid Anthracenes for Facile Full-Colour Luminescence Tuning at Single Blue-Light Excitation. *Nat. Commun.* **2013**, *4*, 1969.
(18) Santhosh Babu, S.; Aimi, J.; Ozawa, H.; Shirahata, N.; Saeki, A.; Seki, S.; Ajayaghosh, A.; Mohwald, H.; Nakanishi, T. Solvent-Free Luminescent Organic Liquids. *Angew. Chem., Int. Ed.* **2012**, *51*, 3391−3395.
(19) Gershuni, S.; Rabinovitz, M.; Agranat, I.; Berlman, I. B. Effect of substituents on the melting points and spectroscopic characteristics of some popular scintillators. *J. Phys. Chem.* **1980**, *84*, 517−520.
(20) Lu, F.; Takaya, T.; Iwata, K.; Kawamura, I.; Saeki, A.; Ishii, M.; Nagura, K.; Nakanishi, T. A Guide to Design Functional Molecular Liquids with Tailorable Properties Using Pyrene-Fluorescence as a Probe. *Sci. Rep.* **2017**, *7*, 3416.
(21) Masutani, K.; Morikawa, M.; Kimizuka, N. A Liquid Azobenzene Derivative as a Solvent-Free Solar Thermal Fuel. *Chem. Commun.* **2014**, *50*, 15803−15806.
(22) Ishi-i, T.; Sakai, M.; Shinoda, C. Benzothiadiazole-Based Dyes That Emit Red Light in Solution, Solid, and Liquid State. *Tetrahedron* **2013**, *69*, 9475−9480.
(23) Lu, F.; Hagiwara, K.; Yoshizawa, M.; Nagura, K.; Ishihara, S.; Nakanishi, T. Luminescence Tuning with Excellent Colour Homogeneity and Steadiness Using Fluorescent Molecular Liquids. *J. Mater. Chem. C* **2019**, *7*, 2577−2582.
(24) Narayan, B.; Nagura, K.; Takaya, T.; Iwata, K.; Shinohara, A.; Shinmori, H.; Wang, H.; Li, Q.; Sun, X.; Li, H.; Ishihara, S.; Nakanishi, T. The Effect of Regioisomerism on the Photophysical Properties of Alkylated-Naphthalene Liquids. *Phys. Chem. Chem. Phys.* **2018**, *20*, 2970−2975.
(25) Allain, C.; Piard, J.; Brosseau, A.; Han, M.; Paquier, J.; Marchandier, T.; Lequeux, M.; Boissière, C.; Audebert, P. Fluorescent and Electroactive Low-Viscosity Tetrazine-Based Organic Liquids. *ACS Appl. Mater. Interfaces* **2016**, *8*, 19843−19846.
(26) Petrova, D.; Weber, B.; Allain, C.; Audebert, P.; Venner, C. H.; Brouwer, A. M.; Bonn, D. Fluorescence Microscopy Visualization of the Roughness-Induced Transition between Lubrication Regimes. *Sci. Adv.* **2019**, *5*, No. eaaw4761.
(27) Ribierre, J.-C.; Aoyama, T.; Muto, T.; Imase, Y.; Wada, T. Charge Transport Properties in Liquid Carbazole. *Org. Electron.* **2008**, *9*, 396−400.
(28) Xu, D.; Adachi, C. Organic Light-Emitting Diode with Liquid Emitting Layer. *Appl. Phys. Lett.* **2009**, *95*, No. 053304.
(29) Hirata, S.; Kubota, K.; Jung, H. H.; Hirata, O.; Goushi, K.; Yahiro, M.; Adachi, C. Improvement of Electroluminescence Performance of Organic Light-Emitting Diodes with a Liquid-Emitting Layer by Introduction of Electrolyte and a Hole-Blocking Layer. *Adv. Mater.* **2011**, *23*, 889−893.
(30) Hirata, S.; Heo, H. J.; Shibano, Y.; Hirata, O.; Yahiro, M.; Adachi, C. Improved Device Lifetime of Organic Light Emitting Diodes with an Electrochemically Stable π-Conjugated Liquid Host in the Liquid Emitting Layer. *Jpn. J. Appl. Phys.* **2012**, *51*, No. 041604.
(31) Kobayashi, N.; Kuwae, H.; Oshima, J.; Ishimatsu, R.; Tashiro, S.; Imato, T.; Adachi, C.; Shoji, S.; Mizuno, J. A Wide-Energy-Gap Naphthalene-Based Liquid Organic Semiconductor Host for Liquid Deep-Blue Organic Light-Emitting Diodes. *J. Lumin.* **2018**, *200*, 19−23.
(32) Bai, X.; Sun, Y.; Jiang, Y.; Zhao, G.; Jiang, J.; Yuan, C.; Liu, M. Circularly Polarized Luminescence from Solvent-Free Chiral Organic π-Liquids. *Angew. Chem., Int. Ed.* **2021**, *60*, 3745−3751.
(33) Takaishi, K.; Matsumoto, T.; Kawataka, M.; Ema, T. Circularly Polarized Luminescence Liquids Based on Siloxybinaphthyls: Best Binaphthyl Dihedral Angle in the Excited State. *Angew. Chem., Int. Ed.* **2021**, *60*, 9968−9972.
(34) Shim, C.-H.; Hirata, S.; Oshima, J.; Edura, T.; Hattori, R.; Adachi, C. Uniform and Refreshable Liquid Electroluminescent Device with a Back Side Reservoir. *Appl. Phys. Lett.* **2012**, *101*, No. 113302.
(35) Machida, T.; Taniguchi, R.; Oura, T.; Sada, K.; Kokado, K. Liquefaction-Induced Emission Enhancement of Tetraphenylethene Derivatives. *Chem. Commun.* **2017**, *53*, 2378−2381.
(36) Lu, F.; Nakanishi, T. Solvent-Free Luminous Molecular Liquids. *Adv. Opt. Mater.* **2019**, *7*, No. 1900176.
(37) Madhu, M.; Ramakrishnan, R.; Vijay, V.; Hariharan, M. Free Charge Carriers in Homo-Sorted I -Stacks of Donor-Acceptor Conjugates. *Chem. Rev.* **2021**, *121*, 8234−8284.
(38) Peng, X.; Wang, L.; Chen, S. Donor−Acceptor Charge Transfer Assemblies Based on Naphthalene Diimides (NDIs). *J. Incl. Phenom. Macrocycl. Chem.* **2021**, *99*, 131−154.
(39) Lokey, R. S.; Iverson, B. L. Synthetic molecules that fold into a pleated secondary structure in solution. *Nature* **1995**, *375*, 303−305.
(40) Wakchaure, V. C.; Pillai, L. V.; Goudappagouda; Ranjeesh, K. C.; Chakrabarty, S.; Ravindranathan, S.; Rajamohanan, P. R.; Babu, S. S. Charge Transfer Liquid: A Stable Donor−Acceptor Interaction in the Solvent-Free Liquid State. *Chem. Commun.* **2019**, *55*, 9371−9374.
(41) Wakchaure, V. C.; Veer, S. D.; Nidhankar, A. D.; Goudappagouda; Nayak, R.; Asokan, K.; Ravindranathan, S.; Babu, S. S. Donor−Acceptor Based Solvent-Free Organic Liquid Hybrids with Exciplex Emission and Room Temperature Phosphorescence. *Chem. Commun.* **2022**, *58*, 1998−2001.
(42) Lakowicz, J. R. Excited-State Reactions. In *Principles of Fluorescence Spectroscopy*; Springer, Boston, MA, 1999.
(43) Guo, J.; Zhen, Y.; Dong, H.; Hu, W. Recent Progress on Organic Exciplex Materials with Different Donor−Acceptor Contacting Modes for Luminescent Applications. *J. Mater. Chem. C* **2021**, *9*, 16843−16858.
(44) Tanabe, Y.; Tsutsui, H.; Matsuda, S.; Shikita, S.; Yasuda, T.; Isoda, K. Pyromellitic-Diimide-Based Liquid Material Forming an Exciplex with Naphthalene. *ChemPhotoChem.* **2023**, *7*, No. e202200287.
(45) Yang, X.; Zhou, G.; Wong, W.-Y. Functionalization of Phosphorescent Emitters and Their Host Materials by Main-Group Elements for Phosphorescent Organic Light-Emitting Devices. *Chem. Soc. Rev.* **2015**, *44*, 8484−8575.
(46) Baroncini, M.; Bergamini, G.; Ceroni, P. Rigidification or Interaction-Induced Phosphorescence of Organic Molecules. *Chem. Commun.* **2017**, *53*, 2081−2093.
(47) Forni, A.; Lucenti, E.; Botta, C.; Cariati, E. Metal Free Room Temperature Phosphorescence from Molecular Self-Interactions in the Solid State. *J. Mater. Chem. C* **2018**, *6*, 4603−4626.
(48) Kabe, R.; Notsuka, N.; Yoshida, K.; Adachi, C. Afterglow Organic Light-Emitting Diode. *Adv. Mater.* **2016**, *28*, 655−660.
(49) Zhang, G.; Palmer, G. M.; Dewhirst, M. W.; Fraser, C. L. A Dual-Emissive-Materials Design Concept Enables Tumour Hypoxia Imaging. *Nat. Mater.* **2009**, *8*, 747−751.
(50) Nidhankar, A. D.; Goudappagouda; Wakchaure, V. C.; Babu, S. S. Efficient Metal-Free Organic Room Temperature Phosphors. *Chem. Sci.* **2021**, *12*, 4216−4236.
(51) Ventura, B.; Bertocco, A.; Braga, D.; Catalano, L.; d'Agostino, S.; Grepioni, F.; Taddei, P. Luminescence Properties of 1,8-Naphthalimide Derivatives in Solution, in Their Crystals, and in Co-Crystals: Toward Room-Temperature Phosphorescence from Organic Materials. *J. Phys. Chem. C* **2014**, *118*, 18646−18658.
(52) Chen, X.; Xu, C.; Wang, T.; Zhou, C.; Du, J.; Wang, Z.; Xu, H.; Xie, T.; Bi, G.; Jiang, J.; Zhang, X.; Demas, J. N.; Trindle, C. O.; Luo, Y.; Zhang, G. Versatile Room-Temperature-Phosphorescent Materials Prepared from N-Substituted Naphthalimides: Emission Enhancement and Chemical Conjugation. *Angew. Chem., Int. Ed.* **2016**, *55*, 9872−9876.
(53) Wei, J.; Liang, B.; Duan, R.; Cheng, Z.; Li, C.; Zhou, T.; Yi, Y.; Wang, Y. Induction of Strong Long-Lived Room-Temperature Phosphorescence of N-Phenyl-2-naphthylamine Molecules by Con-

https://doi.org/10.1021/acs.accounts.3c00670
Acc. Chem. Res. 2024, 57, 670−684

finement in a Crystalline Dibromobiphenyl Matrix. *Angew. Chem., Int. Ed.* **2016**, *55*, 15589−15593.
(54) Komura, M.; Sotome, H.; Miyasaka, H.; Ogawa, T.; Tani, Y. Photoinduced Crystal Melting with Luminescence Evolution Based on Conformational Isomerisation. *Chem. Sci.* **2023**, *14*, 5302−5308.
(55) Goushi, K.; Yoshida, K.; Sato, K.; Adachi, C. Organic Light-Emitting Diodes Employing Efficient Reverse Intersystem Crossing for Triplet-to-Singlet State Conversion. *Nat. Photonics* **2012**, *6*, 253−258.
(56) Lee, S. Y.; Yasuda, T.; Komiyama, H.; Lee, J.; Adachi, C. Thermally Activated Delayed Fluorescence Polymers for Efficient Solution-Processed Organic Light-Emitting Diodes. *Adv. Mater.* **2016**, *28*, 4019−4024.
(57) Zhang, Q.; Li, J.; Shizu, K.; Huang, S.; Hirata, S.; Miyazaki, H.; Adachi, C. Design of Efficient Thermally Activated Delayed Fluorescence Materials for Pure Blue Organic Light Emitting Diodes. *J. Am. Chem. Soc.* **2012**, *134*, 14706−14709.
(58) Venugopal, G.; Kumar, V.; Jadhav, A. B.; Dongre, S. D.; Khan, A.; Gonnade, R.; Kumar, J.; Babu, S. S. Boron- and Oxygen-Doped π-Extended Helical Nanographene with Circularly Polarised Thermally Activated Delayed Fluorescence. *Chem. Eur. J.* **2024**, *30*, 202304169.
(59) Zhang, T.; Xiao, Y.; Wang, H.; Kong, S.; Huang, R.; Ka-Man Au, V.; Yu, T.; Huang, W. Highly Twisted Thermally Activated Delayed Fluorescence (TADF) Molecules and Their Applications in Organic Light-Emitting Diodes (OLEDs). *Angew. Chem., Int. Ed.* **2023**, *62*, e202301896.
(60) Tang, G.; Sukhanov, A. A.; Zhao, J.; Yang, W.; Wang, Z.; Liu, Q.; Voronkova, V. K.; Di Donato, M.; Escudero, D.; Jacquemin, D. Red Thermally Activated Delayed Fluorescence and the Intersystem Crossing Mechanisms in Compact Naphthalimide−Phenothiazine Electron Donor/Acceptor Dyads. *J. Phys. Chem. C* **2019**, *123*, 30171−30186.
(61) Guo, Y.; Guan, H.; Li, P.; Wang, C.; Wu, Z.; Wang, Y.; Yu, Z.; Zhang, Z.; Wang, S.; Zhao, G. Thermally Activated Delayed Fluorescence Enabled by Reversed Conformational Distortion for Blue Emitters. *J. Phys. Chem. Lett.* **2021**, *12*, 9501−9507.
(62) Isoda, K.; Orita, Y. Stimuli-responsive Behaviors for Room-temperature Fluorescent Liquid Materials based on N-Heteroacenes and their Mixtures in Response to HCl Vapor and their Facile Synthesis. *ANAL. SCI.* **2021**, *37*, 469−473.
(63) Tateyama, A.; Nakanishi, T. Responsive Molecular Liquid Materials. *Responsive Mater.* **2023**, *1*, No. e20230001.
(64) Shinohara, A.; Pan, C.; Guo, Z.; Zhou, L.; Liu, Z.; Du, L.; Yan, Z.; Stadler, F. J.; Wang, L.; Nakanishi, T. Viscoelastic Conjugated Polymer Fluids. *Angew. Chem., Int. Ed.* **2019**, *58*, 9581−9585.

https://doi.org/10.1021/acs.accounts.3c00670
Acc. Chem. Res. 2024, 57, 670−684

International Journal of Entomology Research
www.entomologyjournals.com
ISSN: 2455-4758
Received: 11-12-2023, Accepted: 27-12-2023, Published: 12-01-2024
Volume 9, Issue 1, 2024, Page No. 61-65

A Detailed exploration on termites (Isopteran; Termitidae) Ecology of vegetative gradient in Gulbarga University Campus, Kalaburagi

Varis[1], Rabiya Begum[2*], K Vijay Kumar[3], Pruthviraj C B[4], Shashikanta H Majagi[2]
[1] Department of Zoology, SP Arts, Science and JMB Commerce Degree College Shorapur, Yadagir, Karnataka, India
[2] Department of Zoology, Vijayanagara Sri Krishnadevaraya University, Ballari, Karnataka, India
[3] Department of Zoology, Gulbarga University, Kalaburagi, Karnataka, India
[4] Department of Zoology, Kottureshawra Degree College, Kottur, Karnataka, India

Abstract
Termites are social insects belonging to the order Isoptera; it exhibits polymorphism and showing various ecologically important activities along with some destructive activities as they usually feed upon wooden structures. The present investigation yielded in recording of 2 different species of termites belonging to the genus *Odontotermes* (Family: Termitidae) namely, *Odontotermes wallonensis* and *Odontotermes brunneus* from Gulbarga University campus, Kalaburagi. Soil samples collected from the mounds represented by *Odontotermes wallonensis* of different soil types were analyzed for Physio-chemical parameters such as elemental analysis and pH was also recorded. During the study, analysis of 40 termite mounds where done which showed the dominance of *Odontotermes wallonensis* in the taken study area.

Keywords: Ecology, Termites, Kalaburagi, Physio-Chemical characters, Mount soil sample

Introduction

Termites are small, white or brownish terrestrial social insects exhibiting very well-organized polymorphism, categorizing into fertile caste (workers, soldiers, king, and queen) and the sterile caste belonging to order isopteran originated nearly 100 million years ago. Termites are often known as 'kashtaharika' or wood-feeders as per the ancient Sanskrit literature, also termites are commonly named as white ants, 'Udai' or 'deemak'. A total of 3106 species of termites have been described (Sudipta *et al.*, 2017) [14] of which only 371(12.4%) have been reported as destructive and only 104 (3.5%) are considered as serious pests. Bose (1994) reported 95 species of termites belonging to 5 families from southern India. Termites are usually known for their destructive nature as they cause severe damage to the wooden structures but they play vital role in ecosystem by recycling of plant nutrients because of their detritivore's nature and consuming dead plant materials at any level of decomposition (Pooja *et al.*, 2017). Economically termites are not only the serious pests of agriculture and plantations but also, they cause enormous damage to structural wood in different types of houses in all tropical and subtropical countries (Bignell and Eggleton, 1998 & 2000; Qaseem 2015) [12]. Subterranean termites foremost harmful wood tormentor within the world, build their colonies within the soil and frequently work their means on top of the bottom to achieve wood or any other cellulose source.

Present investigations carried out in the campus of the Gulbarga University, Kalaburagi from Jan 2018 to May 2018 to determine the termite diversity and distribution which also involved the analysis of physio-chemical parameters of the mound.

Materials and methods

Study area

The Gulbarga University campus is situated on 860 acres of land 6 kilometers east of Kalaburagi city at an elevation of 1556ft., (17˚18˙46" N latitude and 76˚52˙32" E longitude). The study area exhibits dry deciduous type of vegetation were temperature ranges from 20˚C to 45˚C with average rainfall of about 750mm.The study area was divided into 5 blocks (Fig 1) such as:

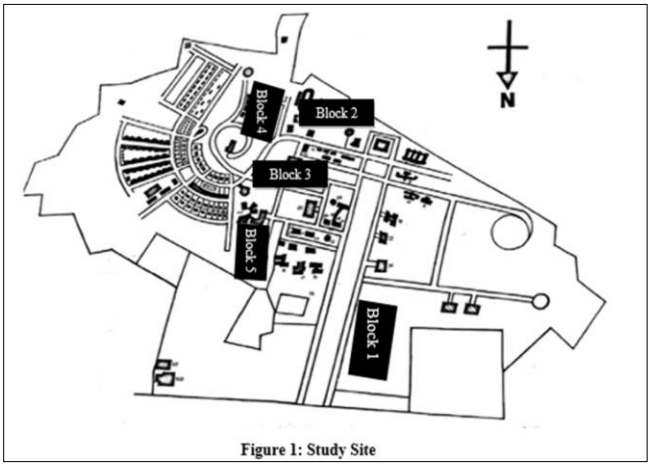

Fig 1: Study site

Block 1: University 1st gate to boy's hostel surrounding area.
Block 2: Administrative block to Arts department and Sports department surrounding
area.
Block 3: Girls Hostel front and back area.
Block 4: Guest House and quarters surrounding area.

Block 5: Botanical Garden and surrounding departments Chemistry, Botany, Physics,
Microbiology, Biochemistry, Biotechnology, material science and USIC

Department
Collections were carried out weekly from Jan 2018 to May 2018 by Quadrate method and Lines transect sampling method (Plate 1-3). Termites were collected and preserved in 70% alcohol for further identification. Later different casts from each species were photographed by stereo zoom microscope.

Analysis of Physio-chemical parameters of termite mounts soil
A total of 3 representative mounds were selected based on nesting soil type (Red, Black and Grey) of Block 1 and 2. Later pH of the soil samples from different mounds determined electrometrically using glass electrode pH meter. The elemental analysis of termite mound soil was carried out at USIC department, Gulbarga University, Kalaburagi.

Results
Survey and distribution of termites: There are 2 different species of termite's namely *Odontotermes wallonensis* and *Odontotermes brunneus* belonging to family Termitidae were dominantly found in different sites of the campus (Plate 4-8). During the present study worker, soldier and queen were observed and recorded. The percentage of occurrence was more with *Odontotermes wallonensis* (57.5%) followed by *Odontotermes brunneus* (42.5%) from the forty recorded nest. The measurements of termite mount were made to analyze variation in nest formation and species specificity (Table 1).

Analysis of Physio-chemical parameters of termite mounts soil: The physio-chemical parameters of different termite mound soil varied with respect to pH, K, Mg and Mn. Manganese was highest in all type of soil samples compared to potassium and magnesium. The pH of all the soil samples is towards basic ranging between7.92 to 8.23 (Table 2).

Plate 1: Vertical section of the mound of *O.wallonensis* showing scattered fungus Combs And royal chamber with queen in the base of the mound.

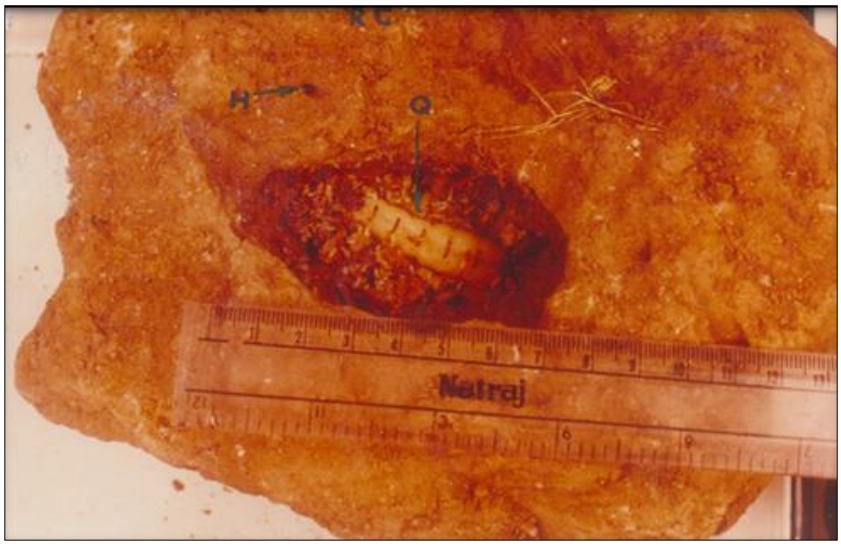

RC = Royal chamber; Q = Queen; H = Holes

Plate 2: Showing vertical section of the royal chamber with queen inside. Royal Chamber of the termite *O. wallonensis* shown with an arrow mark.

Plate 3: Showing nymphs of the reproductive caste of the termite *O. wallonensis*. Showing small wing pads to the nymph

Plate 4: Showing nursery vaults excavated from the established nests of the Termite *O. wallonensis*

Plate 5: Nest of *O. brunneus* with scattered turrets having open holes on the Turrets, Gulbarga University Campus, Gulbarga

Table 1: The height, diameter and temperature of the mound nest of the termites.

Sl.no.	Height (FT)	Diameter(FT)	Temperature(^{0}c)
1	5.5	20	31
2	4	15.5	29
3	3.5	25.5	30
4	4	17	32
5	3.6	15	30
6	6	30.5	31
7	1	33	30
8	2	12.5	32
9	2	22	33
10	1.5	11	34
11	6.6	21.6	34
12	5	17	27
13	3	6.7	26
14	4	8	29
15	3	6.8	29
16	1.5	3.5	31
17	3	7.6	32
18	4.5	15	28
19	3.5	8	29
20	4.6	10	31
21	4	9	30
22	3.5	7	31
23	4	7	31
24	5	11.7	33
25	6	13	30
26	5.5	18	31
27	5	11	32
28	3	7.6	33
29	4.9	28.5	33
30	0.5	11.6	34
31	7	35	33
32	5	27.6	33
33	4.5	27	31
34	2	14	31
35	1.5	10	30
36	5	18	30
37	7	31	29
38	7	20	31
39	5	16	31
40	4	18	30

Table 2: Analysis of Physio-chemical parameters of different termite species soil samples.

Sl. No	Termite species	Soil type	pH	K(mg/l)	Mn(mg/l)	Mg(mg/l)
1.	*Odontotermes wollenses*	Red soil	7.92	8.772	23.539	4.134
		Black soil	8.11	8.427	23.539	4.173
		Grey soil	8.23	8.768	23.539	4.202

Discussion

In Gulbarga university campus there are several types of termite mound were identified such as dry and moist mounds. Termites act both beneficial and harmful to the environment. The harmful effects are they damage crops, properties, and trees; they are beneficial to the ecosystem which enriches the soil fertility. The study area is one of the best places for the termites as it provides a good habitat for the termites. It provides food and shelter for the termites. It is because the atmospheric moisture throughout the year is around 60-80%, additionally plenty of food in terms of cellulolytic material is available. Only 2 species were identified. Observations made on the physicochemical characters of the mounds nest and graphical representation is shown as Graph No. 1- 7. Difference in the height and diameter of mound also depends on the disturbance caused by human beings, rainy winds, foraging domestic and wild herbivore, which destroys these mounds, consequently they reproduce again and again by the workers. As the termite queen grows year by year in length and weight, her fecundity is also enhanced. Thus, the growth of the queen and the enhancement of the fecundity year by year are the root cause of the increase in the population and resultant changes in the dimensions of mound nest and weight of the fungus comb. The mother queen during copulation stores a large number of sperms in her sperm theca and uses them whenever required.

In the present study area, a total of 5 transects were surveyed for the termite mound. The mounds belong to *Odentotermes wallonensis* are constructed largely on the earth surface among these nests maximum mounds were witnessed in botanical garden and minimum at guest house. It may be because botanical garden is a fully vegetative area with loose soil and undisturbed. It protected by fencing hence number of mounds were recorded in contrast. Whereas the guest house area is hilly terrain with disturbance by the devotees, staff, and guest hence a smaller number of mounds was recorded in the entire study. A single wood-boring mound was noticed. A future study on the species of the termites in the study area is required.

Conclusion

In the Gulbarga university campus, the habitat changes have led to the strong modifications of the termite community in terms of the species richness, species composition, biomass, and density. As the sampling in this study was restricted to the soil, the species richness in this report is probably underestimated to a certain extent. Sampling from various niches within the habitats like logs, busy landmass, and etc. anthropoid disturbance strongly affects the functioning of the natural ecosystem through modifications of vegetation, soil properties, and soil fauna communities.

Our synthesis is intended to identify knowledge gaps regarding the controls on termite abundances and distributions and to put into perspective why an understanding of their abundances is needed to project vegetation and function accurately. The *Odontotermes wallonensis* is dominant and distributed throughout the campus. The Physio-Chemical parameters of various termite mound nest soil varied with respect to the different soil type. Mn is comparatively higher than other constituents K and Mg. pH was basic and Potassium content was in normal range with respect to soil fertility. A key conclusion is that the lack of data on the ecology of termites in dry regions is a barrier to generalized, major conceptual advances for this insect guild. Thus, we must emphasize the critical need for further study of these species in non-urban, intact ecosystems, with a particular focus on their assistance identifying termites.

Acknowledgement

The authors are thankful to authorities of Gulbarga University for providing necessary facilities to carry out this work also a special thanks to the USIC Department for helping out in elemental analysis.

References

1. Vasantkumar B, Vijaykumar K. Population density of various castes in different part d of the mound of the termite *Odontotermes wallonensis wasmann* (Isopteran: Termitidae). Lake; Wetlands, Biodiversity & Climate change, 2010.
2. Bignell DE, Eggleton P. Termites in ecosystems. In: Termites: Evolution, Sociality, Symbioses, Ecology. (eds T. Abe, M. Higashi & D. E. Bignell). Kluwer Academic Press, Dordrecht, The Netherlands, 2000.
3. Bishwajeet Paul, Md. Aslam Khan, Sangeeta Paul, Karuppan Shankar Ganesh, Sarbashish Chakravorty. Termites and Indian agriculture. Springer international publishing, Termites and sustainable management, sustainability in plant and crop protection, 2018, 51-98.
4. Bhurli P, Chimkod VB. Effect of *in vitro* environmental conditions on the biological attributes of termite *Odontotermes wallonensis.* International & multidisciplinary research journal,2012:2(12):36-39.
5. Chhotani OB. Fauna of India-Isoptera (Termites). Vol. II. Zoological Survey of India Publication, Calcutta, 1997, 800.
6. Ferry B. Distribution of the important litter decomposing termites (Isoptera) in the western ghats forests of Karnataka (India). Pedobiolodia,1992:36:193-211.
7. Freise F. The significance of ants and termites in tropical forests. An. Brasil. Econ. Forestal.,1949:2:145-154.
8. Pardeshi MK, Kumar D, Bhattacharyya AK. Termite (Insecta: Isoptera) fauna of some agricultural crops of Vadodara, Gujarat (India). Zoological Survey of India,2010:110(I):47-59.
9. Pooja BB, Vybhava KB, Vaibhav PU, Soumya R Patil, Pulikeshi M Biradar. Survey of termite and physio-chemical parameters of termite soil samples collected from Karnataka University Campus, Dharwad. ISOR Journal of environmental science, 2017.
10. Pranesh MK, Harini BP. Comparative morphological divergence among few common Indian species of the family Termitidae: Isoptera. International Journal of Advanced Research,2014:2(4):523-531.
11. Qaseem S, Rajashekhar M, Vijaykumar K. Diversity of termite fauna in urban systems. International journal of multidisciplinary educational research,2015:8(2):53-57.
12. Qaseem S, Rajashekhar M, Vijaykumar K. Preliminary studies on structural wood in urban systems. International journal of multidisciplinary educational research,2015:8(2):15-25.
13. Singh BK, Roy SP. Studies on the role of termites (Insecta: Isoptera) in the decomposition of leaf litters of deciduous tropical forest. The Bioscan,2008:3(1):89-91.
14. Sudipta CK, Shankar, Chanrilla K. Ecological and medicinal importance of termite fauna. The NEHU journal,2017:15(1):79-87.
15. Vasconcelos HL. Effects of forest disturbance on the structure of ground foraging ant communities in Central Amazonia Biodiversity and Conservation,1999:8(3):409-420.

International Journal of Entomology Research

Indexed Journal, Refereed Journal, Peer Reviewed Journal

ISSN: 2455-4758

Publication Certificate

This certificate confirms that **Varis** has published article titled **A Detailed exploration on termites (Isopteran; Termitidae) Ecology of vegetative gradient in Gulbarga University Campus, Kalaburagi** .

Details of Published Article as follow:

Volume	:	**9**
Issue	:	**1**
Year	:	**2024**
Page Number	:	**61-65**
Reference No.	:	**9008**
Published Date	:	**12 Jan, 2024**

Regards
International Journal of Entomology Research
www.entomologyjournals.com
entomol.article@gmail.com

MHD Carreau hybrid nanoliquid flow over a stagnation region of poignant needle: An enhanced heat transmission model

Sunita J[1], Suresh Biradar[2] and Samrat SP[3]
[1]Department of Mathematics, Sharanbasva University, Kalaburagi, Karnataka, India 585103.
[2]Department of Mathematics, Sharanbasva University, Kalaburagi, Karnataka, India 585103.
[3]Department of Mathematics, Shri Prabhu Arts, Science & JM Bohra Commerce College Shorapur, Karnataka, India 585224

Abstract. An unsteady 2D MHD enhanced Carreau hybrid nanoliquid over a stagnation region of poignant needle with chemical reaction is studied numerically. The governing PDEs are condensed into system of nonlinear ODEs and attained equations are tackled by using bvp5c MATLAB scheme. Moreover, the impacts of numerous physical factors over the flow fields are confer and expressed through plots. Numerical results of Nusselt and Sherwood number, wall friction are inspected and displayed thru tables. The main motive of this investigation is to examine the thermal and mass transmission mechanism of Carreau hybrid nanoliquid under the action of magnetic effect and in the absence of magnetic effect. Results obtained reveals thatthe needle thickness factor is capable of diminishing fluid flow, heat transfer and enriching concentration description. The Weissenberg number diminishes the rate of flow whereas the reverse trend isobserved for thermal distribution. Evidently, heat transport mechanism is highly influential in magnetic effects rather in the absence of magnetic effect.

Key words: MHD, thin needle, chemical reaction, hybrid nanoliquid, uneven heat source

1. Introduction

The transference of heat through a diverse medium has tremendous applicability in recent developments. Industries and engineering activities needs heat transference to accumulate inventions of daily desires. Numerous authors haveperformedcritical studies on heat transfer process to help industrial growths. The present paper also tries to convey the importance of heat in several areas. It cooperate the nano and hybrid nano liquids drive thru stretching sheet. Basically, nanoliquids (it contains single nano-sized particles) are noble conductive property to transference heat and avoid the losses of energies. It concoctions base liquids and conductive/inductive metals to rheostat heat performance. Nanoliquids are applied in solar energy procuring devices [1], oil recovery [2], cooling of electronic devices, nuclear reactor, power generation etc. Samrat et al. [3] examined the Casson nanofluid flow thru stretching sheet in presence of thermal radiation. They reveal that the viscidness of liquids has tendency to control the flow and enhance the conduciveness. Dogonchi et al. [4] studied the nanoliquid and its heat flow feature between parallel plates with MHD and radiation. Later, Sulochana et al. [5] elaborated the MHD radiative nanoliquid flow thru a rotary plane with Soret effect. Maboob et al. [6] examined the nanoliquids under the effects of MHD, viscidness and stretching parameter. It is perceived that magnetic effect leads to decrease momentum and increase temperature of the liquid.

During the rapid development and computations in heat transfer nanoliquids do not fulfil the industrial requirement. It's due to oxide and metallic nanoparticles were differently used and the conductive efficiency were diverse, extremely volatile and unstable. So that hybrid nanofluids is implemented to resolve these requirements. Elattar et al. [7] discussed the computational work on hybrid-nanoliquid with hall current over a slender stretch area in the occurrence of chemical reaction. Nadeem et al. [8] reported that hybrid nanoliquids gains higher heat transfer rate as related to nanoliquids. Zainal et al. [9] considered magnetic effects on hybrid nanoliquids flow thru vertical smooth plate. They reported that fluid momentum increases by rising magnetic effects while converse act see in thermal profile. Tlili et al. [10] explained the Brownian movement's impacts to enhance the thermal field and dissipative accelerate both velocity and thermal profile. Waini et al. [11] investigated that stable flow of (HNF) hybrid nanofluid above a porous surface. They have fixed Al_2O_3 volume fraction and varied the other nanoparticles volume fraction and discussed the dual solutions. Alsaedi et al. [12] analysed numerically that flow of hybrid nanoliquid among two coaxial cylinders with magnetic effect. Results

showed that higher volume fraction of Cu leads to decay the thermal profile. Tlili et al. [13] studied the hybrid nanoliquid flow over irregular dimension surface with slip effect.

The flow of nano or hybrid nanoliquid thru moving needle has been studied. It has very helpful in experimental studies to determine velocity and heat transfer behaviour. Soid et al. [14] studied the unnatural convection flow over uninterrupted thin needle in a nanoliquid. The property of needle size on thermal and momentum outline were investigated. The stability analyse of convective flow to a poignant needle engrossed in a nanoliquid were reported by Salleh et al. [15]. Sulochana et al [16] was studied boundary layer analysis of moving thin needle in a nanoliquid with the influence of MHD and joule heating. Waini et al. [17] considered Cu and Al2O3 as nanoparticles and H_2O as a base liquid flow over poignant thin needle. They investigated that the Brownian movements leads to enhance concentration of hybrid liquid. Afridi et al. [18] studied irreversibility analysis of hybrid nanoliquid past a thin needle with dissipative effects.

An unsteady 2D MHD enhanced Carreau hybrid nanoliquid over a stagnation region of moving needle with chemical reaction is studied. The governing PDEs are condensed into system of nonlinear ODEs. The bvp5c MATLAB software is used for tables and graphical representation. Moreover, the effects of numerous physical factors over the flow fields are confer and expressed through graphs. Numerical results of Nusselt and Sherwood number, friction factor is inspected and displayed thru tables. We have got good results with comparing the existing literature.

2. Mathematical formulation

Presume a time independent two dimensional MHD flow of Carreau hybrid nanoliquid under the stagnation region of poignant needle, as depicted in fig. 1. We suppose that (x, r) signifies the axial and radial axis in cylindrical coordinate system, respectively, where c is the needle width. The magnitude of needle is as small as the boundary layer formed on it. Also, we assumed u_0 is a uniform velocity of the needle operating in horizontal direction and u_∞ is the mainstream velocity. A uniform magnetic field strength B_0 is imposed parallel to the path of motion as revealed in figure. The temperature of needle near boundary is greater than the ambient fluid temperature i.e. $T_0 > T_\infty$. Simultaneous solutions are deployed for with magnetized effect and without magnetized effects and irregular heat source effect and radiative impacts are taken into consideration.

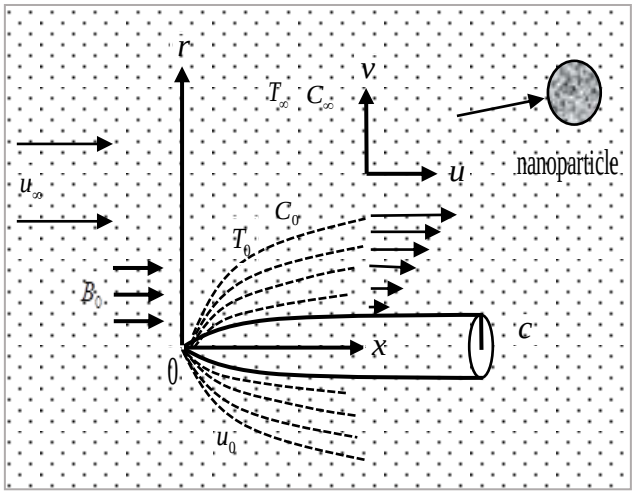

Fig. 1: Flow geometry

Under the above conventions, we formulated the following governing equations

$$\frac{\partial}{\partial x}(ru)+\frac{\partial}{\partial r}(rv)=0, \tag{1}$$

$$\rho_{hnf}\left(u\frac{\partial u}{\partial x}+v\frac{\partial u}{\partial r}\right)=\mu_{hnf}\left\{\frac{1}{r}\frac{\partial}{\partial r}\left(r\frac{\partial u}{\partial r}\right)\left[3(n-1)\Gamma^2\left(\frac{\partial u}{\partial r}\right)^2\right]\right\}-\sigma_{hnf}B_0^2u, \tag{2}$$

$$(\rho c_p)_{hnf}\left(u\frac{\partial T}{\partial x}+v\frac{\partial T}{\partial r}\right)=k_{hnf}\frac{1}{r}\frac{\partial}{\partial r}\left(r\frac{\partial T}{\partial r}\right)+q''', \tag{3}$$

$$\left(u\frac{\partial C}{\partial x}+v\frac{\partial C}{\partial r}\right)=D_B\frac{1}{r}\frac{\partial}{\partial r}\left(r\frac{\partial C}{\partial r}\right)-H(C-C_\infty), \tag{4}$$

the appropriate boundary restrictions are,

$$\left.\begin{array}{l} u=u_0,\ v=0,\ T=T_0,\ C=C_0 \ \text{ at } \ r=R(x) \\ u\to u_\infty, T\to T_\infty, C\to C_\infty \ \text{ as } \ r=\infty \end{array}\right\}, \tag{5}$$

where u,v are the velocity components along x,y direction, respectively, $R(x)$ is the needle dimension.

In the energy equation (3) $q'''=\left(k_f U_0/x\nu_f\right)\{A(T_w-T_\infty)f'+B(T-T_\infty)\}$, is the irregular heat source/sink parameter, in which A and B are the coefficients of space and temperature dependent heat source and sink respectively. The similarity variables in eq. (6) used to reduce the equations (1) - (4) to the non-dimensional form and the effective nanofluid parameters are described in (7) as

$$\xi=\nu_f x f(\eta);\eta=\frac{U_0 r^2}{\nu_f x};u=\frac{\psi_r}{r};v=\frac{-\psi_x}{r};\theta(\eta)=\frac{T-T_\infty}{T_w-T_\infty};\psi(\eta)=\frac{C-C_\infty}{C_w-C_\infty};R(x)=\left[\frac{\nu_f xc}{U}\right]^{\frac{1}{2}}, \tag{6}$$

$$\left.\begin{array}{l} \dfrac{\mu_{hnf}}{\mu_f}=\dfrac{1}{(1-\phi_1)^{5/2}(1-\phi_2)^{5/2}},\quad \dfrac{\rho_{hnf}}{\rho_f}=\dfrac{\rho_{s_2}}{\rho_f}\phi_2+(1-\phi_1)(1-\phi_2)+\dfrac{\rho_{s_1}}{\rho_f}\phi_1(1-\phi_2), \\ \dfrac{k_{hnf}}{k_{nf}}=\dfrac{k_{s_2}+2k_{bf}-2(k_f-k_{s_2})\phi_2}{(k_f-k_{s_2})\phi_2+2k_f+k_{s_2}},\quad \dfrac{k_{nf}}{k_f}=\dfrac{k_{s_1}+2k_f-2(k_f-k_{s_1})\phi_1}{2k_f+(k_f-k_{s_1})\phi_1+k_{s_1}}, \\ \dfrac{(\rho c_p)_{hnf}}{(\rho c_p)_f}=\dfrac{(\rho c_p)_{s_2}}{(\rho c_p)_f}\phi_2+(1-\phi_1)(1-\phi_2)+\dfrac{(\rho c_p)_{s_1}}{(\rho c_p)_f}\phi_1(1-\phi_2), \\ \dfrac{\sigma_{hnf}}{\sigma_f}=\left[1+\dfrac{3\sigma_{s_1}\phi_{s_1}+\phi_{s_2}\sigma_{s_2}-\phi\sigma_f}{\sigma_{s_1}(1-\phi_{s_1})+\sigma_{s_2}(1-\phi_{s_2})+(2+\phi)\sigma_f}\right], \end{array}\right\}, \tag{7}$$

In the above equation (6) and (7) we notice that, $\xi, r=R(x), \varphi, \rho, \mu, k, \sigma$ and c_p describes the stream function, magnitude of the needle, volume fraction, density, viscosity, thermal conductivity, electrical conductivity and specific heat. The suffixes hnf and f represents the hybrid nanofluid and base liquid case.

The non-dimensional equations are obtained by using eq. (6-7) given by:

$$2\eta A_1\left(\frac{3(n-1)}{2}Wef''^2 f'''\right)+A_2\left(ff''-A_3Mf'\right)=0, \tag{8}$$

$$2A_4\left(\eta\theta''+\theta'\right)+A_5\,\mathrm{Pr}\, f\theta'+\left(Af'+B\theta\right)=0, \tag{9}$$

$$\psi''\eta+\psi'+Sc\left(Kr\psi+\frac{f\psi'}{2}\right)=0 \tag{10}$$

where $A_1=\dfrac{\mu_{hnf}}{\mu_f};A_2=\dfrac{\rho_{hnf}}{\rho_f};A_3=\dfrac{\sigma_{hnf}}{\sigma_f};A_4=\dfrac{k_{hnf}}{k_f};A_5=\dfrac{(\rho c_p)_{hnf}}{(\rho c_p)_f};$ (11)

transformed boundary restrictions are

$$\left.\begin{array}{l} f(c)=\dfrac{\lambda c}{2};\ f'(c)=\dfrac{\lambda}{2};\ \theta(c)=1;\ \psi(c)=1 \text{ at } \eta=c \\ f'(\eta)\to\dfrac{(1-\lambda)}{2};\ \theta(\eta)\to\dfrac{\lambda}{2};\ \psi(\eta)\to\dfrac{\lambda}{2} \ \text{ as } \eta\to\infty \end{array}\right\}, \tag{12}$$

where prime denotes the differentiation with respect to η and the dimensionless parameters namely, magnetic

field, Prandtl number, chemical reaction, ratio of needle velocity to the composite velocity and composite velocity, respectively are given as

$$\left.\begin{aligned} M=\frac{\sigma_{hnf}B_0^2}{2U_0\rho_f};\Pr=\frac{(\mu c_p)_f}{k_f};Kr=\frac{H}{U}\lambda=\frac{u_0}{U_0};U_0=u_0+u_\infty, \end{aligned}\right\}, \tag{13}$$

The physical entities of engineering interest are skin friction coefficient C_f , local Nusselt number Nu_x and local Sherwood number Sh_x which are given as

$$\left.\begin{aligned} C_{fx}&=\frac{4c^{1/2}A_1}{\mathrm{Re}_x^{1/2}}\left(\frac{3(n-1)}{2}We^2(f''(c))^3\right)\\ Nu_x&=-\left(\frac{2c^{1/2}A_4}{\mathrm{Re}_x^{-1/2}}\right)\theta'(c),\\ Sh_x&=-\left(\frac{2c^{1/2}D_B}{\mathrm{Re}_x^{-1/2}}\right)\psi'(c), \end{aligned}\right\}, \tag{14}$$

where $\mathrm{Re}_x=U_0x/\nu_f$.

3. Conversation of outcomes

In this fragment, the impact of apposite non-dimensional parameters like magnetic field (M), non-uniform heat source(A,B), Weissenberg number(We), nonlinearity index(n), needle thickness (c)and chemical reaction (Kr) on $f'(\eta),\theta(\eta)$ and $\psi(\eta)$ are deliberated by plotting the curves and C_{fx},Nu_x and Sh_x through tables. For the purpose of computational justification, the non-dimensional parameters are assigned the values as $M=2,A=B=0.5,\lambda=1,c=0.1,Sc=3,Kr=0.2,n=3,We=0.3,\phi_1,\phi_2=0.05$. The main drive of this research is to deliberate the comparative outcomes of heat and mass transport mechanism for with and without magnetic field effect cases.

Figs. 2, 3 & 4 unveil the response of needle thickness on momentum, energy and concentration fields. It depicts that the rise in needle thickness decreases the flow rate and energy profile whereas concentration fieldsare enriched. This happens because the needle size perturbs the free stream resulting in the drop of velocity as well as thermal fields. Figs. 5 - 6 illustrate the reverberations of nonlinearity index on velocity and temperature profiles. It is documented rise in velocity and fall in temperature. The sway of Weissenberg number is portrayed in the plots 7 and 8. The fluid velocity decays with extending values of Weissenberg number, while a reverse trend is experienced in case of thermal distribution. Increasing magnitude of We upsurges the relaxation time by decreasing fluid velocity. Figs. 9 and 10 put forward the consequences of non-uniform heat source parameter on thermal distribution respectively. The cumulative values of A and B demonstrate the relation of heat source, which direct the temperature field to rise.

The graphical trend of $\psi(\eta)$ with chemical reaction is displayed in fig. 11. It is noticed that the elevation of the Kr turns down $\psi(\eta)$. This happens because the molecular diffusivity reduces as the chemical reaction parameter enhances, resulting in the decline of $\psi(\eta)$.Figs. 12 and 13 set forth the impression of ϕ_1,ϕ_2 on $f'(\eta)$ and $\theta(\eta)$. The upliftment of the volume of nanoparticles lowers the $f'(\eta)$ and hikes the $\theta(\eta)$. Hike in temperature is same for both the cases of magnetic and without magnetic field.

The thermophysical properties of the nanoparticles Nimonic 80 A, Ti6Al4V and the base fluid water are enlisted in table 1. Further, tables 2, 3 and 4 inscribes the influence of prominent non-dimensional parameters on C_{fx},Nu_x and Sh_x with and without magnetic field cases respectively. Clearly the skin friction factor is augmented function of n and We , while it is decreasing function of c and ϕ_1,ϕ_2 for both the cases.By table 3

we reckon that n, c, We enhance the rate of heat transfer whereas A, B and ϕ_1, ϕ_2 descends it. Further, it is noted from table 4 that c, n, We and ϕ amplify the rate of mass transfer while Kr tend to dwindle it for both with and without magnetic effect cases. Table 5 portrays the validation of the present result for nonlinearity index upon local Nusselt number with the published literature for limiting cases and we discern a good agreement between them.

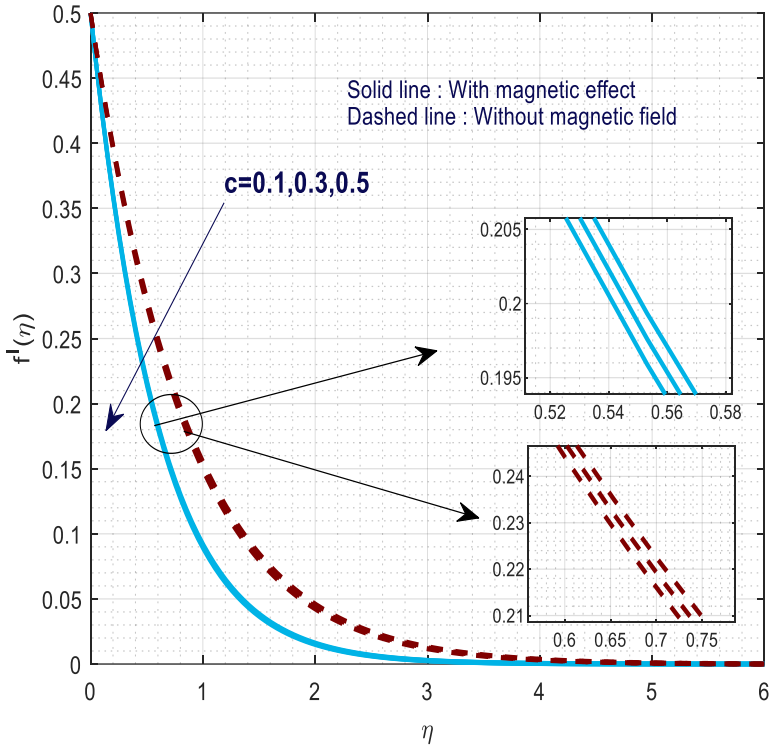

Fig. 2 Response of $f'(\eta)$ with c

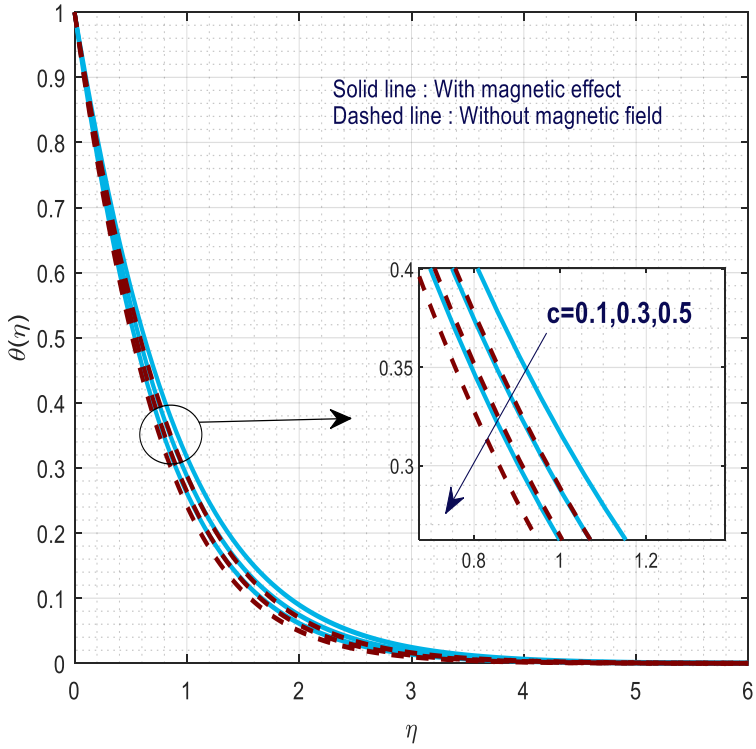

Fig. 3 Response of $\theta(\eta)$ with c

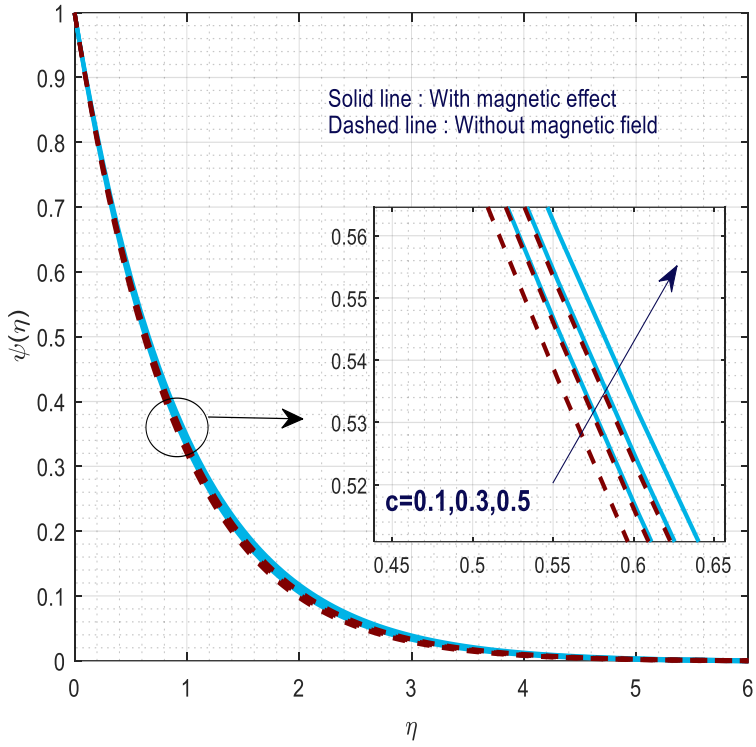

Fig. 4 Response of $\psi(\eta)$ with c

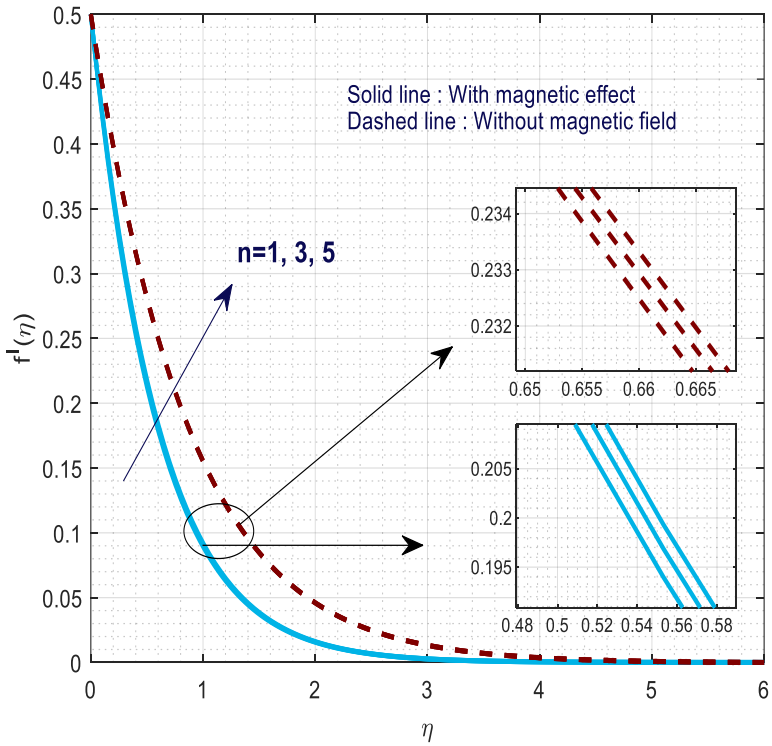

Fig. 5 Response of $f'(\eta)$ with n

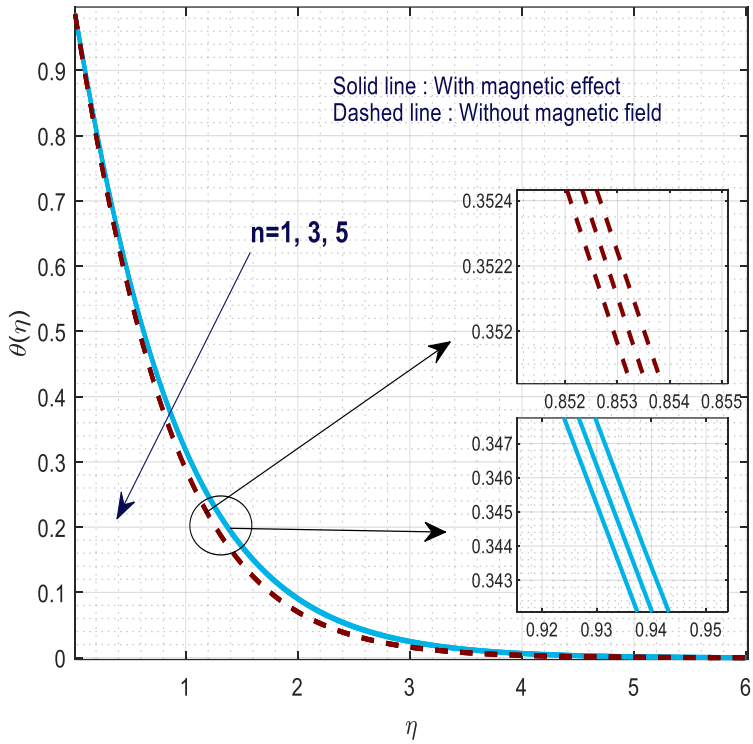

Fig. 6 Response of $\theta(\eta)$ with n

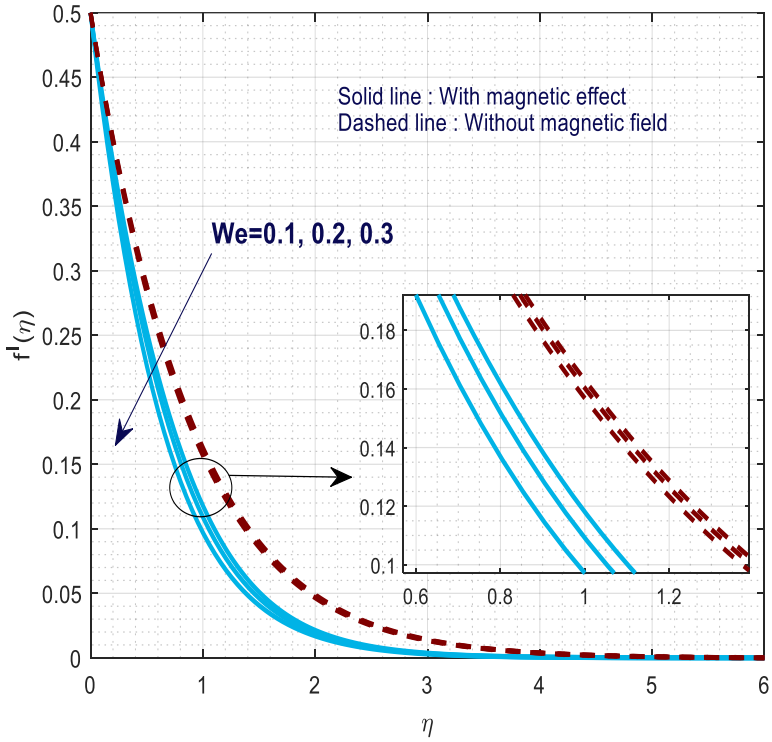

Fig. 7 Response of $f'(\eta)$ with We

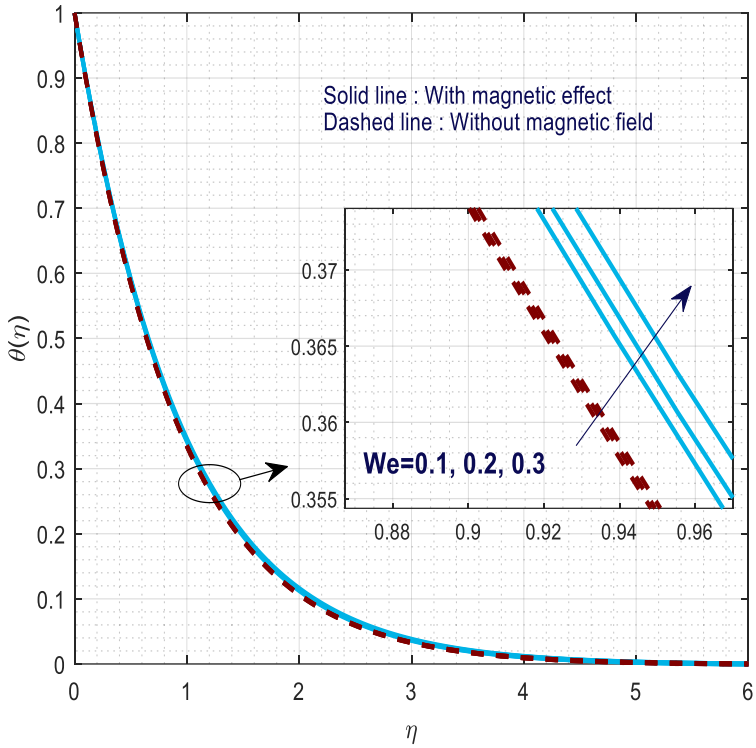

Fig. 8 Response of $\theta(\eta)$ with We

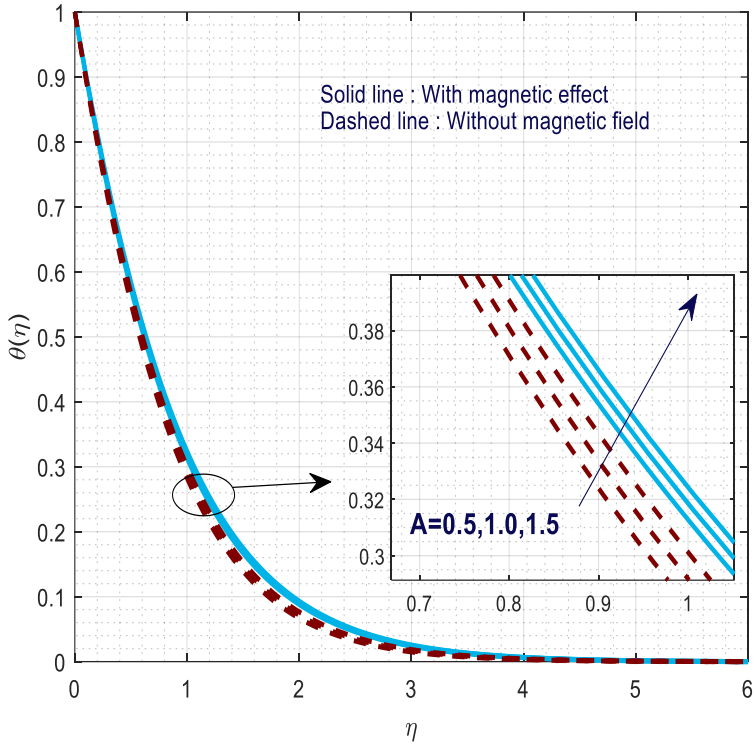

Fig. 9 Response of $\theta(\eta)$ with A

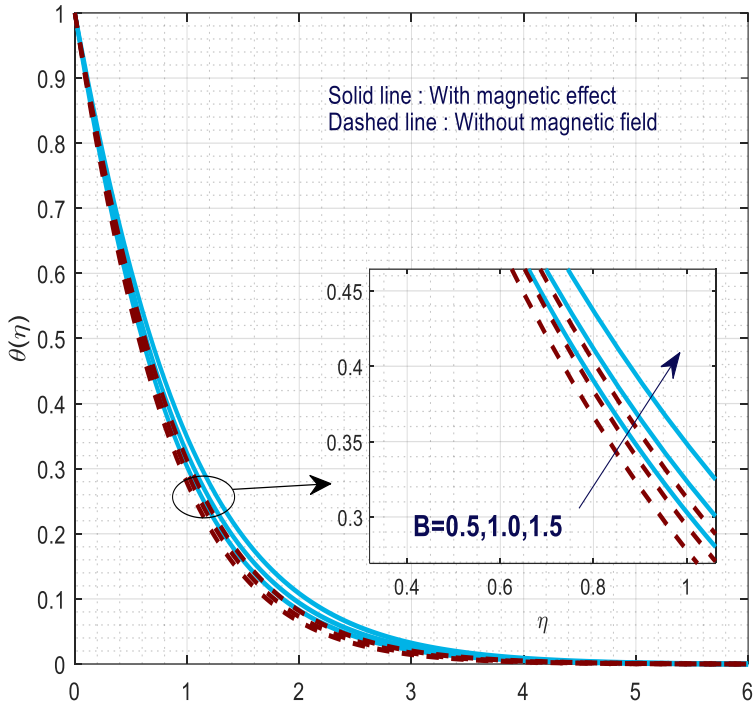

Fig. 10 Response of $\theta(\eta)$ with B

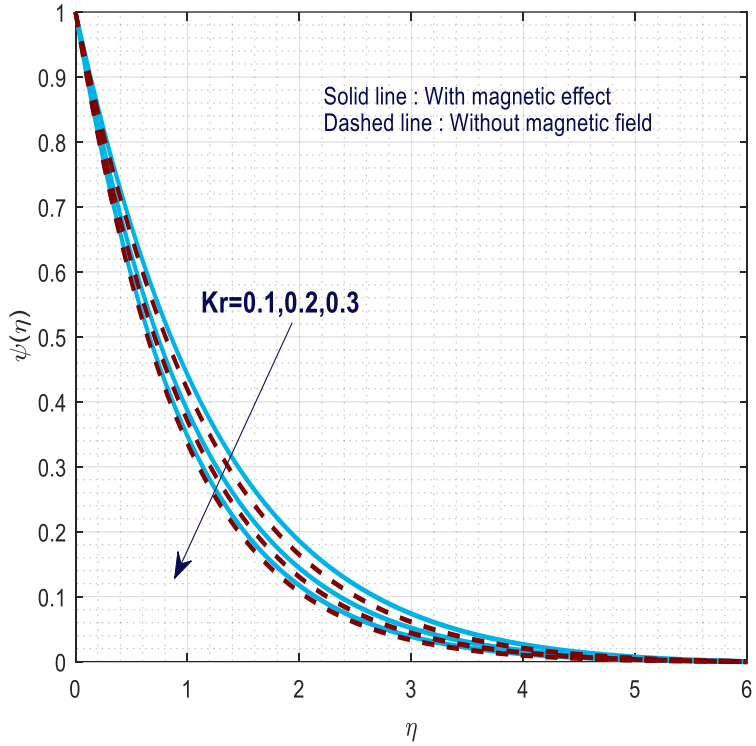

Fig. 11 Response of $\psi(\eta)$ with Kr

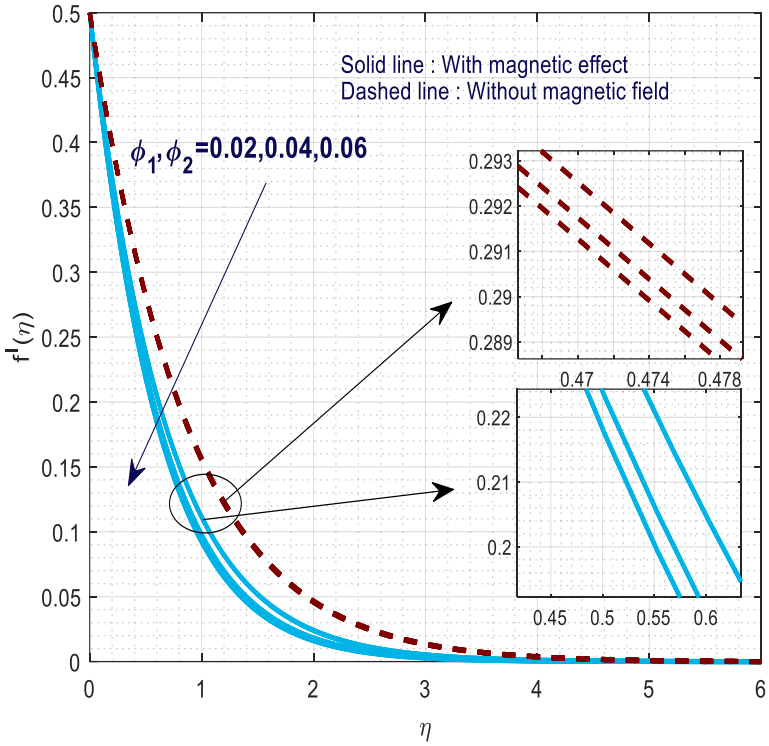

Fig. 12 Response of $f'(\eta)$ with ϕ_1, ϕ_2

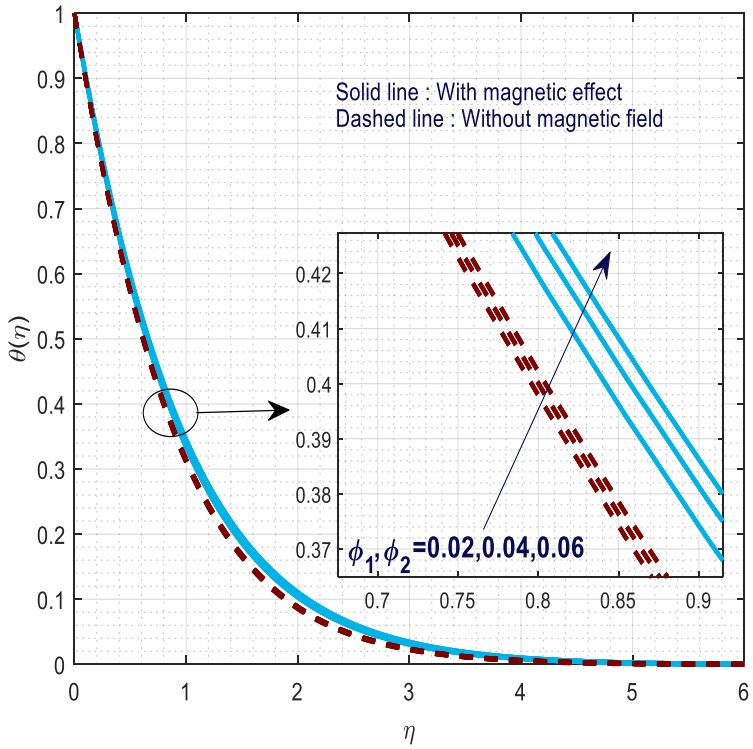

Fig. 13 Response of $\theta(\eta)$ with ϕ_1, ϕ_2

Table 1 Physio-thermal characteristic of nanoparticles and the base liquid

Physical Property	*Nimonic* 80*A*	*Ti*6*Al*4*V*	*Water*

$C_p(J/KgK)$	448	0.56	4179
$\sigma(S/m)$	8.8 x 10^{-5}	5.8 x 10^{-5}	21 x 10^{-5}
$\rho(Kg/m^3)$	8190	4420	997.1
$k(W/mK)$	112	7.2	0.613

Table 2 Variation in C_{fx} with magnetic effect and without magnetic effect cases

c	n	We	ϕ	C_{fx}	
				$M=2$	$M=0$
0.1				-1.317710	-0.930325
0.2				-1.879418	-1.338487
0.3				-2.321275	-1.667191
	1			-1.391434	-0.929356
	2			-1.348550	-0.926519
	3			-1.317558	-0.924020
		0.1		-1.234116	-0.915190
		0.2		-1.113789	-0.896626
		0.3		-1.056486	-0.885359
			0.02	-1.317558	-0.809218
			0.04	-2.403155	-0.924020
			0.06	-5.189737	-1.061504

Table 3 Variation in Nu_x with magnetic effect and without magnetic effect cases

c	n	We	A	B	ϕ	Nu_x	
						$M=2$	$M=0$
0.1						1.134889	0.906750
0.2						1.720297	1.385072
0.3						2.249101	1.823452
	1					0.854506	0.902346
	2					0.876781	0.922604
	3					0.898648	0.942840
		0.1				0.864666	0.903232
		0.2				0.876181	0.925913
		0.3				0.882957	0.937388
			0.5			0.871793	0.920714
			1.0			0.852075	0.893902
			1.5			0.832358	0.867092
				0.5		0.895339	0.935331
				1.0		0.839310	0.885942
				1.5		0.776377	0.832203
					0.02	1.462437	1.524467
					0.04	1.437439	1.516795
					0.06	1.418020	1.509340

Table 4 Variation in Sh_x with magnetic effect and without magnetic effectcases.

c	n	We	Kr	ϕ	Sh_x	
					$M=2$	$M=0$
0.1					0.658825	0.670567
0.2					0.953467	0.969497
0.3					1.194456	1.213405
	1				0.647406	0.662285
	2				0.647985	0.662365

	3				0.648463	0.662438
		0.1			0.650034	0.662721
		0.2			0.653173	0.663435
		0.3			0.655122	0.663949
			0.1		0.648463	0.662438
			0.2		0.580375	0.598628
			0.3		0.492582	0.518940
				0.02	0.648463	0.662318
				0.04	0.649703	0.662438
				0.06	0.652818	0.662639

Table 5 validation of results for Nusselt number for power law index parameter

n	Nu_x	
	Sulochana et al.[19]	Present Results
1	1.498468	1.49845
2	3.020768	3.02075
3	4.538099	4.53812
4	6.053664	6.05367

4. Concluding Remarks

Beholding the improved heat transfer ability of the nanofluids the current research article emphasis the impression of chemical reaction and dissipative effects on MHD nanofluid flow consisting alloys of Nimonic 80 and Ti6Al4V across needle surface for both with and without magnetic effect cases. Further Matlab bvp5c software is employed to tackle the occurring set of ODE's with associated boundary constraints.

- The needle thickness is capable of diminishing fluid flow, heat transfer and enriching concentration description.
- The non-linearity index revamp the fluid flow and deteriorate thermal transmission of the nanofluid for both the cases
- The Weissenberg number diminishes the rate of flow whereas the reverse trend isobserved for thermal distribution.
- An impact of magnetic field leads to condense velocity of the flow and enhance thermal field.
- Thermal transfer performance of the hybrid nanoliquid is tremendous in the magnetic field effect case than without magnetic field case.

References

1. Hamzat, A. K., Omisanya, M. I., Sahin, A. Z., RopoOyetunji, O., &AboladeOlaitan, N. (2022). Application of nanofluid in solar energy harvesting devices: A comprehensive review. Energy Conversion and Management (Vol. 266). Elsevier Ltd. https://doi.org/10.1016/j.enconman.2022.115790
2. Khoramian, R., Kharrat, R., &Golshokooh, S. (2022). The development of novel nanofluid for enhanced oil recovery application. Fuel, 311, 122558. https://doi.org/10.1016/j.fuel.2021.122558
3. Samrat, S. P., Sulochana, C., &Ashwinkumar, G. P. (2019). Impact of Thermal Radiation on an Unsteady Casson Nanofluid Flow Over a Stretching Surface. International Journal of Applied and Computational Mathematics, 5(2). https://doi.org/10.1007/s40819-019-0606-2
4. Dogonchi, A. S., Divsalar, K., &Ganji, D. D. (2016). Flow and heat transfer of MHD nanofluid between parallel plates in the presence of thermal radiation. Computer Methods in Applied Mechanics and Engineering, 310, 58–76. https://doi.org/10.1016/j.cma.2016.07.003
5. Sulochan, C., Samrat, S. P. & Sandeep, N. (2018). Magnetohydrodynamic radiative nanofluid flow over a rotating surface with Soret effect. Multidiscipline Modeling in Materials and Strctures, 14, 168-188. https://doi.org/10.1108/MMMS-05-2017-0042
6. Mabood, F. Khan, W. A., & Ismail, A. M., (2015). MHD boundary layer flow and heat transfer of nano fluids over a nonlinear stretching sheet : A numerical study. Journal of Magnetism and Magnetic Materials, 374, 569-576.
7. Elattar, S., Helmi, M. M., Elkotb, M. A., El-Shorbagy, M. A., Abdelrahman, A., Bilal, M., & Ali, A. (2022). Computational assessment of hybrid nanofluid flow with the influence of hall current and chemical reaction over a slender stretching surface. Alexandria Engineering Journal, 61(12), 10319–10331. https://doi.org/10.1016/j.aej.2022.03.054

8. Nadeem, S., Abbas, N., & Malik, M. Y. (2020). Inspection of hybrid based nanofluid flow over a curved surface. Computer Methods and Programs in Biomedicine, 189. https://doi.org/10.1016/j.cmpb.2019.105193
9. Zainal, N. A., Nazar, R., Naganthran, K., & Pop, I. (2020). MHD mixed convection stagnation point flow of a hybrid nanofluid past a vertical flat plate with convective boundary condition. Chinese Journal of Physics, 66(January), 630–644. https://doi.org/10.1016/j.cjph.2020.03.022
10. Tlili, I., Samrat, S. P., & Sandeep, N. (2021). A computational frame work on magnetohydrodynamic dissipative flow over a stretched region with cross diffusion : Simultaneous solutions. Alexandria Engineering Journal, 60(3), 3143–3152. https://doi.org/10.1016/j.aej.2021.01.052.
11. Waini, I., Ishak, A., & Pop, I. (2020). Flow and heat transfer of a hybrid nanofluid past a permeable moving surface. Chinese Journal of Physics, 66(January), 606–619. https://doi.org/10.1016/j.cjph.2020.04.024
12. Alsaedi, A., Muhammad, K., & Hayat, T. (2022). Numerical study of MHD hybrid nanofluid flow between two coaxial cylinders. Alexandria Engineering Journal, 61(11), 8355–8362. https://doi.org/10.1016/j.aej.2022.01.067
13. Tlili, I., Nabwey, H. A., Samrat, S. P., & Sandeep, N. (2020). 3D MHD nonlinear radiative flow of CuO-MgO/methanol hybrid nanofluid beyond an irregular dimension surface with slip effect. Scientific Reports, 10(1), 1–14. https://doi.org/10.1038/s41598-020-66102-w
14. Soid, S. K., Ishak, A., & Pop, I. (2017). Boundary layer flow past a continuously moving thin needle in a nanofluid. Applied Thermal Engineering, 114, 58–64. https://doi.org/10.1016/j.applthermaleng.2016.11.165
15. Salleh, S. N. A., Bachok, N., Arifin, N. M., Md Ali, F., & Pop, I. (2018). Magnetohydrodynamics flow past a moving vertical thin needle in a nanofluid with stability analysis. Energies, 11(12), 1–15. https://doi.org/10.3390/en11123297
16. Sulochana, C., Samrat, S. P., & Sandeep, N. (2017). Boundary layer analysis of an incessant moving needle in MHD radiative nanofluid with joule heating. International Journal of Mechanical Science. 129, 326–331.
17. Waini, I., Ishak, A., & Pop, I. (2020). Hybrid nanofluid flow past a permeable moving thin needle. Mathematics, 8(4). https://doi.org/10.3390/math8040612
18. Afridi, M. I., Tlili, I., Goodarzi, M., Osman, M., & Khan, N. A. (2019). Irreversibility analysis of hybrid nanofluid flow over a thin needle with effects of energy dissipation. Symmetry, 11(5). https://doi.org/10.3390/sym11050663
19. Sulochana, C., Savita, &Ashwinkumar, G. P. (2022). Joule heating effect on MHD flow of tangent hyperbolic mixed nanofluid embedded with MgO and CuO nanoparticles. International Journal of Ambient energy. 95http://doi.org/10.1080/01430750.2023.2198531.
20. Rao, K. N., et al. "Comparative study by numerical investigation of heat transfer in circular tube by using hybrid nanofluids." *International Journal of Mechanical and Production Engineering Research and Development* 10.3 (2020): 969-982.
21. Thakur, M. O. H. I. T., D. Gangacharyulu, and G. U. R. P. R. E. E. T. Singh. "Effect of temperature and multiwalled carbon nanotubes concentration on thermophysical properties of water base nanofluid." *Int J Mech Prod Eng Res Dev (IJMPERD)* 7 (2017): 4151-160.
22. Joy, N. I. V. I. N. "Design and Analysis of an Integrated Exhaust Manifold with Turbocharger for Considerable Reduction of Over Heating of Bearing System." *International Journal of Mechanical and Production Engineering Research and Development 8.2 (2018)* 601608 (2018).
23. Moorthy, CH VKNSN, et al. "Computational analysis of a CD nozzle with 'SED'for a rocket air ejector in space applications." *International Journal of Mechanical and Production Engineering Research and Development (IJMPERD)* 7.1 (2017): 53-60.
24. Thilak, K. Raj, R. Kiruthika, and M. Sakthivel. "Experimental and Analytical Study of Roof Heat Effect on the Performane of Solar Desalination System." *International Journal of Electrical & Electronics Engineering Research* 4.2 (2014).
25. Rao, K. N., et al. "Comparative study by numerical investigation of heat transfer in circular tube by using hybrid nanofluids." *International Journal of Mechanical and Production Engineering Research and Development* 10.3 (2020): 969-982.

.